MAMMONE, RICHARD JAMES

ROBUST SUPERRESOLVING RESTORATION WITH APPLICATIONS

City University of New York PH.D. 1981

ROBUST SUPERRESOLVING RESTORATION

WITH APPLICATIONS

by

RICHARD JAMES MAMMONE

A dissertation
submitted to the Graduate Faculty in Engineering
in partial fulfillment of the requirements
for the degree of
Doctor of Philosophy
The City University of New York

1981

This manuscript has been read and accepted for the Graduate Faculty in Engineering in satisfaction of the dissertation requirement for the degree of Doctor of Philosophy.

4/30/81
date

Gerge Eichmann
Chairman of Examining Committee

4/30/81
date

Paul R. Kamel pro
Executive Officer

Prof. G. Eichmann

Prof. D. Schilling

Prof. P. Stebe

Prof. F. Thau

Prof. G. Lidor

Dr. I. Kadar
Supervisory Committee

The City University of New York

Abstract

ROBUST SUPERRESOLVING RESTORATION

WITH APPLICATIONS

by

Richard James Mammone

Advisor: Professor G. Eichmann

A new robust method of solving ill-conditioned problems is presented. The method employs a priori constraints on the estimate, i.e. that the estimate, the first and/or higher order differences are bounded. The ill-conditioned system is reduced by elimination of the effectively redundant equations. This provides a reduction in computational complexity and acts to stabilize the inversion problem.

Since the resulting reduced system of equations is under-determined, there are many possible "solutions." We shall select that particular vector for the solution which yields the minimal norm of the residual error. Since this solution vector is of the same dimension as the effective rank, the method prefers restorations of inputs with sparse vector representations. The method is demonstrated in three

applications: image processing, spectral estimation, and Apodization. Each application pertains to increasing the resolution of a measured signal. The resolution is increased beyond the limit imposed by the uncertainty principle of signal processing (superresolving). The method is demonstrated to be very effective in all three applications via computer simulations. The first chapter of this thesis contains material of an introductory nature. In Chapter 2 the contemporary methods of increasing resolution or equivalently extrapolating the spectrum of a signal are given. In general, these methods are found to be computationally very expensive and highly sensitive to noise. In Chapter 3, a new method of increasing the resolution of an image is presented. The method reduces the computational effort necessary to restore images degraded by an ill-conditioned operator. The restorations of noncoherent and coherent diffraction limited images are treated in detail. In Chapter 4, extrapolation in the time domain of a bandlimited signal is investigated. Alternately, the resolution of the frequency spectrum is increased. Thus, super-resolving spectral estimation is demonstrated. In Chapter 5, the design of a superresolving Apodization screen is presented. This screen will permit a spot-size of smaller circumference than previously possible. This smaller spot-size finds immediate application in the recent development of laser video discs. The video information is in the form of holes in the video disc. This Apodization will

allow smaller holes to be burnt into the disc; thus discs of higher density can be made. Chapter 6 presents the general summary and conclusions obtained in the thesis. Future research is suggested in further applications of the algorithm presented.

ACKNOWLEDGEMENTS

I would like to take this opportunity to thank Professor George Eichmann for providing me with the opportunity to explore this topic and for his invaluable assistance in obtaining the desired results.

Special thanks to my fiance Ms. Valerie Altman for her patience and understanding during this endeavor, and for her unending assistance in preparing this manuscript.

R.J.M.

TABLE OF CONTENTS

LIST OF FIGURES

Chapter 1

INTRODUCTION

1.0 Introduction

Resolution is the measure of the discernable distance between two points. A frequently used resolution limit is the Rayleigh distance. This is the distance between impulses such that the maximum of the first impulse response falls on the first zero of the second impulse response, when the impulses are the input to an ideal low pass filter (ILPF). This is shown in Fig. 1.0-1 and can be stated as

$$TW_c \geq 1 \qquad (1.0\text{-}1)$$

where T is the time between impulses and W_c is the bandwidth of the ideal low pass filter transfer function. This is the well known uncertainty principle [1] in signal analysis.

This distance is related in a reciprocal fashion to resolution. If by processing a waveform, the resolution is increased beyond that limit imposed by this uncertainty principle, then the process is called superresolving. In this thesis a method is presented which is shown to be superresolving. The violation of the uncertainty principle requires a priori information about the original image. This information can be given in the form of linear

equalities or inequalities. The fact that the original signal is positive and bounded provides sufficient constraints for many applications. This increase in the resolution of a signal can be employed in many fields. In this dissertation we focus on three applications: image restoration, spectral estimation and apodization.

1.1 Superresolving Image Restoration

Consider an ideal low-pass system with a transfer function

$$H(\omega) = \begin{cases} 1 & |\omega| \leq W_c \\ 0 & |\omega| > W_c \end{cases} \qquad (1.1\text{-}1a)$$

with corresponding impulse response function

$$h(t) = \frac{\sin W_c t}{\pi t} \qquad (1.1\text{-}1b)$$

and let the input be $f(t)$ with Fourier transform $F(\omega)$. Then the Fourier transform of the output of the low pass filter is

$$G(\omega) = H(\omega)\, F(\omega) \qquad (1.1\text{-}2)$$

Since

$$G(\omega) = \begin{cases} F(w) & |\omega| \leq W_c \\ 0 & |\omega| > W_c \end{cases} \qquad (1.1\text{-}3)$$

The input $f(t)$, in general, cannot be reconstructed from its image $g(t)$ because all components of $F(\omega)$ above $|\omega| = W_c$ are lost. However, if $f(t)$ is of compact support, i.e.

$$f(t) = 0 \quad \text{for } |t| > \frac{T}{2} \tag{1.1-4}$$

then it can be recovered in terms of its response

$$g(t) = \int_{-T/2}^{T/2} f(\zeta) \frac{\sin W_c(t-\zeta)}{\pi(t-\zeta)} d\zeta \tag{1.1-5}$$

The above follows from the fact that the transform $F(\omega)$ of a signal of finite extent is an analytic function of ω. Therefore, if $f(t)$ is known in the interval $(-W_c, W_c)$ (or any other interval), it can be determined, at least in principle, for all ω. In the following we discuss a direct method for recovering $f(t)$ from $g(t)$.

1.2 The Prolate Spheroidal Function Method

In order to extrapolate the lost high frequency content of $f(t)$ we introduce the prolate spheroidal (PSF) functions $\{\phi_n(t)\}$. These functions are eigenfunctions of the integral equation

$$\int_{-T/2}^{T/2} \phi_n(\zeta) \frac{\sin W_c(t-\zeta)}{\pi(t-\zeta)} d\zeta = \lambda_n \phi_n(t) \qquad n = 0,1... \tag{1.2-1}$$

where the constants $\{\lambda_n\}$ are the eigenvalues of the above integral equation. We then define the truncated PSF

$$\phi_{Tn}(t) = \begin{cases} \phi_n(t) & |t| \leq \frac{T}{2} \\ 0 & |t| > \frac{T}{2} \end{cases} \tag{1.2-2}$$

which results when $\phi_n(t)$ is truncated above $|t| = \frac{T}{2}$, and if applied as input to the system (1.1-1), then the resulting output equals $\lambda_n \phi_n(t)$.

The functions $\{\phi_n(t)\}$ are orthogonal in both intervals $(-\infty, \infty)$ and $(-T/2, T/2)$, i.e.

$$\int_{-\infty}^{\infty} \phi_n(t)\phi_m(t)\, dt = \begin{cases} 1 & n = m \\ 0 & n \neq m \end{cases} \qquad (1.2\text{-}3)$$

and

$$\int_{-T/2}^{T/2} \phi_n(t)\phi_m(t)\, dt = \begin{cases} \lambda_n & n = m \\ 0 & n \neq m \end{cases} \qquad (1.2\text{-}4)$$

The PSF form a complete set in the above intervals. By this we mean that any function g(t), bandlimited as in Eq. (1.1-3) can be written as a convergent series

$$g(t) = \sum_{n=0}^{\infty} c_n \phi_n(t) \qquad (1.2\text{-}5)$$

and a function f(t) of limited extent, as in (1.1-4) can be written as a convergent series

$$f(t) = \sum_{n=0}^{\infty} d_n \phi_{Tn}(t) \qquad (1.2\text{-}6)$$

As we see from Equations (1.2-3) and (1.2-4), the coefficients c_n and d_n are given by

$$c_n = \int_{-\infty}^{\infty} g(t)\phi_n(t)\, dt \qquad (1.2\text{-}7)$$

and

$$d_n = \frac{1}{\lambda_n} \int_{-T/2}^{T/2} f(t)\, \phi_n(t)\, dt \qquad (1.2\text{-}8)$$

respectively. Using these functions we may now solve the bandlimited extrapolation problem.

Let the unknown input f(t) be expanded into a PSF series, as in Eq. (1.2-6), then the output

$$g(t) = \sum_{n=0}^{\infty} \lambda_n d_n \phi_n(t) \qquad (1.2\text{-}9)$$

since the response to $\phi_{Tn}(t)$ is $\lambda_n \phi_n(t)$. From Eqs. (1.2-5) and (1.2-9) it follows that

$$d_n = \frac{c_n}{\lambda_n}. \qquad (1.2\text{-}10)$$

Thus, the constants $\{d_n\}$ can be found from Eq. (1.2-10) where $\{c_n\}$ are the coefficients of the expansion of the known function g(t). This is the PSF method of solution of the bandlimited image restoration problem.

1.3 Superresolving Spectral Estimation

The dual of the previous problem, i.e. exchanging the roles of frequency and time, can also be solved in an identical fashion. In the dual problem we are given a time truncated version of a bandlimited signal. From the given time interval we can extrapolate outside the interval using the PSF method. Thus the Fourier Transform of the measured signal

is of infinite duration and blurred by the time truncation operator, and the Fourier Transform of the solution is bandlimited and can have more detail. Thus bandlimited extrapolation in the time domain is identical to increasing the resolution in the frequency domain. Again, if this increase in resolution is greater than the limit given by the uncertainty principle, then this increase in spectral resolution is called superresolving spectral estimation.

1.4 Superresolving Apodization

Consider an optical system with point spread function h(r) where r is the radial distance. By a proper scaling we can assume that the radius of the exit pupil equals one and that the output field H at the exit pupil equals the two-dimensional Fourier transform of h(r). If the system is an ideal diffraction-limited system then, for a spherical lens with circular aperture

$$h(r) = \frac{2J_1(r)}{r} \qquad (1.4\text{-}1)$$

where J_1 is the Bessel function of the first kind of order one. This function is the two-dimensional analog of the one dimension sampling function used previously.

The object of Apodization is to modify H (for example, by coating the lens) so as to improve the system performance. Since the image of an object is obtained by convolving

its amplitude with h(r) for coherent signals or its intensity with $|h(r)|^2$ for incoherent signals, it is desirable for satisfactory performance to chose H so as to reduce the spread of h. However, since $H(\omega)$ must be such that

$$H(\omega) = 0 \quad |\omega| > a \tag{1.4-2}$$

it follows from a radial uncertainty principle that the parameter a of Eq. (1.4-2) must be greater or equal to unity and thus h(r) cannot be made arbitrarily narrow.

An Apodization is called superresolving if the transfer function $H(\omega)$ can be replaced with a transfer function of smaller bandwidth.

The case with which we are primarily concerned is that of coherent and incoherent optical systems and where the density of the coating on the lens is constrained to lie between zero and unity. We shall accomplish this for a radial symmetric optical system. The method presented begins with a desired $H(\omega)$ and via mathematical programming techniques will provide the optimal aperature coating for the given $H(\omega)$. This technique provides superresolving results.

1.5 The Ill-Posed Nature of the Problem

The method of achieving superresolving results given in Section 1.2, although convergent, is not very practical. This is due to the ill-posed nature of the problem. That is, the stated method is highly sensitive to noise. This

can be seen by observing the behavior of the eigenvalues defined by Eq. (1.2-1). It can be shown [2] that these eigenvalues go approximately as a unit step as a function of the index, i.e.

$$\lambda_i \simeq \begin{cases} 1 & i \leq r' \\ 0 & i > r' \end{cases} \qquad (1.5\text{-}1)$$

where the index r' is a function of the time-bandwidth product. The PSF method of the solution requires that the components of the measured signal be divided by these eigenvalues, see Eq. (1.2-10). This division by, effectively, zero creates the numerical instability. For any real measured signal there always will be some high order noise components. These high order noise components will not allow this division to go past the r'^{th} order eigenvalue component. Thus a possible alternative is to form the truncates series expansion

$$f_a(t) = \sum_{n=0}^{r'} \frac{c_n}{\lambda_n} \phi_{Tn}(t) \qquad (1.5\text{-}2)$$

where the subscript "a" indicates a truncation approximation. This stabilized PSF or the regular PSF method requires the signal to be decomposed into orthogonal components of a numerically complicated signal space. The PSF are not easily generated, and the integrations which must be performed before the final series expansion can be evaluated, are numerically cumbersome. Foregoing the computation

difficulties involved, this method cannot yield super-resolving restorations since the high order components correspond to the high frequency signal components. Thus to gain stability, most of the high frequency information is eliminated. This is precisely the information the super-resolution seeks to recover.

In order to take advantage of numerical methods of solution, we employ some quadrature rule on the integral of Eq. (1.1-5) to obtain a set of N algebraic equations. This converts the continuous problem into a discrete and finite set of equations. We shall assume, without loss of generality, that the number of samples measured is equal to the number of input samples. Thus,

$$\underline{g} = \underline{H}\underline{f} \tag{1.5-3}$$

where g and f are the N dimensional measured and input signal vectors and H is an NxN matrix obtained from the quadrature rule. This discrete formulation is still ill-conditioned [3].

To illustrate the ill-conditioning, we diagnoalize H into a modal form via a singular value decomposition (SVD). We obtain

$$\underline{H} = \underline{U}\underline{\Lambda}^{\frac{1}{2}}\underline{V}^{T} \tag{1.5-4}$$

where $\underline{U}$ and $\underline{V}$ are orthogonal matrices and $\underline{\Lambda}$ is a diagonal matrix consisting of the eigenvalues of $\underline{H}\underline{H}^{T}$. The superscripts

T and ½ indicate matrix transpose and matrix square root respectively, i.e. the square root of a diagonal matrix is simply the matrix obtained by taking the positive square root of the diagonal elements, which are known to be positive. These eigenvalues exhibit the same behavior as for the continuous use. That is, they go abruptly to effectively zero. Thus, the inverse of H given by

$$\underline{H}^{-1} = \underline{V}\ \underline{\Lambda}^{-\frac{1}{2}}\ \underline{U}^{T} \qquad (1.5\text{-}5)$$

where $\Lambda^{-\frac{1}{2}}$ possess the reciprocal elements of $\underline{\Lambda}^{\frac{1}{2}}$, thus forcing any norm $||\underline{H}^{-1}||$ to become effectively unbounded since the eigenvalues of $\underline{H}$ behave approximately as a unit step as a function of the index, that is, the same behavior as exhibited in the continuous case of Eq. (1.5-1). It can be surmised from Eq. (1.5-4) that the measured signal contains very strong attenuated higher order components. So we might make the approximation that Eq. (1.5-6) is true with equality signs replacing the approximately equal signs. Thus r' becomes the rank of H' thus formed, where r' is sometimes called the pseudorank of the $\underline{H}$ matrix. Therefore of the N equations only r' are needed to form a basis and the remaining N-r' equations are redundant.

If the elements of $\underline{\Lambda}^{-\frac{1}{2}}$ are replaced with this approximation, the resulting $\underline{H}'$ matrix will have rows that

that are linearly dependent. Only r rows will be linearly independent, thus (N-r) equations can be discarded. The undetermined set of equations results in

$$g' = \underline{H}'_f \qquad (1.5\text{-}6)$$

where g' is an r'dimensional vector (a subset of g) and H' is an r x N matrix obtained by discarding redundant equations. Since the number of unknowns (N) is greater than the number of equations, there are many solutions to Eq. (1.5-6). Eq. (1.5.6 is effectively Eq. (1.5-3) for purposes of numerical computation.

It will be instructive to examine the distribution of the linearly dependent rows in the matrix H. This will give the optimal distribution of the input signal since the solution will be better posed if the r'or less non-zero elements lie on linear independent nodes of the quadrature grid. In order to find this spacing, take the Taylor series expansion of $h(t,\zeta)$ where the dependence on the shift ζ is explicitly shown:

$$h(t+\Delta t, t_1+\Delta t_1) = h(t,t_1) + \frac{\partial h}{\partial t}\Big|_{t,t}^{\Delta t} + \frac{\partial h}{\partial t}\Big|_{t,t_1}^{\Delta t} + E \qquad (1.5\text{-}7)$$

where E is the remainder term, we wish to use the Taylor series to compare elements of

the rows of H that lie in the same vertical column. Thus we set the set increment $\Delta t_1 = 0$ and have

$$h(t+\Delta t, t_1) \approx h(t,t_1) + \frac{\partial h}{\partial t}\Big|_{t,t_1}^{\Delta t} \tag{1.5-8}$$

We now choose the value of t and t_1 about the expansion is made to be points t_k and t , which are chosen to generate the matrix $\underline{H}$. The time samples t_k correspond to the rows and time t_{1j} corresponds to the columns of the $\underline{H}$ matrix. Thus,

$$h(t_k+\Delta t, t_{1j}) = h(t_k, t_j) + \frac{\partial h}{\partial t}\Big|_{t_k,t_{1j}} \Delta t + E \tag{1.5-9}$$

We now use the approximation

$$\frac{\partial h}{\partial t}\Big|_{t_k,t_j} \Delta t \approx \left[\frac{h(t_k,t_{ij}) - h(t_{k-i},t_{1j})}{t_k - t_{k-1}}\right] \Delta t \tag{1.5.10}$$

Substituting Eq. (1.5-10) into Eq. (1.5-9), we have

$$h(t_k+\Delta t, t_{1j}) \approx h(t_k,t_{1j}) + \frac{\Delta t}{t_k - t_{k-1}} \left[h(t_k,t_{1j}) - h(t_{k-1},t_{1j})\right]\Delta t \tag{1.5-11}$$

Finally, choosing Δt such that $t_k+\Delta t = t_{k+1}$

$$h(t_{k+1},t_{1j}) \approx h(t_k,t_{1j}) + \frac{t_{k+1}-t_k}{t_k - t_{k-1}} [h(t_k,t_{1j}) - h(t_{k-1},t_{1j}] \tag{1.5-12}$$

The right hand side of this equation is the desired linear combination. This equation is true for K+1 = 2,3,...,M-1. For k+1 = 0,1, there are insufficient rows in the matrix to make the combination. Therefore, any row of $\underline{H}$ is approximately a linear combination of two adjacent rows of $\underline{H}$. This is an alternate statement of the ill-conditioning of the $\underline{H}$ matrix. Furthermore, the accuracy of the Taylor series approximation is dependent upon how closely together we choose the sampling points t_k and t_{1j}. As we subdivide the intervals more finely, the sampling distance points are closer together and the approximation described in (1.5-12) becomes more accurate, therefore attempting to make the approximation more accurate. However, choosing more points does not lead to a "better" solution for the function f. It leads to a "worse" solution because the matrix H becomes increasingly ill-conditioned with more redundant sampling points. Thus, trying to solve an equality of the form (1.1-5) is only made more difficult by the choice of more sampling points. Due to the Toeplitz structure of $\underline{H}$, the linear dependence between adjacent rows yields linear dependence between adjacent columns and the r' linearly independent samples are uniformly spaced at the maximum possible distance. This is the same sampling distribution for which the input signal is most easily restored.

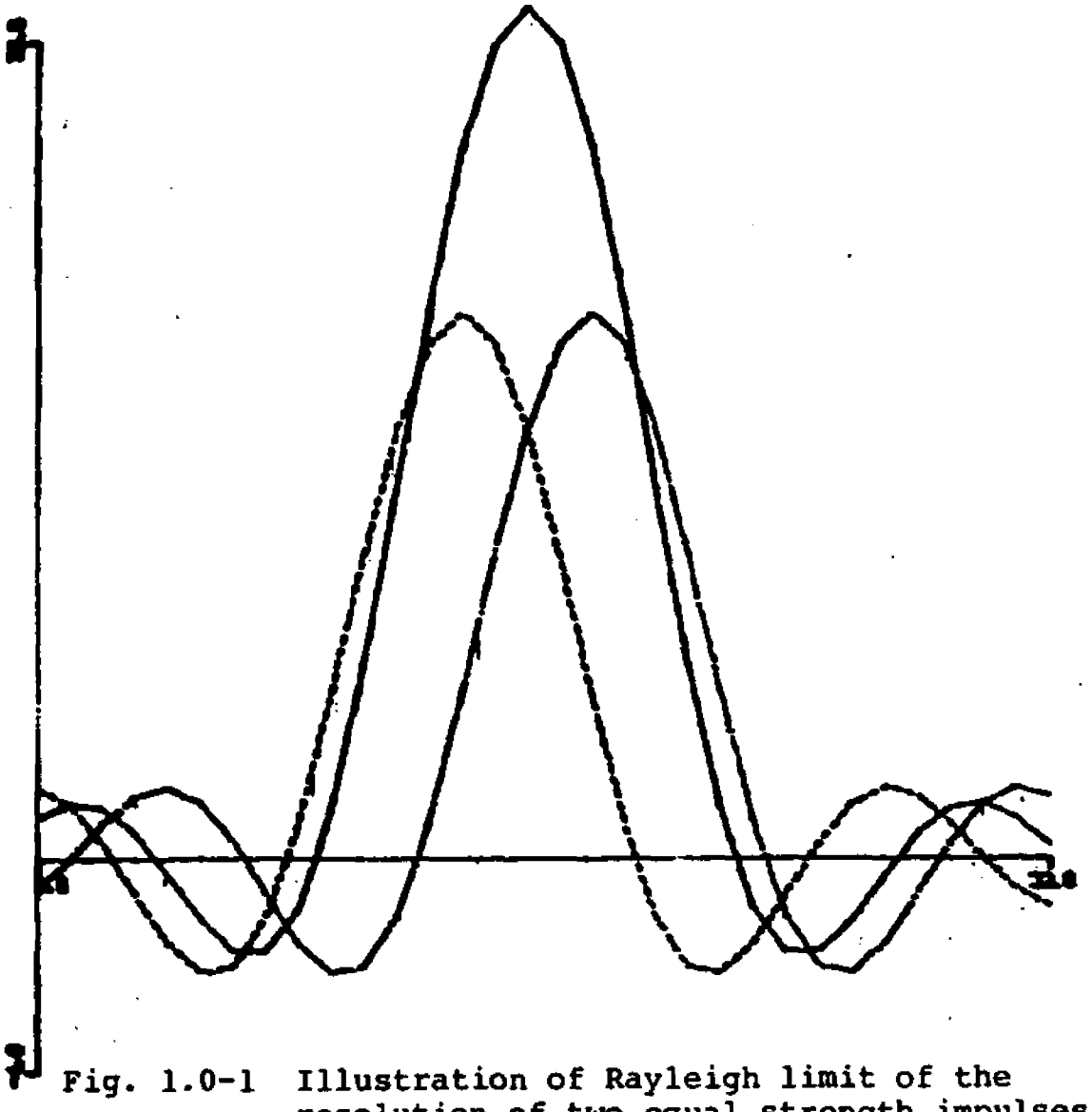

Fig. 1.0-1 Illustration of Rayleigh limit of the resolution of two equal strength impulses

Chapter 2

INTRODUCTION TO SUPERRESOLVING METHODS

2.0 Background

In this chapter we shall examine the existing algorithms designed to increase the resolution of a measured signal. These algorithms come from a wide diversity of fields and the approaches taken in formulating the problems are as varied as the number of methods. Most of the methods are designed for a specific use but can be adopted easily to any of the applications discussed in this thesis.

The existing methods fall into several different categories. In general linear methods which do not impose constraints (positivity appears highest in priority) on the input signal being sought, do not produce superresolving results. There are ad hoc methods of imposing positivity constraints but the solution found is not optimal in any sense and in most cases it is not even clear that the method will converge to a particular solution. These are statistical methods which require statistical information of the underlying signal space. This information is very seldom known a priori. We must assume some convenient statistics, thus negating the desired optimal conditions. Alternately one might try to deduce the

the statistics from the measured signal, usually replacing one ill-posed problem with another. The linear predictive type MEM and MLM are very popular but they require that the order of the predictor be exactly correct. This is not a simple task. The methods which regularize the problem never offer superresolving results since the estimate must be smooth.

In the following we shall present an overview of the available methods and discuss the relative advantages and disadvantages.

2.1 Autoregressive and Maximum Entropy Methods

These new techniques are not only strongly related to each other, but to other fields as well. They include work done in the past on system identification where the objective is to model an unknown system using a linear adaptive model with adjustable poles and zeroes [4], linear predictive coding [5], among others.

The AR method uses a finite autoregression fit to the time series data and calculates the spectrum from the autoregression coefficients (as well as the error variance. A key problem is to determine the order of the autoregression to be used. The difficulty is not unlike that confronting the user in a pattern recognition

problem in determining the optimum number of features to use, given a finite data set. Akaike's [6] Information Criterion is the most popular method used to determine the order of the regression, because of its effective use of the final prediction error FPE. In essence, the AR parameters are fit by a least squares to the covariance sequence of the observed data (the sets of equations to be solved for the coefficients are exactly those used for linear predictive encoding (LPE)). When the order of the estimate is the same as the order of the model that generated the data, the parameters are known to be maximum likelihood estimates. The question as to the order of the model has been the brunt of much of the recent work by Akaike and others.

The method presented does not show this ambiguity since there is no parametric model involved. The degradation operator is discretized using a quadrature rule. Therefore we assume perfect knowledge of the degradation in the form of a convolution relationship.

Maximum Entropy is a method credited primarily to Berg, which provides an estimate of the power spectral density which maximizes the entropy of a stationary random process from the first N lags of the autocorrelation function. It has been shown [7] that this method is, in fact, equivalent to fitting an AR data model to the available time series data and closely related to work appearing in the statistical literature previously. With this similarity it is only necessary to describe one of these techniques in detail. The following parallels the explanation of AR given by Griffiths [8] which appears in numerous other references as well.

The AR method of spectral analysis may be described in terms of a whitening model. The input data sequence x(k) is filtered by a whitening operator having an impulse response with z transform

$$H(z) = 1 - a_1 z^{-1} - a_2 z^{-2} \ldots a_L z^{-L} \qquad (2.1\text{-}1)$$

where z^{-1} has been used to denote a unit delay. As is well known,

$$S_\varepsilon(\omega) = S_x(\omega) \; |H(\omega)|^2 \qquad (2.1\text{-}2)$$

In AR analysis, the L coefficients $a_1, a_2, \ldots, a_L$ are chosen

so as to minimize the power at the filter output. Zero output power is not possible due to the fact that the leading coefficient is unity. Markel and Grey [5] have shown that minimizing the output power is equivalent to providing the flattest possible output spectral density $S_\varepsilon(\omega)$. The appropriate equations for these coefficients are called the normal equations or correlation equations, and are given in matrix form by

$$\begin{bmatrix} r_x(0) & r_x(1) & \cdots & r_x(L-1) \\ r_x(1) & r_x(0) & \cdots & r_x(L-2) \\ \vdots & & & \\ r_x(L-1) & & \cdots & r_x(0) \end{bmatrix} \begin{bmatrix} a_1 \\ a_2 \\ \vdots \\ a_L \end{bmatrix} = \begin{bmatrix} r_x(1) \\ r_x(2) \\ \vdots \\ r_x(L) \end{bmatrix} \qquad (2.1\text{-}3)$$

where $r_x(\ell)$ is the autocorrelation of the input data sequence at lag ℓ. If the resulting coefficients provide a truly flat output spectral density, i.e.

$$S_\varepsilon(\omega) = \gamma, \text{ for all } \omega \qquad (2.1\text{-}4)$$

then, combining the input spectral density $S_x(\omega)$ may be expressed as

$$S_x(\omega) = \frac{\gamma}{|H(\omega)|^2} \qquad (2.1\text{-}5)$$

Since

$$H(\omega) = 1 - \sum_{\ell=1}^{L} a_\ell \; e^{-j\omega\ell} \qquad (2.1\text{-}6)$$

and, as shown by Makhoul [45],

$$\gamma = r_x(0) - \sum_{\ell=1}^{L} a_\ell r_x(\ell) \qquad (2.1\text{-}7)$$

the input power spectrum can be determined directly from the a_ℓ, which are called the AR coefficients.

Of course, one cannot always expect a flat output spectrum for finite values of L, which is the order of the AR model referred to before. This occurs only if the second-order statistics of x(k) can be reproduced exactly by a sequence which is generated by filtering white noise with a filter containing no zeroes and L or fewer poles [7]. For this reason, AR spectral analysis is often called the all-pole-model method of spectral analysis.

The theory outlined above assumes that the data autocorrelation function $r_x(\ell)$ is known exactly for lags $\ell = 0$ through $\ell = L$. In practice, this function must be determined from direct measurement on the data. Two common methods are currently being used. They are the Yule-Walker and Burg procedures. Yule-Walker (YW) involves the following three steps:

1. Estimate $r_x(\ell)$ for $\ell = 0,1,\ldots,L$
2. Substitute these values and solve for the AR coefficients $a_1,\ldots,a_L$
3. Compute a spectral estimate $S_A(\omega)$ and the results

of steps 1 and 2.

In Burg's method the a_ℓ coefficients and autocorrelation values are estimated simultaneously from the data values using a recursive algorithm. Once these parameters have been found, the spectral estimate $S_A(\omega)$ is computed as in step 3 above. Burg's method will, in general, provide a different estimate than that given by the YW procedure. There is some evidence suggesting that higher resolution may be achieved for the case of sinusoids in white noise using Burg's algorithm, but this is still an open question for the case of random data.

The critical set of equations are the normal equations (to determine the coefficients) which frequent the literature. If the data is only available sequentially, for example, it is possible to iteratively estimate the correlation coefficients and sequentially update them and, in turn, the coefficients.

To demonstrate briefly the similarity, the MEM states that the least assumptions should be made about the unobserved points. This may be restated by saying that the spectrum estimated should be maximally random (maximum entropy) and still be consistent with the observed data. The equation Entropy ~ $\int_o^\omega \log P(f)\, df$ (where intentionally different notation is used) is the entropy of a Gaussian stationary

process. The object is to find a P(f) that maximizes this entropy and agrees with the measured values of the autocorrelation function. The MEM solution for this is

$$P(f) = \frac{P(N+1)/\omega}{\left| 1 + \sum_{n=1}^{N} \alpha(n+1)\ e^{-j2\pi f n\ \Delta t} \right|^2} \qquad (2.1\text{-}8)$$

where P(N+1) and $\alpha(n+1)$ are obtained from

$$\begin{bmatrix} c(0) & c(1) & \cdots & c(N) \\ c(1) & c(0) & & \\ & \ddots & & \\ \vdots & & \ddots & \vdots \\ c(N) & & \cdots & c(0) \end{bmatrix} \begin{bmatrix} 1 \\ \alpha(2) \\ \alpha(3) \\ \vdots \\ \alpha(N+1) \end{bmatrix} = \begin{bmatrix} P(N+1) \\ 0 \\ 0 \\ \vdots \\ 0 \end{bmatrix} \qquad (2.1\text{-}9)$$

This matrix equation may be recognized as identical to that of the AR method as well as that resulting from designing a N + 1 point predictor.

AR methods are particularly well suited for short record lengths. In fact, it has been stated that Burg's method is simply not practical for long records to go to the other extreme.

In addition to the classic advantages of AR methods for obtaining higher resolution on shorter records of data, and the difficulty with sensitivity to noise, there are other

factors to consider not all of which can be presented here. For example, given a situation where there are two neighboring peaks of equal width in the spectrum to be estimated, the AR method will tend to emphasize the stronger of the two signals. A narrower variance of the stimate will be obtained and the results will be misleading in that they may indicate premature termination of the estimation procedure, or reflect on the signals as having different widths, strengths, etc. The AR methods are critically dependent on the number of terms used in the model, with too many or too few yielding erroneous results.

2.2 Papoulis-Gerchberg Method

In recent years there have been some innovative methods developed for spectral estimation. One of the most significant has been that by Papoulis [9] and Gerchberg [10]. This method is applicable to bandlimited signals. The algorithm is an iteration involving the fast Fourier transform. In the reference [9], the convergence properties, the effects of noise, aliasing, etc. are described in detail. The method may be used to extrapolate bandlimited functions as well.

Given a bandlimited function f(t) and a segment of it $g_o(t)$

$$G_o(\omega) = \int_{-T}^{T} g_o(t)\ e^{-j\omega t}\ dt \qquad (2.2\text{-}1)$$

The n^{th} iteration step proceeds as follows: Form the

$$F_n(\omega) = G_{n-1}(\omega)\ \rho_\sigma(\omega) \tag{2.2-2}$$

where

$$\rho_\sigma(\omega) = \begin{cases} 1 & |\omega| < \sigma \\ 0 & |\omega| > \sigma \end{cases} \tag{2.2-3}$$

by truncating $G_{n-1}(\omega)$ and compute its inverse transform

$$f_n(t) = \int_{-\sigma}^{\sigma} F(\omega)\ e^{j\omega t}\ d\omega \tag{2.2-4}$$

Now form

$$g_n(t) = f_n(t) + \left[f(t)-f_n(t)\right]\ \rho_T(t) = \begin{cases} g(t) & |t| < T \\ f_n(t) & |t| > T \end{cases} \tag{2.2-5}$$

by replacing the segment of $f_n(t)$ in the interval $(-T,T)$ by the known segment $g(t)$ of $f(t)$. Finally,

$$G_n(\omega) = \int_{-\infty}^{\infty} g_n(t)\ a^{-j\omega t}\ dt \tag{2.2-6}$$

at the n^{th} step.

Note that $f_n(t)$ is bandlimited and given by

$$f_n(t) = g_{n-1}(t) * \frac{\sin \sigma t}{\pi t} \tag{2.2-7}$$

By this continued resubstitution and multiple use of the FFT in transforming from one domain to the other, the bandlimited spectrum is estimated. In the time domain since bandlimiting the spectrum is equivalent to extending the signal

(again the uncertainty principle), the extrapolation of the signal beyond the original duration interval provided may be performed as well. The procedure has been shown effectively for bandlimited signals. A closed form procedure similar in approach, has been developed by J. Cadzow [11], where the numerical implementation does not require the truncation of generally infinite time signals, and therefore avoids the error producing truncations. More significantly, in the same work, Cadzow develops a closed form rule for generating the desired extrapolation in one step. W. Steenaart [12] has also extended this class of extrapolation methods of Papoulis to a matrix formulation where the total process is achieved by one matrix operation resulting in savings in computation and yielding more accurate results in some cases.

Kadar and Kurz [13] have robustized this process to measurement noise outliers in unspecified burst noise of high variance. The modified method also eliminates the need for stopping constraints.

This algorithm converges very slowly in general requiring enormous computational time. The method is linear, although not shift variant, so that the addition of constraints cannot be employed to speed the convergence.

The method is also limited to the discrete Fourier transform

(DFT) approximation to the Fourier transform due to the large number of iterations usually required for a solution. Inherent in the DFT approximation are the concepts of periodic and discrete time and frequency sequences. Since the analysis was performed for the Fourier transform it is not clear that the DFT will provide convergence at all. This might explain the large number of iterations reported [9].

2.3 Backus-Gilbert Method

Backus and Gilbert [14] suggested to minimize separately in some convenient sense the output noise and the output departure of the restored signal from the true object. This can be accomplished by defining the restoration filter $Y(\omega)$ for the problem

$$G(\omega) = H(\omega)F(\omega) + N(\omega) \tag{2.3-1}$$

$$F'(\omega) = Y(\omega)G(\omega) \tag{2.3-2}$$

where $F'(\omega)$ is the Fourier transform of the signal estimate, $G(\omega)$ is the Fourier transform of the measured signal with the noise added, and $Y(\omega)$ is the inversion process that we are seeking. The total mean-square output noise is then

$$N_o = \int_{-\infty}^{\infty} |Y(\omega)N(\omega)|^2 \, d\omega \tag{2.3-3}$$

where $N(\omega)$ is the Fourier transform of the noise. As a measure of the resolution of the estimate, Backus and

Gilbert used a measure of the width of the effective total transfer function, i.e.

$$\ell_o = \int_{-\infty}^{\infty} t^2 y(t) h(t)\, dt \qquad (2.3\text{-}4)$$

where $y(t)$ and $h(t)$ are the point spread functions corresponding to $Y(\omega)$ and $H(\omega)$ respectively. The smaller (2.3-3) can be made, the closer the total point spread is to a Dirac delta function $\delta(t)$. Thus the higher the resolution of the estimate. It is shown in [14] that the combined criterion

$$\lambda_1 N_o + \lambda_2 \ell_o \qquad (2.3\text{-}5)$$

may be solved for the deconvolution of the function $y(t)$ for different sets of parameters λ_1, λ_2. These solutions result in useful tradeoff curves of attainable (shortest) resolution "length" ℓ_o as a function of tolerable noise level for a fixed N_o.

However, this approach has the following drawbacks: First, since it is a linear method, its output $f'(t)$ (the inverse Fourier transform of $F'(\omega)$) is unconstrained and accordingly can have negative regions. The measure for resolution (2.3-3) is quite arbitrary and is, to a good extent, insensitive to the sidelobe structure of the overall point spread function. Hence, the statement of an achieved resolution length l_o does not impart information on the

erroneous oscillations in the output estimate.

2.4 Schell and Biraud Methods

One obvious way to force a positive output f'(t) is to set

$$f'(t) = a(t)^2 \tag{2.4-1}$$

and then try to find a(t) in frequency space. Let

$$F'(\omega) = A(\omega) * A(\omega) \tag{2.4-2}$$

where * denotes the convolution operator. $A(\omega)$ must be consistent with the image. Thus,

$$G(\omega) = H(\omega)[A(\omega) * A(\omega)] \tag{2.4-3}$$

over the data bandwidth $|\omega| \lesssim W_c$. Another way of stating this is

$$\hat{F}(\omega) = G(\omega)/H(\omega) = A(\omega) * A(\omega) \quad |\omega| \lesssim W_c \tag{2.4-4}$$

But the left-hand side of Eq. (2.4-4) is the inverse-filter estimate. We note that samples values of the inverse-filter solution $\hat{F}(\omega)$ may be used as inputs to a positive constrained algorithm.

Due to noise in the measured image, the inputs $\hat{F}(\omega)$ will be in error. Hence, rather than demand strict equality in Eq. (2.4-4), the weaker condition

$$\int_{-W_c}^{W_c} |\hat{F}(\omega) - A(\omega) * A(\omega)|^2 \, d\omega \tag{2.4-5}$$

that the above function be a minimum, is invoked.

On the other hand, at frequency $\omega = 0$, where $H(\omega) = 1$, the error due to inverse-filtering is minimal. Hence here the stronger equality requirement is used:

$$\hat{F}(0) = A(\omega) * A(\omega)\,|\,\omega = 0 \qquad (2.4\text{-}6)$$

Eqs. (2.4-5) and (2.4-6) comprise Biraud's [15] definition of the problem.

The two sides of Eq. (2.4-6) represent the areas under the curves $\hat{f}(t)$ and $f'(t)$. The requirement of equality means that our final output $f'(t)$ must be purely a redistribution (without amplification) of the energy under the band-limited input curve $\hat{f}(t)$. Since $f(t)$ is linearly linked to the exact $f(t)$, the equality (2.4-6) actually fixes the total energy in the estimate $f'(t)$ and that of the time signal $f(t)$ plus noise. Since this tends to be a reliable estimate, it could be expected to aid in producing a convergent solution to (2.4-5). In fact, this is empirically found to be true.

It is important to note at this point that in order to approximate $F(\omega)$ over $|\omega| \lesssim W_c$ in Eq. (2.4-5) and (2.4-6), $A(\omega)$ need only be defined over the half-interval $|\omega| \lesssim W_c/2$. This is a property of the convolution operation in Eq. (2.4-5). However, if $A(\omega) \neq 0$ for frequencies $|\omega| > W_c/2$, these components also contribute to Eqs. (2.4-5) and (2.4-6).

They are mixed into the interval $|\omega| \lesssim W_c$ by the convolution operation. This is a way of packing more degrees of freedom of $A(\omega)$ into the data interval $|\omega| \lesssim W_c$ so as to further reduce the minimum attained in (2.4-5).

Schell [16] and Biraud [15] have solved the problem (2.4-5) and (2.4-6) in different ways, but each with an iterative algorithm.

The essential ingredient in Biraud and Schell's approaches is the necessity for exceeding the data bandwidth if a positive output consistent with the inputs is to be obtained. That is, providing the noise propagation error is small enough. In practice, the method is tolerant to quite significant levels of noise in the inputs, and extrapolation by factors of two or more is the rule rather than the exception. However, these benefits accrue only for objects that consist of a general array of impulses against known (hence, zero) background. For example, an object consisting of random steps does not restore by this method much better than by plain inverse filtering. The edge gradients are enhanced better than by inverse filtering, but there is as much objectionable spurious oscillation in the plateau regions. This drawback is the tendency of all extant, positive-constrained restoring schemes.

2.5 Jansson-Van Cittert Method

Van Cittert suggested a method of inversion [17] based on successive convolution of the measured signal with the degradation operator. It was shown that as the number of iterations went to infinity, the estimate converged to the inverse filter estimate. For a finite number of iterations the estimate yielded a smooth version of the inverse. The method was highly unstable and its use was intended for limited applications.

Jansson [18] found a modification of the technique which has transformed it into a useful tool for enhancing spectral data. Jansson modified Van Cittert's basic algorithm to read, with initial iteration conditions, $k = 0$, $f(t) = g^{o}(t)$ then iterate

$$\text{(i)} \quad g^{k}(t) = h(t) * f^{k}(t) \tag{2.5-1}$$

$$\text{(ii)} \quad f^{k+1}(t) = f^{k}(t) + r(t)[g(t)-g^{k}(t)] \tag{2.5-2}$$

where

$$r(t) = c[1-2|f^{k}(t)-\tfrac{1}{2}|] \quad c = \text{constant} \tag{2.5-3}$$

$$\text{(iii)} \quad k \rightarrow k+1$$

$$\text{(iv)} \quad g^{k}(t) = h(t) * f^{k}(t)$$

where $f^{k}(t)$ on the right side of step (i) incorporates updated values $f^{k-1}(t)$ from step (ii) as they are formed from preceding $g^{k}(t)$ values. For simplicity, we suppress

this dependence from the notation.

This approach differs from Van Cittert's by the insertion of a relaxation factor r(t) at step (ii). This step is the key modification of the method. The dependence of r(t) upon $f^k(t)$ is such that r(t) → 0 as either $f^k(t)$ → 0 or 1. Hence, if at any t an iterate $f^k(t)$ is close to either 0 or 1, by step (ii) the next iterate $f^{k+1}(t)$ and all subsequent ones will remain at that value. This constrains the output f'(t) to obey $0 \leq f'(t) \leq 1$. Precisely this physical requirement occurs with absorption spectra, for which the algorithm was designed.

Regarding step (ii) above, we see that initially r is linear in $f^0(t)$, which in turn is linear in the image g(t). But then f'(t) in step (ii) becomes quadratic in the image g, f^2 is cubic in g, etc. In general, then the output f'(t) is highly non-linear in the image data. The factor r(t) then transforms the linear, unconstrained Van Cittert technique into a nonlinear, constrained method.

The Jansson method requires many iterations of the convolutions operation, thus requiring enormous computer time. The method does not provide an optimal estimate in any sense. Furthermore, this algorithm could not provide inversion for ill-posed point spread functions since each convolution only attenuates high frequency information. No

matter how many times you refilter the signal, the high frequency information cannot be restored.

2.6 Summary and Comparison

The methods described in the preceding sections require a prohibitive amount of computer time for two-dimensional images. These methods are not designed specifically for ill-posed problems. Thus, the question of stability is not usually addressed. The effective lower rank of the linear system of equations is not used to any computational advantage.

The preference for impulsive type image for the superresolving restorations are discussed. It is shown that this preference is related to the ill-conditioned nature of the problem and not the particular restoration method employed. The method presented in this thesis will address these topics. The approach taken will focus on the minimal rank equations, thereby reducing the computational effort necessary. Since the effective system of equations is underdetermined, there are many "solution" vectors f. Thus the need for further constraints is apparent. The method presented here appends constraints in the form of linear inequalities, i.e. positively, bounded etc. to the formulation. The resulting system of linear equalities and inequalities is satisfied by a subset of the solutions to the previous unconstrained problem. The solution is

selected from this subset by choosing the vector which minimizes the norm of the vector difference between the measured signal and the degraded estimate.

This selection of the optimal r-tuple solution vector is formed by taking all r-tuple solutions and eliminating those r-tuples that do not satisfy the a priori constraints, and from those remaining select the r-tuple which is closest in some sense to the measured signal. This method is demonstrated in three applications and yields super-resolving restoration even in the presence of significant noise.

Chapter 3

SUPERRESOLVING IMAGE RESTORATION

3.0 Introduction

The problem of restoring a linearly degraded image has been the subject of much investigation for some time [19]. The mathematical formulation of the image restoration problem is common to many problems in other fields. Some of these applications appear in such diverse fields as: Atmospheric Physics [16], Geophysics [14], Numerical Analysis [20], Radio Astronomy [17,18] and Spectroscopy [15]. In general, the inversion of a linear degradation can be accomplished in numerous ways [19]. When measurement errors (noise) are negligible and the degradation process is well behaved, direct inversion of the degradation process can be obtained. In the case where the noise cannot be neglected, methods such as Weiner filtering [23] are appropriate. Many image restoration problems are ill-conditioned. That is, the measurement error is greatly amplified in the restoration process such that the error dominates the estimate.

For the case of smooth images, stable methods of restoration have been described [20,22, 31,37]. These methods generally append smoothness constraints to the image restoration problem formulation. Methods of image restoration

which impose positivity constraints for stability, have also been described [26-29]. These methods show a preference for impulsive type images [19]. In this chapter, a new method of restoration is presented which employs pre-filtering of the measured image followed by minimization of a norm of the error subject to various linear constraints. The error is the vector difference between the degraded estimate and the measured signal. Three different norms were investigated; ℓ_1, ℓ_2 and ℓ_∞. The ℓ_1 norm of the error is the sum of the absolute values of the error. The ℓ_2 norm of the error is the sum of the squares of the error values, and the ℓ_∞ norm of the error is the maximum value of the error. The ℓ_1 norm was found to give the best performance in terms of resolution. The new method, which provides restorations of images from their diffraction limited images, is demonstrated by computer simulations.

3.1 The Diffraction Limited Image

The specific example considered will be that of restoring a diffraction limited image of finite extent. All physical imaging systems have resolution limitations imposed by the diffraction effects of the neccessarily finite aperture of the system. This effect is characterized by an ideal low pass filter (ILPF) in the spatial frequency domain. That is, the imaging system passes Fourier components of the image with spatial frequencies less than some cut-off spatial frequency f_c and totally eliminates frequency

components above f_c. It has been shown [1,2,30] that for images of finite extent the spectral components of the signal which have been removed can be deduced by analytic continuation of the passband spectrum. This extrapolation in the spatial frequency domain of the image represents an increase in the resolution of the image in the spatial domain. An image restoration process which provides this increase in resolution is called a superresolving image restoration (SIR) process. Conventional methods of image restoration are not superresolving. Methods which provide this superresolving capability are of much recent interest [19].

The SIR problem requires the solution of a Fredholm equation of the first kind (FEFK). The integral equation corresponding to the coherent one-dimensional case is

$$g(x) = \int_{-b}^{b} \frac{\sin f_c \pi (x-y)}{\pi (x-y)} f(y)\, dy \qquad (3.1\text{-}1)$$

where g(x) is the diffraction limited (DL) image, f(y) is the original image of length 2b and f_c is the cut-off frequency of the transfer function. The kernel of the integral corresponds to the coherent impulse response function. If non-coherent optics were to be considered, g and f could represent intensities. The kernel for the noncoherent case becomes the square of the coherent impulse

response. This represents a triangle transfer function. This transfer function has twice the bandwidth of the coherent transfer function. Thus the mathematical formulation of a coherent DL imaging system is more difficult to restore than a noncoherent system. The coherent case thus provides a good benchmark, since improvement of the resolution of an image can only be obtained by an increase in the spectral extent.

The numerical solution of Eq. (3.1-1) requires that this equation be discretized. This can be accomplished using numerical quadrature methods. The result is a system of linear equations which may be written in matrix form

$$g = \underline{H}f + n \qquad (3.1\text{-}2)$$

where g and f are the sampled DL and original images respectively, n is the sampled noise vector and $\underline{H}$ is the matrix representation of the integral operator using a quadrature rule. Without loss of generality, we shall take H to be a square N x N matrix. Thus, g,f and n are all N dimensional vectors. The system of equations (3.1-2) is underdetermined since there are 2N elements in the f and n vectors and only N equations. The difficulty in neglecting the noise n in solving (3.1-2) is due to the nearly linear dependence between adjacent rows of H. Thus the samples of g must vary very slowly. The noise adds a high frequency variation on

g which makes g inconsistent with the DL image vectors possible without noise. A method of stabilizing the problem is then to smooth the elements of the vector g. Ideally this smoothing can be accomplished by passing the image g through an ILPF. This would filter out the components due only to noise. This preprocessing would be straight forward if the DL image is provided in its entirety. However, the original image must be of finite duration in order for a solution to exist [33,34]. Thus the DL image must be infinite in extent. Therefore some finite interval of the DL image must be selected. This choice is arbitrary and for convenience we shall choose this interval to be equal to the length of the original image f, that is, 2b.

3.2 Presmoothing the Image for Reduction of Noise Effects

The method of smoothing the measured image can be seen by examining the singular value decomposition (SVD) of the degradation matrix $\underline{H}$. From Eq. (3.1-2) without noise, we note

$$g = \underline{H}f = \underline{U}\,\underline{\Lambda}^{\frac{1}{2}}\,\underline{V}^{T}\,f \qquad (3.2\text{-}1)$$

where $\underline{U}$ and $\underline{V}^{T}$ are orthogonal matrices and $\underline{\Lambda}$ is a diagonal matrix comprised of the eigenvalues of $\underline{H}\underline{H}^{T}$. The standard form of the SVD is used, where the eigenvalues are in decreasing order, from left to right in $\underline{\Lambda}$. These eigenvalues fall abruptly to practically zero, indicating the ill-conditioned nature of $\underline{H}$. This SVD decomposition is commonly

interpreted as a decomposition of the image into eigenimages [37]. The higher order eigenvalues correspond to the higher order eigenimages. The amount of zero crossing is proportional to the order. Thus the high order components correspond to the high frequency content of the image. We may rewrite (3.1-2) in a transformed coordinate system

$$G = \underline{\Lambda}^{\frac{1}{2}} F \tag{3.2-2}$$

where

$$G = U^{-1} g$$

$$F = V^{T} f$$

The interpretation of G and F is similar to that of a Discrete Fourier Transform (DFT). It is seen that the high order components (high frequency components) are greatly attenuated. This is to be expected since an ILPF in the DFT domain is consistent with low pass filtering in the diagonized coordinate system. The advantage of using this coordinate system (similar to the discrete prolate spheroidal sequences (DPSS) [35] is found in that all of the eigenvalues remain nonzero. Thus an inverse of H exists and is given by

$$f = \underline{V}\ \underline{\Lambda}^{-\frac{1}{2}}\ \underline{U}^{T}\ g \tag{3.2-3}$$

or in transform coordinates

$$F = \underline{\Lambda}^{-\frac{1}{2}}\ \underline{G} \tag{3.2-4}$$

where $\underline{\Delta}^{-\frac{1}{2}}$ indicates a diagonal matrix where the elements are the reciprocals of the elements of $\underline{\Delta}^{\frac{1}{2}}$.

Although the high order SVD components of the image are greatly attenuated, it is assumed the error statistics are of an independent gaussian process. The error possesses the same statistics in the orthogonal transformed domain. Thus the high order SVD components of the measured image are primarily due to the error. Hence we shall eliminate the high order components in the measured image before the inversion process. If constraints are not imposed on the inversion process, the unconstrained least squares estimate would result. This method has been previously implemented [31,37] to provide stable restoration of ill-posed problems. This method is not capable of providing superresolving restorations, since the high frequency components of the solution are discarded yielding an overly-smooth estimate. In order to reduce the effects of noise we first eliminate the higher order singular value components of the image. At the same time, a mechanism for extrapolation of the high order components must be provided. The latter is accomplished using linear programming techniques.

The smoothing is accomplished by preprocessing the measured image via the singular value transform (SVF) relationship

$$\tilde{g} = U\tilde{G} \qquad (3.2\text{-}5)$$

where $\tilde{G}$ is G modified by replacing all elements of index g greater than i, with zero. The index i corresponds to the i^{th} eigenvalue of the matrix $\underline{H}$; it is less than some choosen small number. If $\tilde{g}$ thus obtained is premultiplied by the inverse of H, the result would be the unconstrained least squares estimate. Thus, the direct inverse of the smoothed image cannot reconstruct the high frequency components of the image. The new method does extrapolate the high frequency content. This method imposes the constraints that the image estimate be bounded. Any linear inequality constraints can be appended to the formulation. Thus we have

$$\begin{aligned} \underset{\sim}{f} &\geq 0 \\ \underset{\sim}{f} &\leq \underset{\sim}{f}_{max} \end{aligned} \qquad (3.2\text{-}6)$$

where $\underset{\sim}{f}_{max}$ is the vector corresponding to the a priori upper bounds on f. Any vector f satisfying (3.1-2) subject to (3.2-6) must be consistent and stable. But, due to the underdetermined nature of (3.1-2) there are many such N dimensional solution vectors of (3.1-2). We desire to choose the solution closest to the corresponding measured DL image. The method which we will use to perform this selection of the closest vector is to choose a norm of the residual between the measured image and degraded estimate and then minimize this norm.

This minimization of the norm is accomplished by a method

of optimization known as linear programming [32].

3.3 Linear Programming

Linear programming will be used to solve Eq. (3.1-2) subject to (3.2-6). The general linear programming problem can be formulated as follows:

$$\text{a) Minimize } z = c^T x \tag{3.3-1}$$

subject to

$$\text{b) } P_1: \quad A_1 x \geq B_1 \tag{3.3-2}$$

$$\text{c) } P_2: \quad A_2 x = B_2 \tag{3.3-3}$$

$$\text{d) } P_3: \quad x \geq 0 \tag{3.3-4}$$

where P_1 is the number of inequality constraints, P_2 is the number of equality constraints, and P_3 is the total number of positive variables. The vector c is referred to as the cost or objective vector, the vectors B_1 and B_2 as the constraint vectors, the vector x as the program vector, and $\underline{A}_1$ and $\underline{A}_2$ are the coefficient matrices. The objective function z is the inner product of the objective and program vectors. The most frequently used algorithm to solve linear programming problems is called the simplex algorithm. This algorithm produces one of three mutually exclusive results: first an indication that the problem is infeasible. The problem is feasible if all of the constraints can be simultaneously satisfied for some choice of variables. The problem is infeasible otherwise. Second,

an indication that the problem is feasible but the optimal solution is unbounded; or, third, an optimal solution (if one exists). In the process of arriving at the result, additional variables, called slack variables, are added to the problem formulation. These variables convert the inequalities into equalities thereby increasing the total number of variables to $P_1 + P_3$. If the problem has a finite optimal solution, then the total number of nonzero variables in the optimal program vector is only $P_1 + P_2$.

Linear programming techniques will be applied in three different formulations. That is, the minimization of the ℓ_1, ℓ_2 and ℓ_∞ norm of the residual error. In the next section we discuss the ℓ_1 formulation.

3.4 The ℓ_1 Formulation of the Image Restoration Problem

The formulation of the image restoration as a linear ℓ_1 programming problem can now be addressed. We define two N dimensional vectors n^+ and n^- such that they contain the negative and positive components of n respectively. For any given row, one of the two vectors n^+ and n^- has one zero element and the other has a positive element. Thus we may write:

$$g = \underline{H}f + n^+ - n^- \qquad (3.4\text{-}1)$$

such that n^+, n^- and f are all positive N dimension vectors. If we consider the positive sum for row i,

$$n^{+}_{i} + n^{-}_{i} = |g_i - h_i f| \qquad (3.4\text{-}2)$$

where h_i is the i^{th} row of $\underline{H}$. This is seen to be the absolute value of the residual of the difference between g and hf. Taking the sum over all N rows yields the ℓ_1 norm of the residual error. This will be the cost function that will be minimized subject to the constraints of Eq. (3.2-6). The linear programming formulation of minimal problem is:

$$\text{Minimize:} \quad n_1^{+}+n_1^{-} + n_2^{+}+n_2^{-} + \ldots + n_n^{+}+n_n^{-} \qquad (3.4\text{-}3)$$

$$\text{Subject to:} \quad g = \underline{H}f + n^{+}-n^{-}$$

$$f \leq f_{max}$$

$$f \geq 0$$

The solution program vector will contain only $P_1 + P_2$ non-zero elements for the P unknowns. Assuming that all the slack variables of the solution program vector are nonzero, this leaves only P_2 degrees of freedom for the $2P_1$ unknowns f and n. This results from the underdetermined nature of (3.1-2). Thus, in general the solution vector will contain zeros for half of the elements of f and n. This effect is independent of the norm chosen. It is physically very unsatisfying for images in general, but for input images which have a large number of zero elements this model is appropriate. This type of image is called an impulsive image. Other image restoration methods [19] also favor impulsive type images. If in the input image an element

is binary, that is the element of f is either zero or f_{max}, then the inequality (3.2-6) will be satisfied as an equality. This forces a slack variable out of the solution vector. Thus another nonzero element will enter the f or n vectors. If the entire original image f is binary, N inequalities will be satisfied as equalities. This leaves the N degrees of freedom required so as to allow f and n to contain no zero elements. Thus binary images can also be restored faithfully by this technique.

An alternate interpretation of minimizing the residual can be obtained by examining the process in terms of the solution vector. Minimization of the ℓ_1 norm is bounded by zero. If this bound is obtained, then the residual error is zero and the solution vector acquires all N degrees of freedom necessary. This case pertains to a direct inversion of the degradation matrix $\underline{H}$. In general, this inversion is not possible since the measured image g is usually not consistent with all of the constraints (3.2-6). Thus n will contain non-zero elements and f must contain corresponding zero elements as well.

3.5 Other Norms and Constants

Following a similar procedure, the minimal ℓ_∞ norm estimate can be obtained by linear programming. The ℓ_∞ norm is the

$$\sup_{0<i<N} \{n_i\}$$

where the sup represents the maximum element of the set $\{n_i\}$. This norm can be used as an objective function in the formulation given by (3.3-1). In order to formulate the restoration problem in a linear programming format for the minimization of the ℓ_1 norm, we define E as a scalar variable denoting the largest positive deviation of the degraded estimate of the measured image. We then write the minimal ℓ_∞ formulation as

$$\text{Minimize } E \tag{3.5-1}$$

$$\text{Subject to: } g \geq Hf + e_N E$$

$$g \leq Hf - e_N E$$

The equations can be solved by the method of linear programming. Optionally, the constraining (3.2-6) can be appended to this formulation. This type of formulation is frequently called a minimax solution. It is identical in computational complexity to the minimal ℓ_1 norm technique discussed previously.

The image restoration problem can also be formulated as a minimal ℓ_2 problem and solved using the methods of quadratic programming [33,34]. The ℓ_2 norm is the sum of squares of the elements, i.e. $n_1^2 + n_2^2 + \ldots n_N^2$. Quadratic programming computer codes are modified simplex linear algorithms. The modification involves a significant increase in the effective dimension of H and thus also an increase in computational complexity. Computer programs

are available [35]. The general least squares problem with constraints is discussed in [36], which also provides a computer code for the ℓ_2 algorithm. However, the minimization of the ℓ_2 norm of the residue with constraints did not provide superresolving restorations in any of the simulations we have performed. This method also displayed numerical instabilities which seemed to limit its usefulness.

A more general class of images can be restored if further smoothness constraints are appended to the formulation (3.4-3). If the measured and DL images are highly oversampled and the derivatives of the original image are known to be bounded, we can impose the following derivative constraints

$$f_{i+1} - f_i \leq \delta f_i \tag{3.5-2}$$

where f_{i+1} and f_i are adjacent image elements of the input and δf_i are predetermined constants. For high sampling densities and small δf_{max} inequality (3.5-2) can be satisfied as an equality of the image restoration problem, thus increasing the degrees of freedom of f and n.

3.6 Computer Simulation and Results

The methods were simulated using the Simplex Linear Programming subroutines contained in the International Mathematical and Statistical Library (IMSL) Fortran callable

subroutine package. CUNY's IBM 370 computer system was used. The benchmark example is the diffraction limitation of a coherent one dimensional system. The first figure, Fig. 3.6-1, illustrates reconstruction of two impulses spaced 1/8 the Rayleigh distance with no added measurement noise. The image is composed of 32 samples, the entire duration of the image is two normalized units. The spatial frequency cut-off is one half reciprocal units. The two equal strength impulses are separated by one sample. Thus the separation is 1/8 the Rayleigh distance. The direct inverse solution (dotted line) demonstrates very unstable behavior even though the only noise is due to the finite precision of the computer used and arithmetic errors which are propagated numerically through the inversion process. The exact solution is the two impulses (solid line). The unconstrained least squares solution (dotted line) provides a very stable but overly smooth estimate for the two impulses (solid line). The unconstrained ℓ_2 solution consists of the first r' low order eigenimages of solution, where r' is the pseudo-rank of the $\underline{H}$ matrix; that is, r' is chosen such that the corresponding eigenvalue $\lambda_{r'}$ is sufficiently large so as to avoid instabilities when $\underline{H}$ inverted. Eigenvectors of higher order are discarded. In order to determine the pseudo-rank of a matrix, a measure of the instability of the $\underline{H}$ matrix is used. A figure of merit, also called the condition number of the

$\underline{H}$ matrix is given by

$$c(H) = \frac{\lambda_{max}}{\lambda_{min}} = \frac{\lambda_1}{\lambda_N} \qquad (3.6\text{-}1)$$

A condition number of 10^{12} is usually considered moderately [37] unstable while a condition number of 10^{16} represents a very severe ill-conditioned matrix.

The condition number for the unfiltered problem of Fig. 3.6-1 is 10^{18}. This number was reduced by SVD filtering to a condition number of 10^{+6} in Fig. 3.6-2. If less terms are retained in the estimate, a still smoother estimate results. This is indicated in Fig. 3.6-3 where the condition number has been reduced to 10^{4}. Thus the price paid for stabilizing the inversion process (i.e., reducing the effective condition number) is an overly smooth estimate.

Fig. 3.6-4 illustrates a perfect restoration of two impulses separated by 1/8 the Rayleigh distance by the minimal $\theta_1 \rightarrow \ell_1$ norm method. The dotted curve is the diffraction limited image. It is approximately the main lobe of a sinc function center at the center of the scale. The method completely restored the two impulses. The estimate is the chain dot curve completely coincident with the exact curve (solid line).

The ℓ_∞ method did not provide the high resolution performance

obtained with the ℓ_1 method for two point restoration. Fig. 3.6-5 gives an indication of this difference. The ℓ_∞ estimate (chain-dot) curve is shifted, the second impulse is down by 80% and the inter-impulse trough is down to 50% of the actual peak amplitude. There is also a small artifact which appears just to the left of the first impulse. Although this estimate might actually be acceptable for many applications, it is clear that the ℓ_1 estimate is preferable.

The method of restoration is robust to noise yielding estimates with signal to noise ratios (SNR) of comparable magnitudes to the SNR of the measured signal. Here the SNR of the estimate is defined as

$$\text{SNR} = 10 \log \left\{ \frac{\sum_{i=1}^{N} (f_i \text{ estimate} - f_i \text{ original})^2}{\sum_{i=1}^{N} (f_i \text{ original})^2} \right\} \qquad (3.6\text{-}2)$$

and the SNR of the measurement is defined as

$$\text{SNR} = 10 \log \left\{ \frac{\frac{1}{N} \sum_{i=1}^{N} (g_i \text{ measured})^2}{\sigma^2 \text{ noise}} \right\} \qquad (3.6\text{-}3)$$

The particular SNR use will be clear from the context.

Fig. 3.6-6 illustrated the ℓ_1 estimate (chain-dot curve) with no SVD prefiltering of two impulses separated by ½ the Rayleigh distance. White Gaussian noise with zero mean and a σ =.3 has been added to the measured image. The corresponding SNR of the measured image is 21 db. The restored image had an SNR of 14 db. Thus, in order to obtain an increase in resolution of a factor of 2, it cost 7 db in SNR. The diffraction limited image dotted line has a jagged appearance due to the added noise. Fig. 3.6-7 illustrates the effect of the SVD prefiltering on the method. The example is identical to that in Fig. 3.6-6, except prefiltering of the measured image has been performed. The diffraction limited image (dotted line) appears much smoother than in Fig. 3.6-6. The improvement in the estimate is obvious. The estimate (chain-dot curve) lies almost completely coincident to the exact image (solid-line) curve. The peak values of the estimate are 10% lower than the exact solution and the inter-impulse trough is ~10% higher than the exact solution. The importance of SVD prefiltering can also be observed in the ℓ_1 case. Fig. 3.6-8 illustrates the ℓ_∞ estimate of two impulses separated by ½ the Rayleigh distance without SVD preprocessing. White noise was added to the measured image with zero mean and σ = .1. The corresponding SNR of the measured image is 26 db. The restored image (chain-dot) is seen to be very poor. The impulses are shifted and attenuated and there

are small artifacts by the origin and to the far right. Note the jagged appearance of the measured diffraction limited image (dotted curve) due to the addition of noise. Fig. 3.6-9 illustrates the SVD preprocessing on the same measured image of Fig. 3.6-8. Due to the SVD prefiltering, a smoothed diffraction limited image (dotted line) results. The effects are dramatic, almost perfect restoration is obtained. The estimate (chain-dot) and exact solution (solid line) are coincident. Note the small artifacts to the far right and left have not been eliminated since they possess a low frequency spectrum.

In some applications it is important to ascertain if a weak impulse is being dominated by a strong impulse, i.e. the double star problem. Fig. 3.6-10 illustrates the ability of the ℓ_1 method to distinguish between two unequal impulses of strength 10 and 10^5 separated by ¼ the Rayleigh distance. Note that Figs. 3.6-10 to 3.6-14 are drawn on a logarithmic scale.

The diffration limited image (dotted curve) appears as though it were a sinc function, i.e. impulse response due to only the stronger impulses. The ℓ_1 estimate (chain dot) finds the heights of the impulses exactly and is only ~50% off on the interimpulse trough, however centered on the stronger impulse. The restored image (chain dot) restores the magnitudes of the two impulses exactly, with the interimpulse gap down about 50% from the small pulse. The SNR

of the measured signal is 31 db and that of the restored is 25 db. The SNR is not a good indication of the resolving power here since the stronger image dominates. Fig. 3.6-12 illustrates the effects caused when the noise possesses a variance greater than one tenth of the amplitude of the smaller impulse. The unequal impulse problem can be solved by this method if the variance of the noise is much smaller than the value of the weaker impulse. Fig. 3.6-11 illustrates the acceptable performance of the method when the two impulses are spaced ½ the Rayleigh distance and the strengths of the impulses are 10 and 100. Since the variance of the noise is 1 there is no problem in the restoration. Note the diffraction DL image (dotted curve) is approximately a sinc function. Here again we have two impulses of strengths 10 and 100 separated by ½ the Rayleigh distance. Now the added noise has a variance of $\sigma = 6$ the DL image (dotted curve) appears no different than that of Fig. 3.6-11 due to the relative magnitude of the noise. Yet the reconstruction (chain dot) falls short of the exact solution (solid line).

This condition can be relaxed if a finer sampling grid is employed. Fig. 3.6-13 illustrates the acceptable restoration of two unequal impulses of strengths 10 and 10^9 where the variance $\sigma = 10$ and the sample spacing corresponds to ½ of the Rayleigh distance. The two impulses are again separated by ½ of the Rayleigh distance but now this

distance places two zero samples between the impulses. Thus the only error in the reconstructed image (chain dot) is a widening of the larger impulses relative to the exact solution (solid line). This is probably due to the effective broadening of the measured and filtered DL image (dotted line). Then we can remove the superresolving Rayleigh constraints of equal strength impulses. Since for the unequal amplitude impulses the DL image blurs long before the zero of one impulse response is coincident with the maximum of the other, the image can be restored even when significant noise is present. Fig. 3.6-14 illustrates this fact. Observe the DL image appearing as though created by only the larger impulse although the two impulses are separated by 4 Rayleigh distance. Here the two impulses are of strengths 10 and 10^5 and the variance of the noise $\sigma = 100$. The restored image (chain dot) is seen to be acceptable for most applications. Both impulses are resolved. The larger impulse experiences a small artifact to the right and the smaller impulse is shifted to the left by one sample and is attenuated.

The near linear dependence between adjacent rows was discussed in Chapter One. Here we illustrate the effect on the restored images. For the case of the $\underline{H}$ operator yielding 1/8 Rayleigh distance between adjacent points, the pseudo-rank is four. Thus we expect to find at most four input samples. Fig. 3.6-15 illustrates the fact that if

the spacing between impulses is not sufficient, then the restored image (chain dot) may not be an acceptable estimate of the exact solution (solid line). Fig. 3.6-16 indicates what happens if the impulses are maximally spaced. Here the expected four impulses can be restored (chain dot). Fig. 3.6-17 indicates that even if maximally spaced, five different impulses cannot be restored since the pseudo-rank is four.

Most images of interest will have more non-zero elements than the pseudo-rank of the degradation operator $\underline{H}$. Different types of smoothness constraints can be appended to the formulation, as in (3.5-1), to increase the pseudo-rank of the modified degradation matrix. Fig. 3.6-18 illustrates the effects of these smoothness constraints. Fig. 3.6-18 illustrates the restoration (chain dot) of the linear image (solid line) from the DL image (dotted curve). The jagged appearance of the restored image is due to the coarse sampling of this specific function.

The noncoherent diffraction limited restoration problem, as discussed in Section 3.1, has twice the bandwidth of the coherent case. The difference between the pseudo-rank and condition numbers of some frequently reported cases is shown in Fig. 3.6-19. As expected, the non-coherent case is better conditioned. This fact is brought out in Figs. 3.6-20 to 3.6-23. Fig. 3.8-20 demonstrates that perfect

restoration is obtained down to an impulse separation of 1/10 of the Rayleigh limit. This is a marked improvement of that achieved in the coherent case (Fig. 3.6-4), where we achieved perfect restoration at 1/8 the Rayleigh distance. The DL image (dotted line) appears similar to the coherent case of 1/8 Rayleigh separation. The estimate (chain dot) is obscured by the close fit with the exact solution (solid line). The effects of noise on the restoration process are illustrated by Figs. 3.8-21 to 3.6-23. Here the DL image is illustrated by the dotted curve. The exact solution of two equal strength impulses separated by ½ the Rayleigh distance is depicted by the solid line curve and the estimate is shown by a chain dot line. Each figure represents a 2 db increase in the SNR of the measured image and a corresponding increase in the restored image of 2 db. Fig. 3.6-21 illustrates a measured image of SNR of 20 db and a restoration of 5 db, in Fig. 3.6-24. The measured image has a SNR of 22 db and the restored image has a SNR of 7 db. In Fig. 3.6-25 the measured image has an SNR of 24 db and the restored image has and SNR of 9 db. These figures are typical of the results obtained over many simulations not illustrated here.

We have thus shown that the discussion of Chapter 1 regarding the effect of noise on DL image are well founded. The discrepancies in performance between the different chosen norms could be explained by the increase in

dimensionality of the problem and corresponding numerical error incurred in using the ℓ_∞ and ℓ_2 over the ℓ_1 norm. The ℓ_∞ requires a doubling of the number of equations while the ℓ_2 norm requires an even larger increase in the dimension of the problem. Therefore the ℓ_1 is superior. The benefits of SVD prefiltering have strongly been demonstrated. The resulting algorithm performs superresolving restoration even in the presence of significant error.

3.7 Summary and Conclusion

A new approach to image restoration has been introduced. The method presented shows a preference for impulsive and binary images. This is due to the underdetermined nature of the problem. Any optimal solution that is linearly constrained will have the same limitations. That is, the solution vector will consist of as many nonzero elements as there are equality constraints. By satisfying the inequalities as equalities the degrees of freedom are increased. Two straightforward methods of providing this condition is by limiting the possible images to be impulsive or binary. The method presented is optimal in the sense of the norm chosen. The formulation allows for the easy addition of further linear constraints. Smooth input images can be restored by imposing bounds on the first as well as higher order differences. The method is superresolving, that is, restoration of two point sources separated by less than the Rayleigh distance can be

restored. The effect of measurement errors is decreased by SVD preprocessing. This is a smooth process which greatly eliminates the effects of the measurement errors. The method has demonstrated very practical restorations increasing the resolution of the diffraction limited image by a factor of two with significant measurement error. Restorations yielding resolution increases of a factor of eight were demonstrated when no measurement error was introduced. Restoration of two impulses separated by ⅛ Rayleigh distance was achieved for both the coherent and the incoherent cases with SNR of 20 dB.

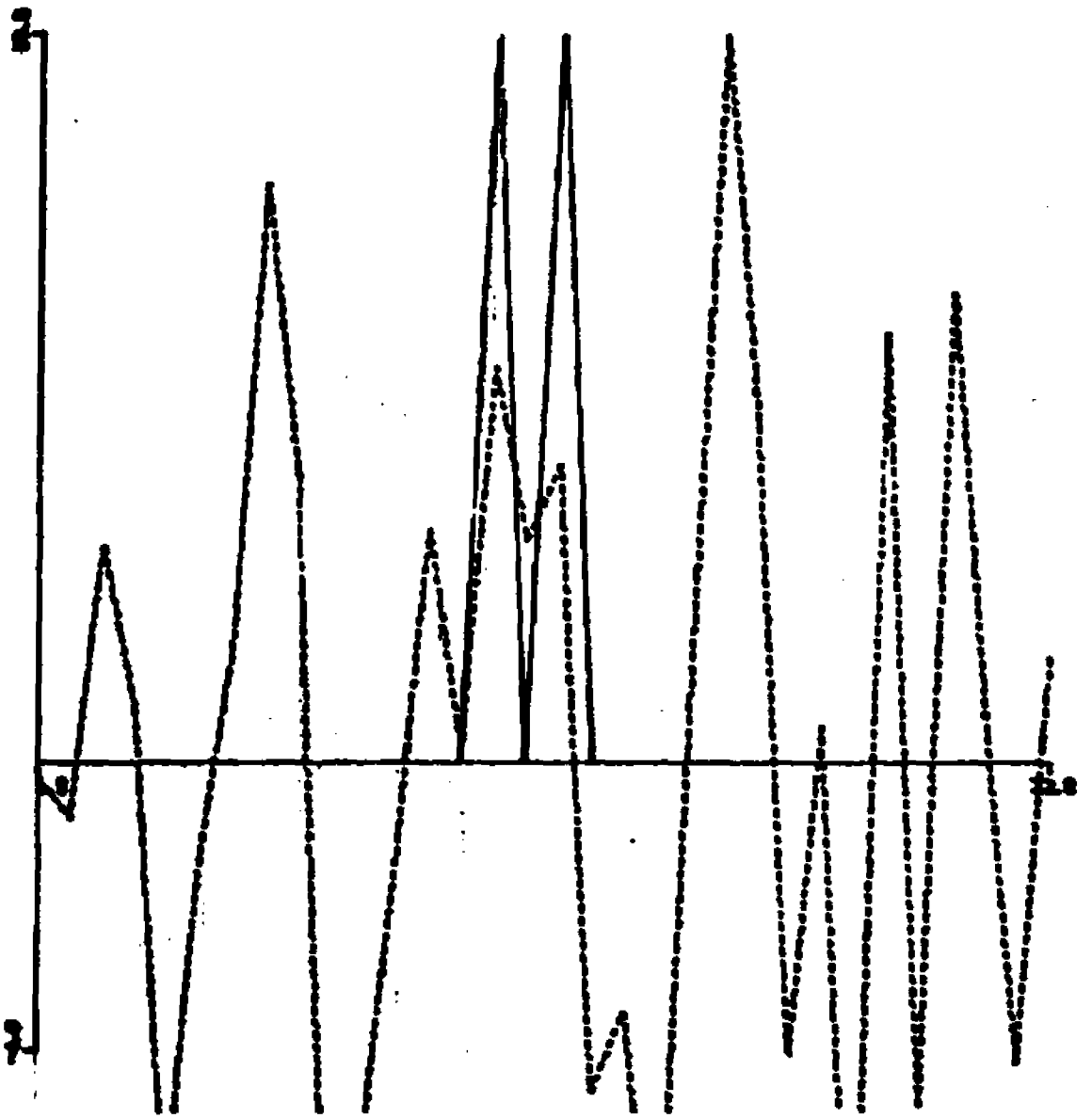

Fig. 3.6-1 Direct inverse solution for two impulses separated by 1/8 the Rayleigh distance

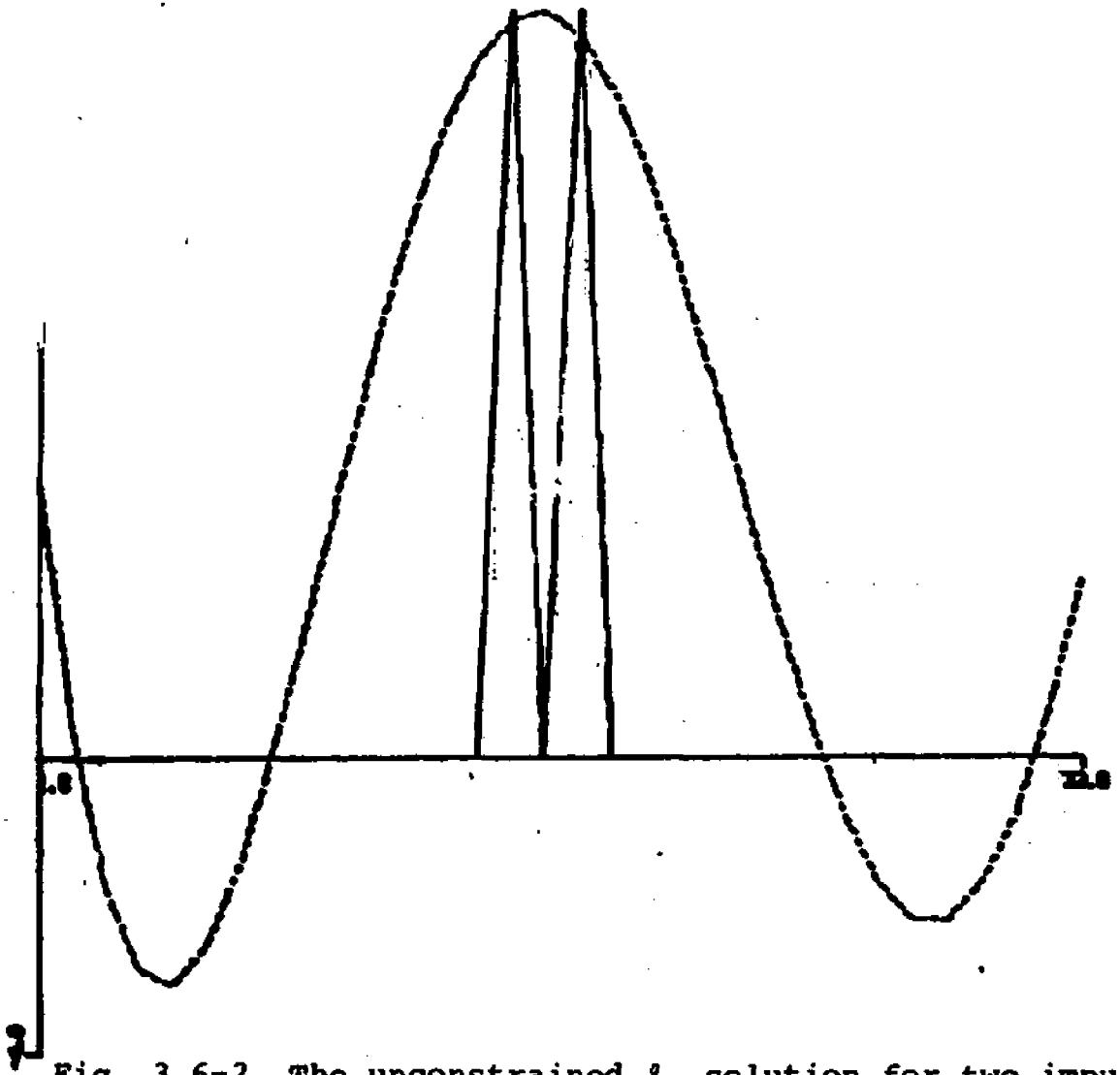

Fig. 3.6-2 The unconstrained ℓ_2 solution for two impulses separated by 1/8 of the Rayleigh distance. The condition number is 10^6

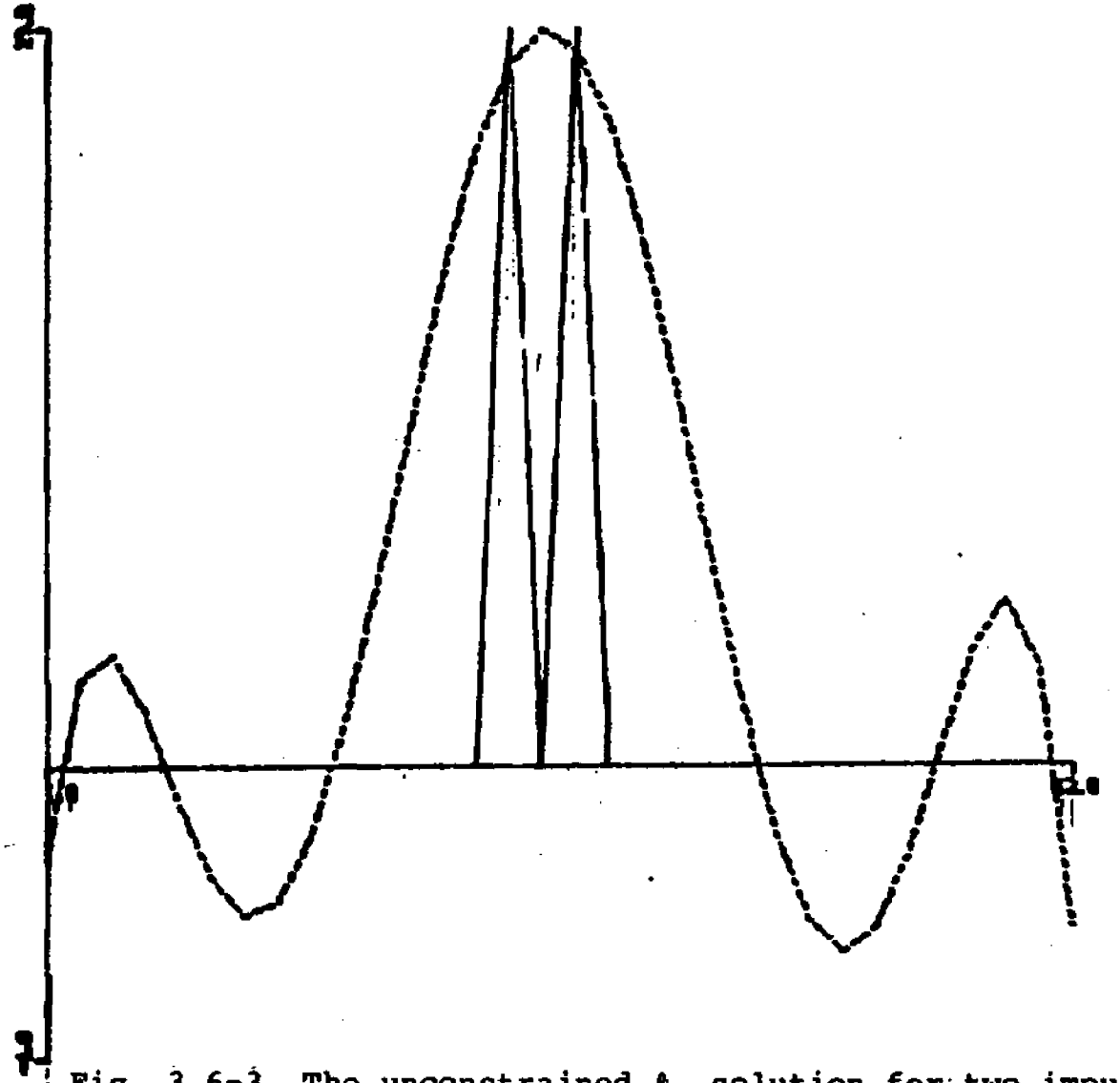

Fig. 3.6-3 The unconstrained ℓ_1 solution for two impulses separated by 1/8 of the Rayleigh distance, the condition number is 10^4

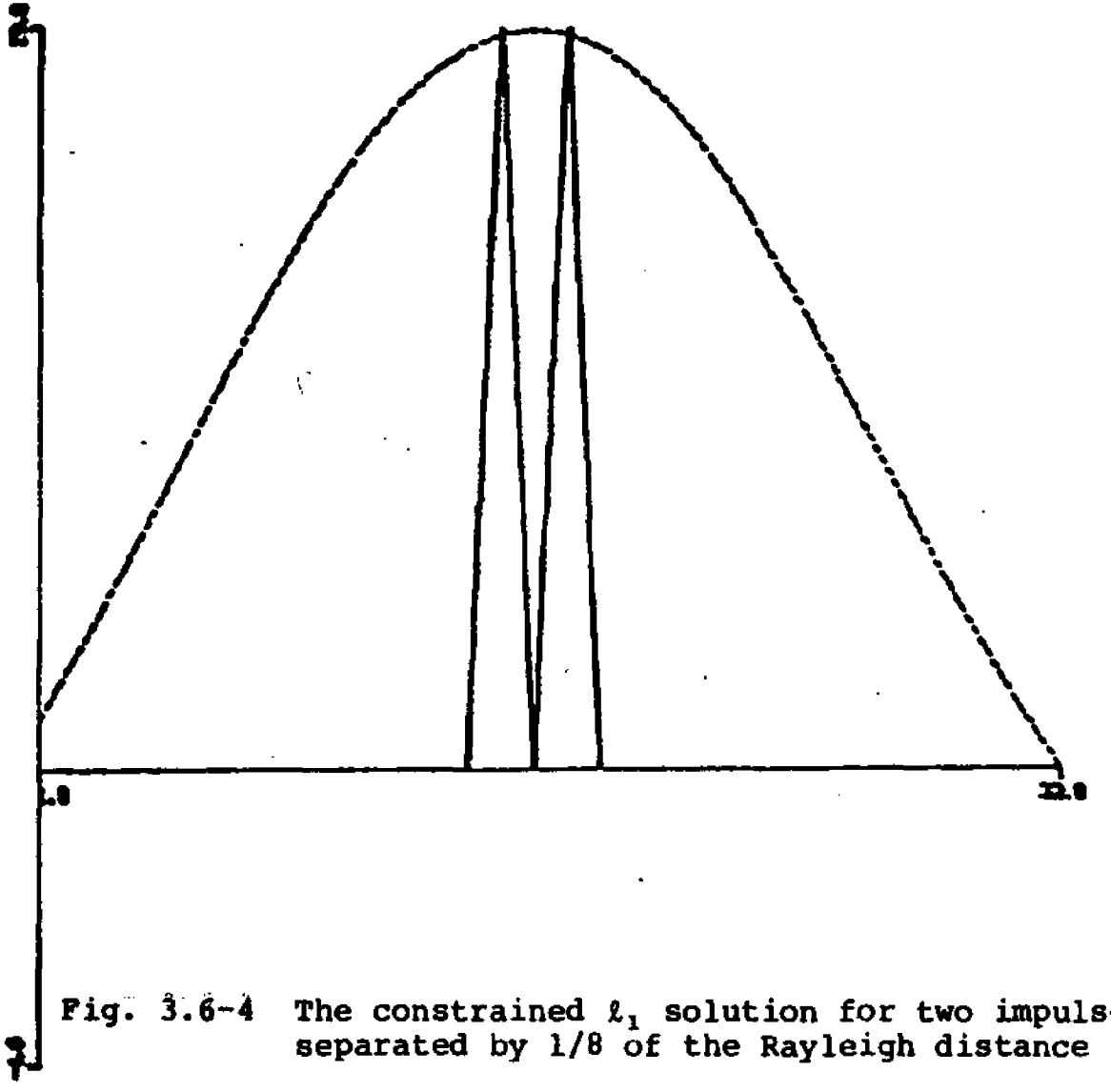

Fig. 3.6-4 The constrained ℓ_1 solution for two impulses separated by 1/8 of the Rayleigh distance

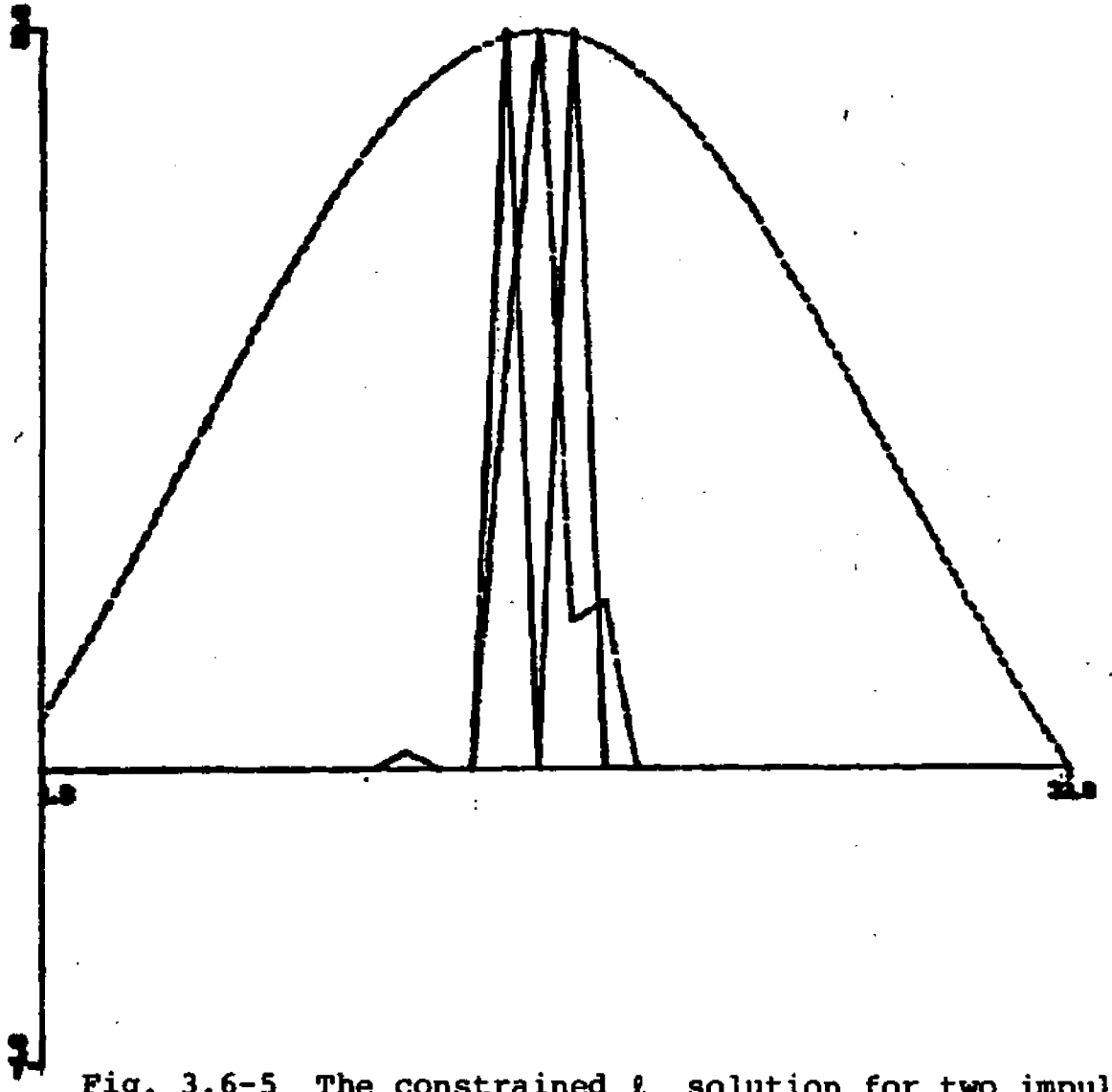

Fig. 3.6-5 The constrained ℓ_∞ solution for two impulses separated by 1/8 of the Rayleigh distance

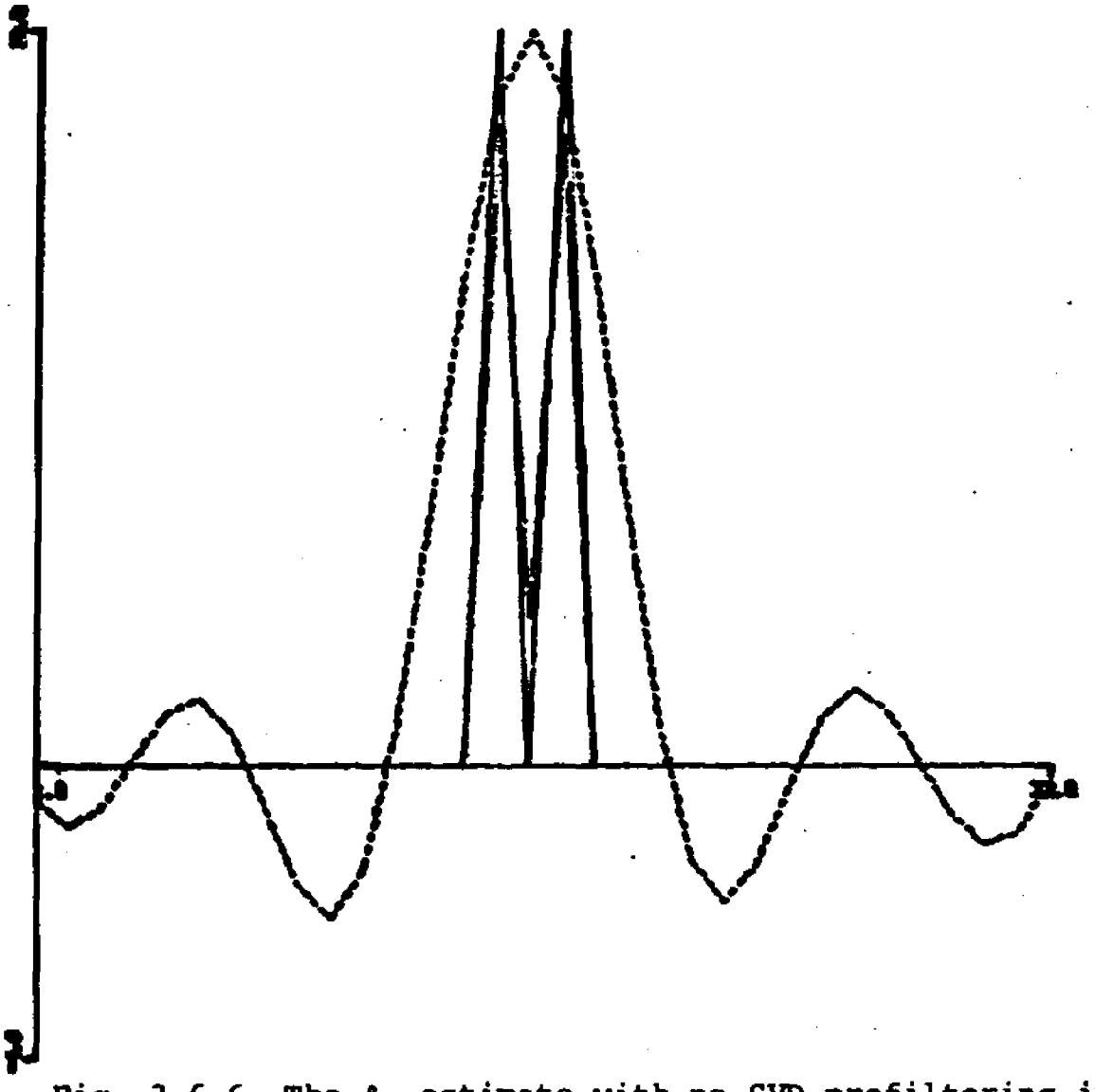

Fig. 3.6-6 The ℓ_i estimate with no SVD prefiltering impulses separated by ½ the Rayleigh distance with white noise added σ= .3

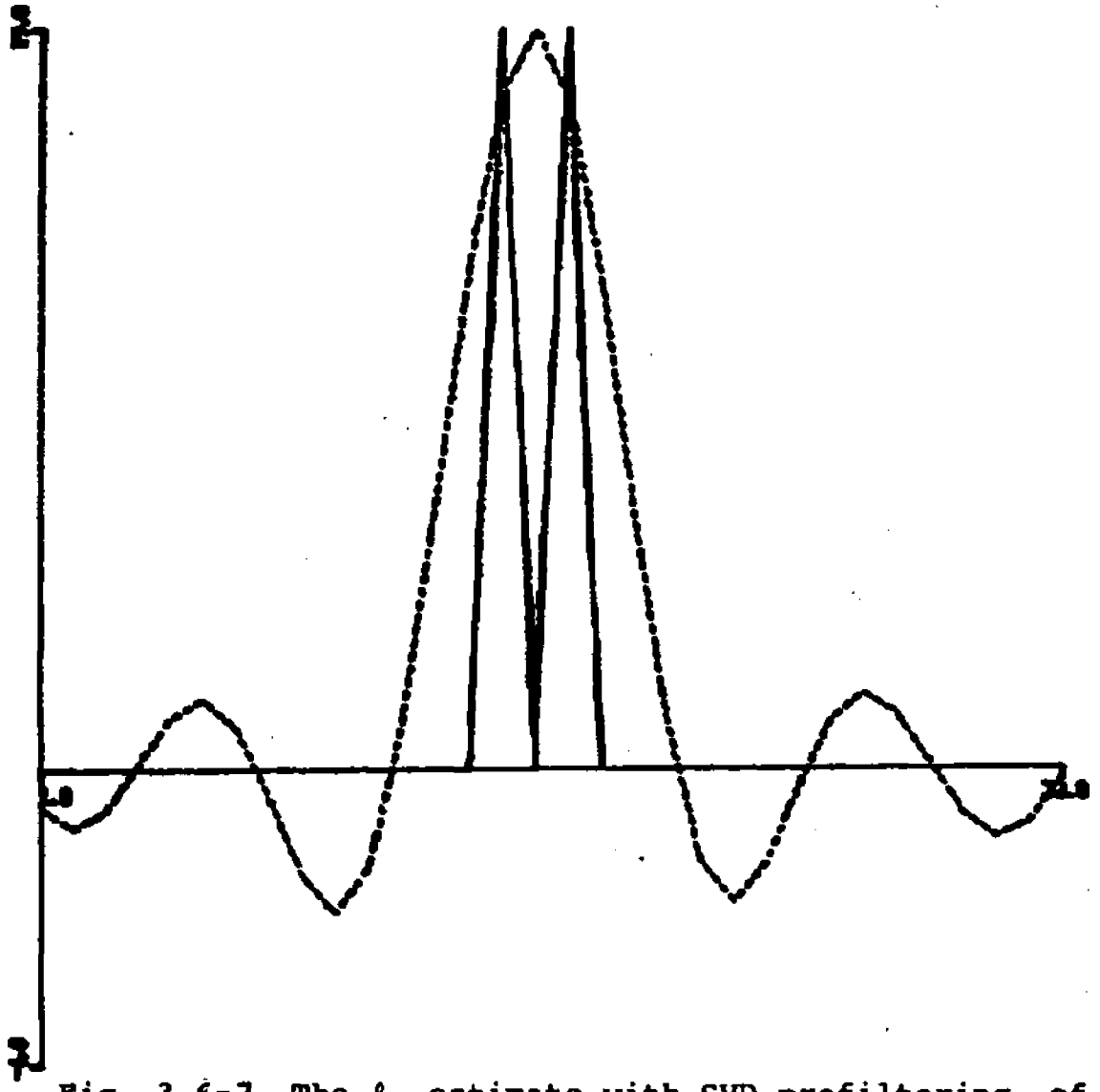

Fig. 3.6-7 The ℓ_1 estimate with SVD prefiltering, of two impulses separated by ½ the Rayleigh distance with white noise added σ=.3

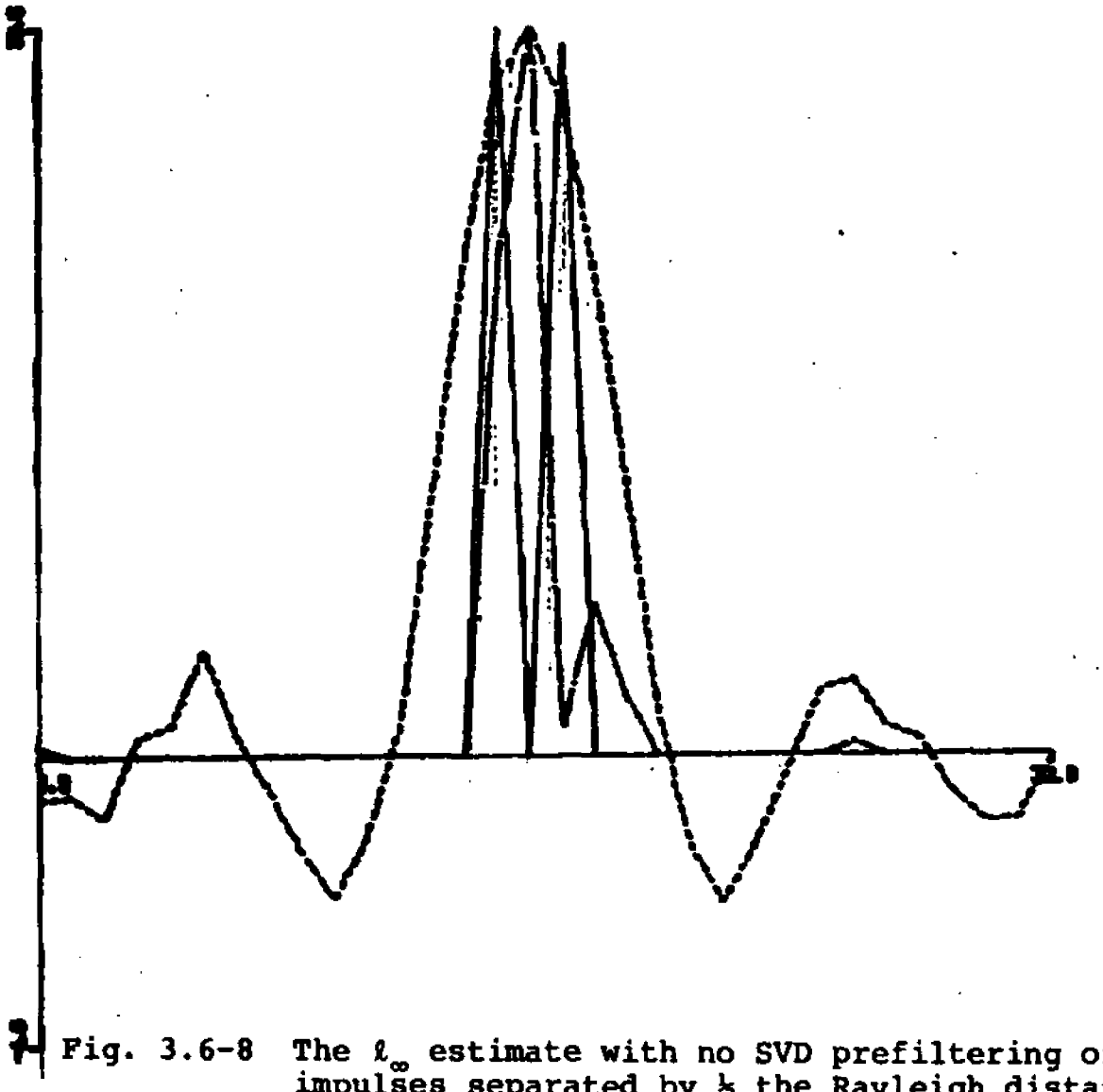

Fig. 3.6-8 The ℓ_∞ estimate with no SVD prefiltering of two impulses separated by ½ the Rayleigh distance with white noise added σ=.1

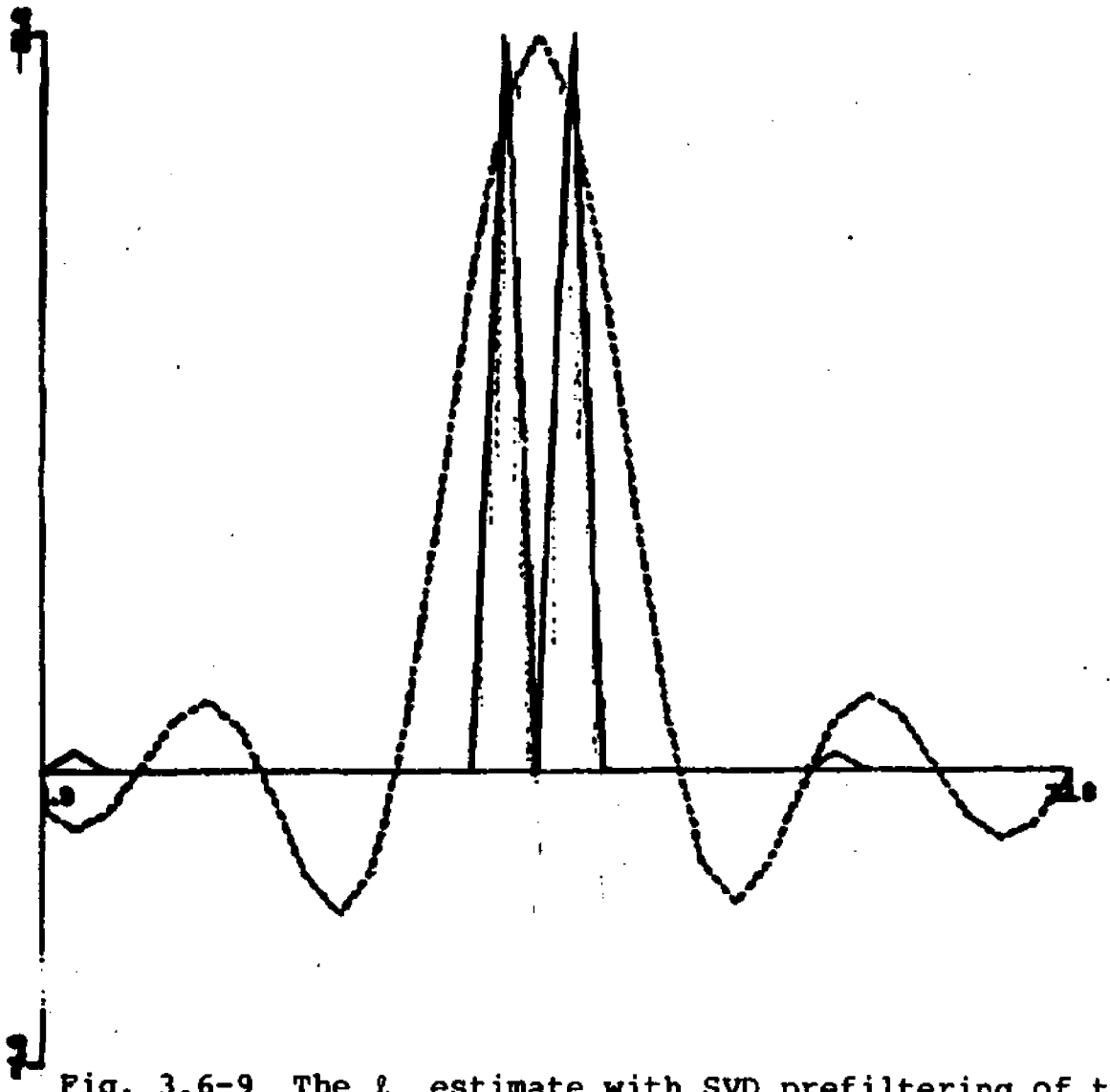

Fig. 3.6-9 The ℓ_∞ estimate with SVD prefiltering of two impulses separated by ½ the Rayleigh distance with white noise added σ=1.

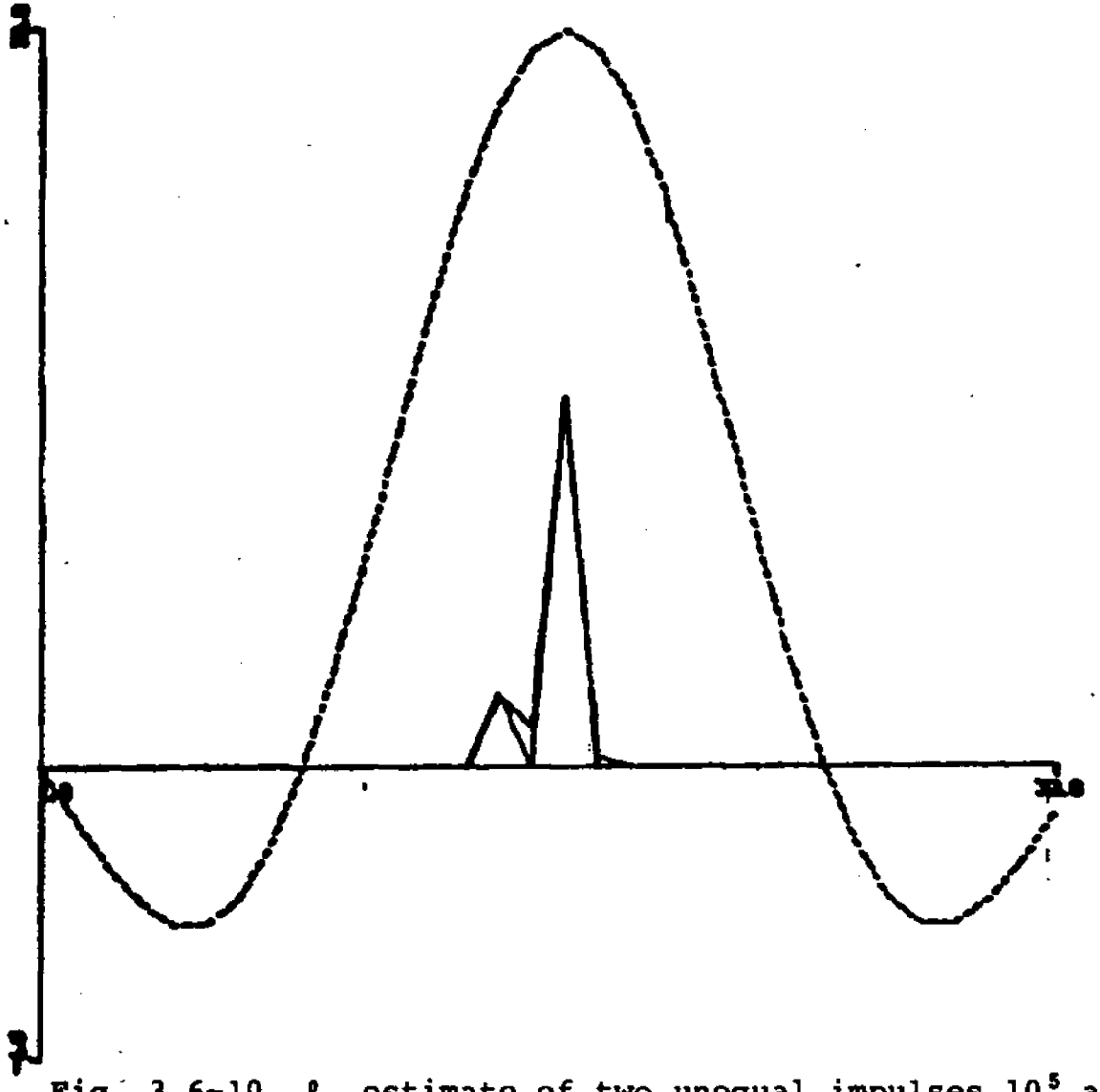

Fig. 3.6-10 ℓ_1 estimate of two unequal impulses 10^5 and 10 separated by ¼ the Rayleigh distance

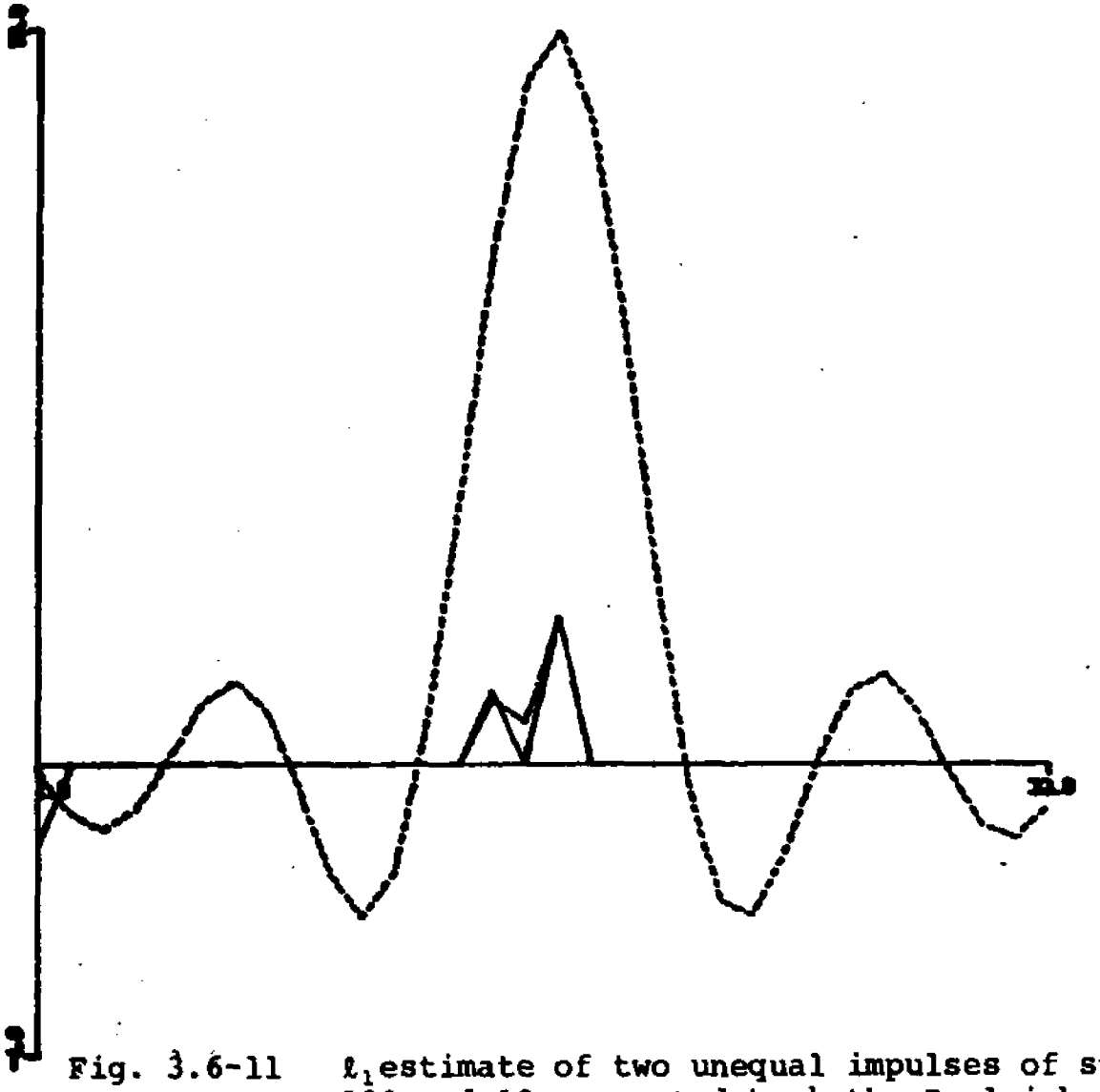

Fig. 3.6-11 ℓ_1 estimate of two unequal impulses of strengths 100 and 10 separated by ½ the Rayleigh distance with noise σ= 1.0

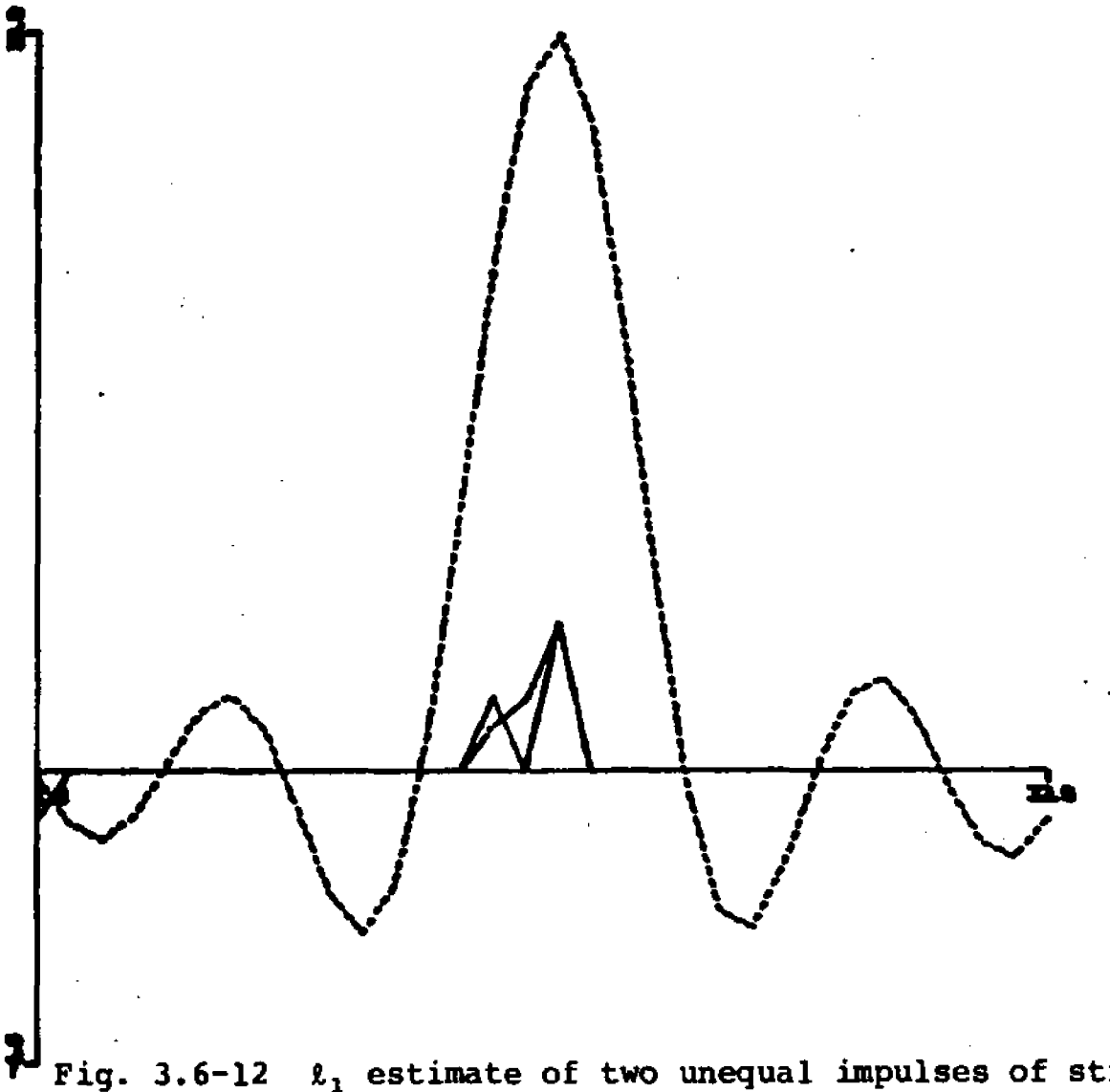

Fig. 3.6-12 ℓ_1 estimate of two unequal impulses of strengths 100 and 10 separated by ½ the Rayleigh distance with noise r=6.0

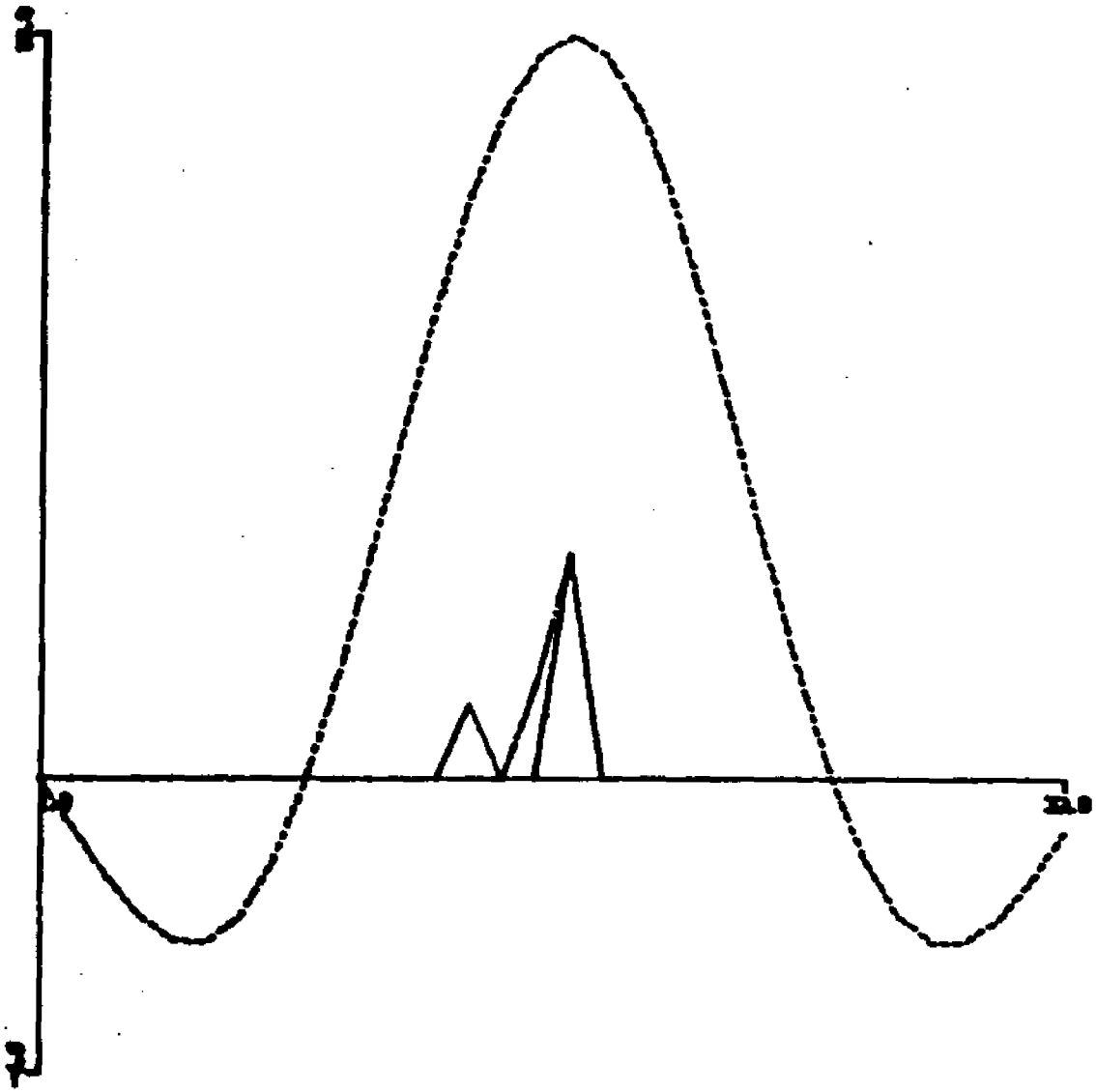

Fig. 3.6-13 ℓ_1 estimate of two unequal impulses of strengths 100 and 10^3 separated by ½ the Rayleigh distance with finer sampling and noise σ=10.0

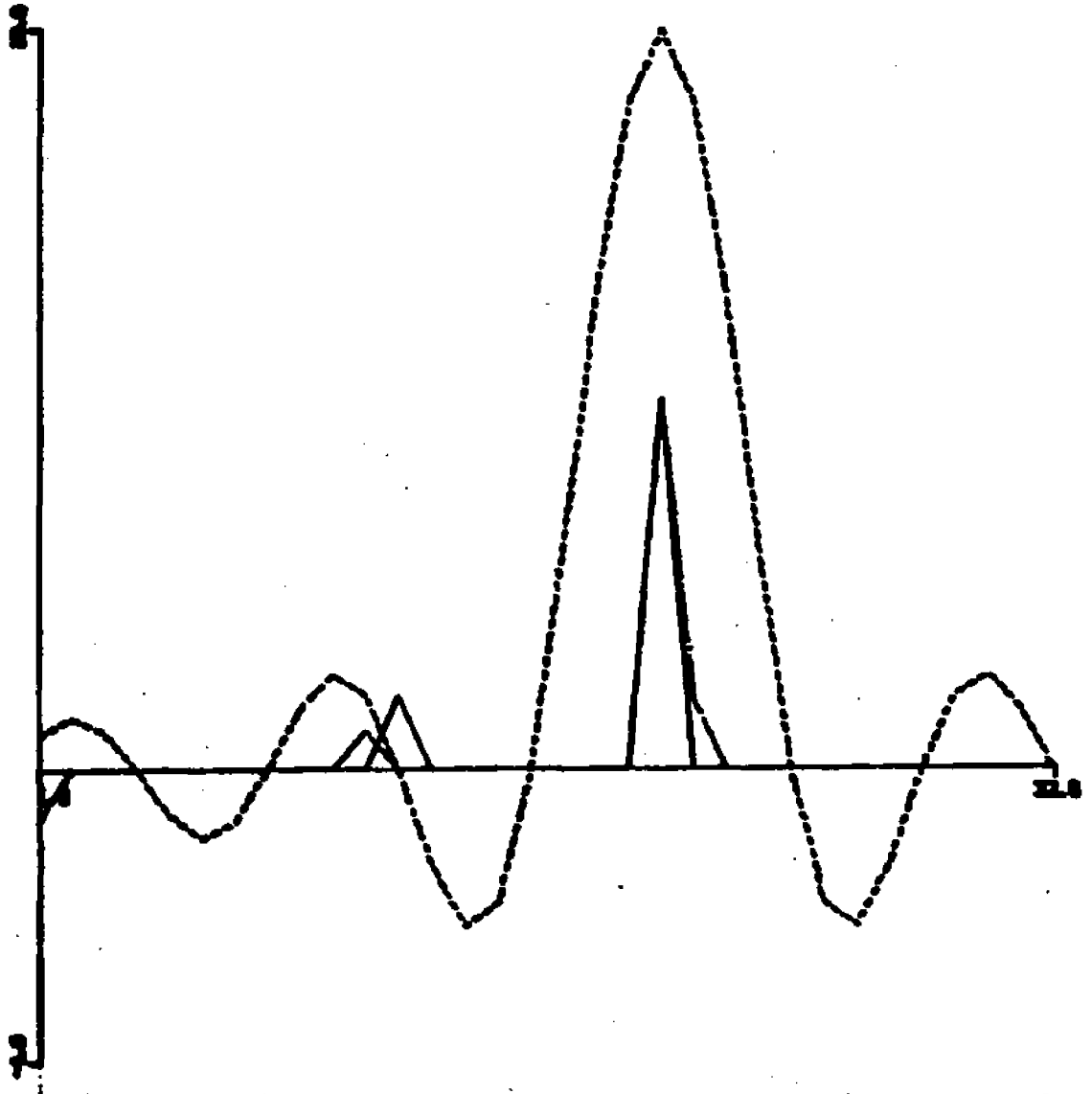

Fig. 3.6-14 ℓ_1 estimate of two unequal impulses of strengths 10 and 10^5 separated by four Rayleigh with noise $\sigma = 100.0$

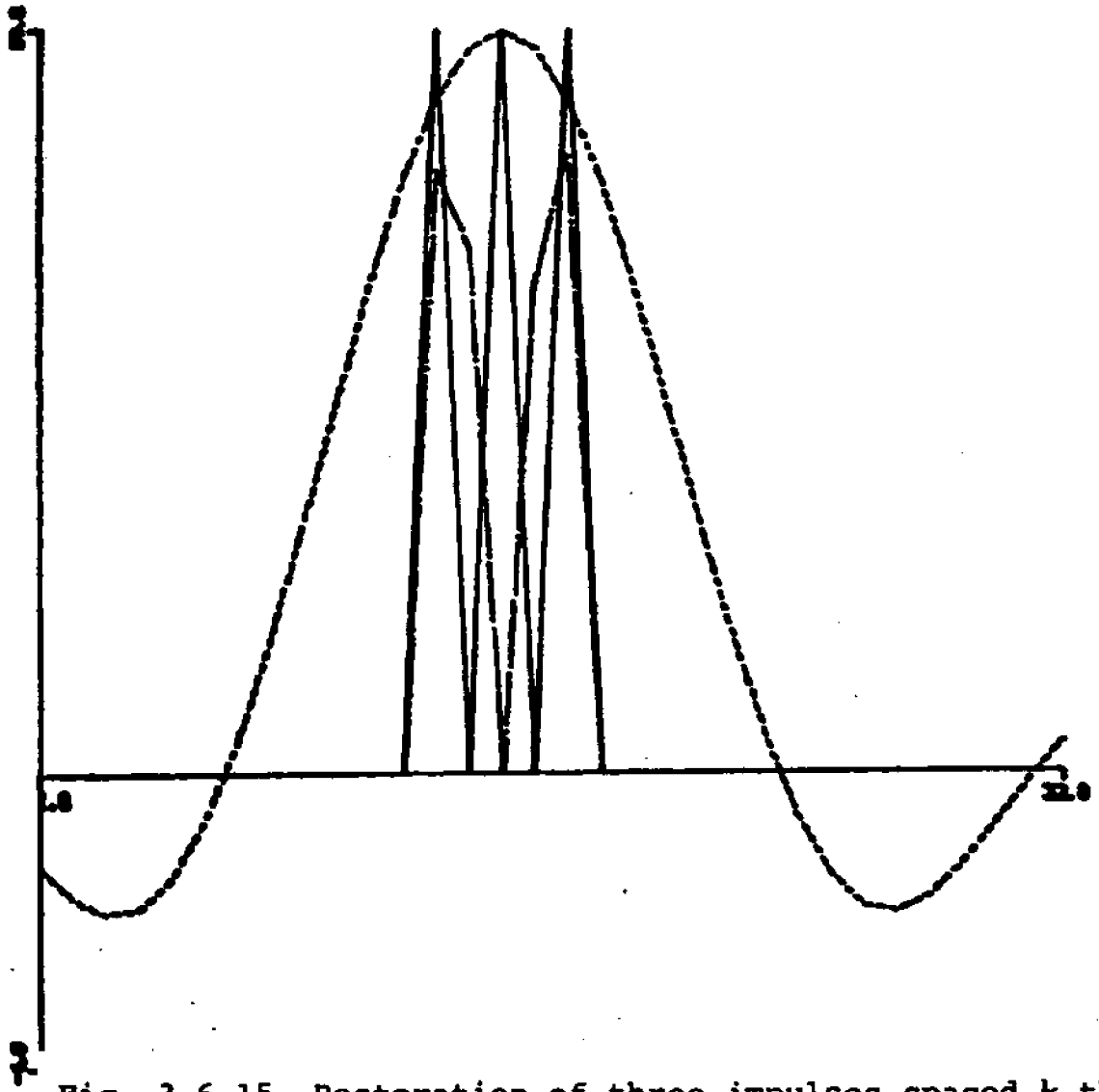

Fig. 3.6-15 Restoration of three impulses spaced ¼ the Rayleigh distance

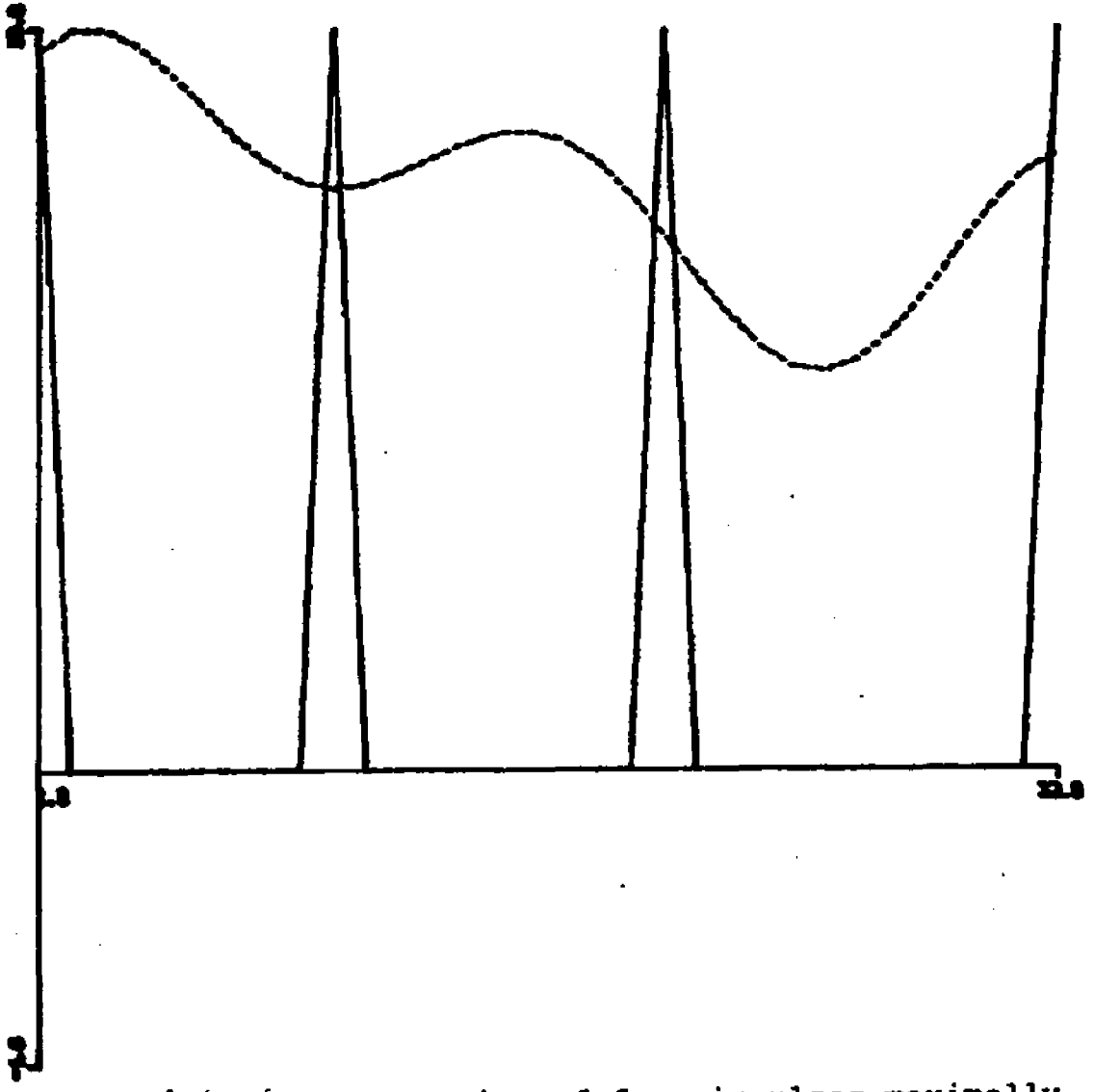

Fig. 3.6-16 Restoration of four impulses maximally spaced

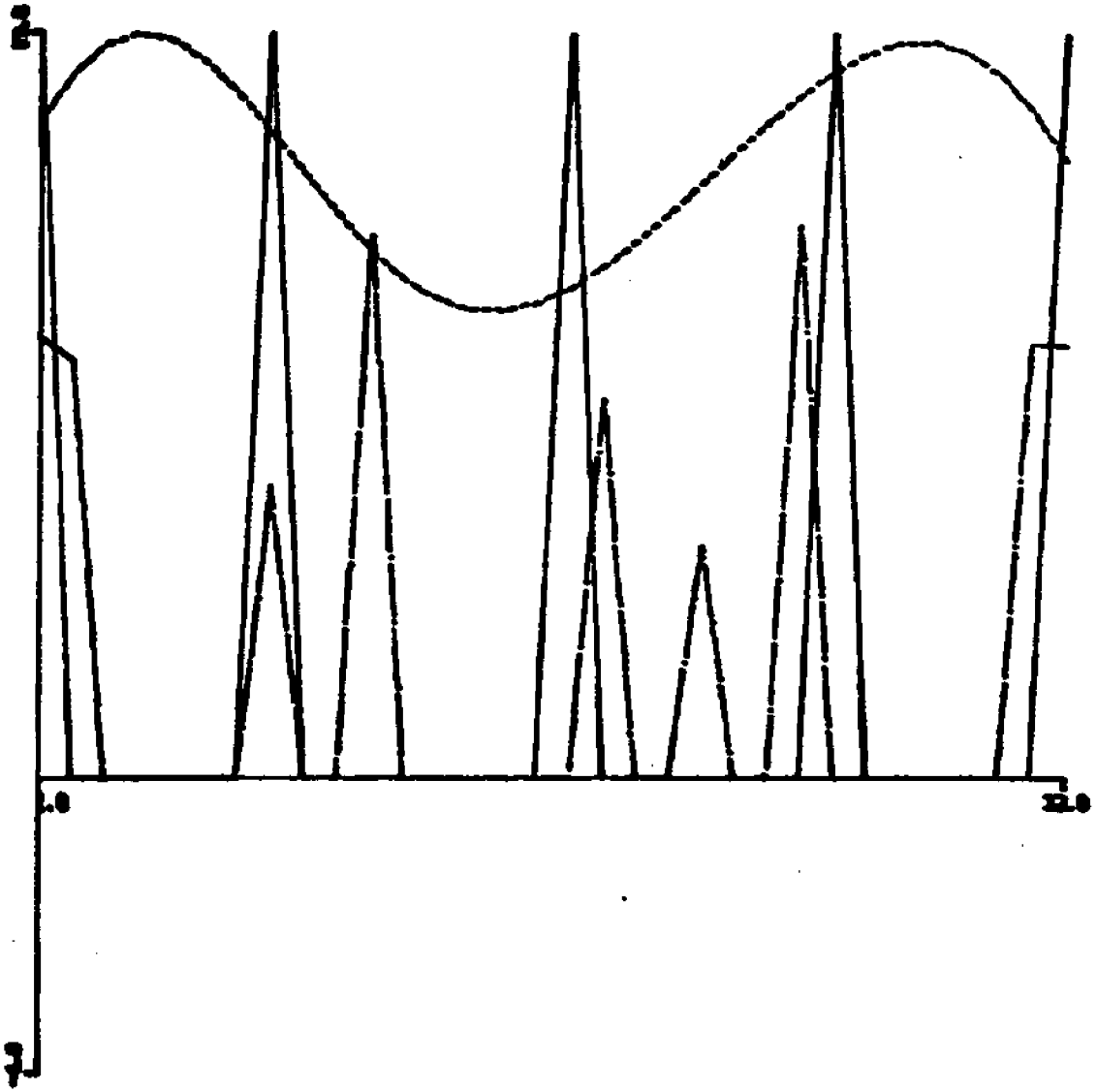

Fig. 3.6-17 Restoration of five impulses maximally spaced

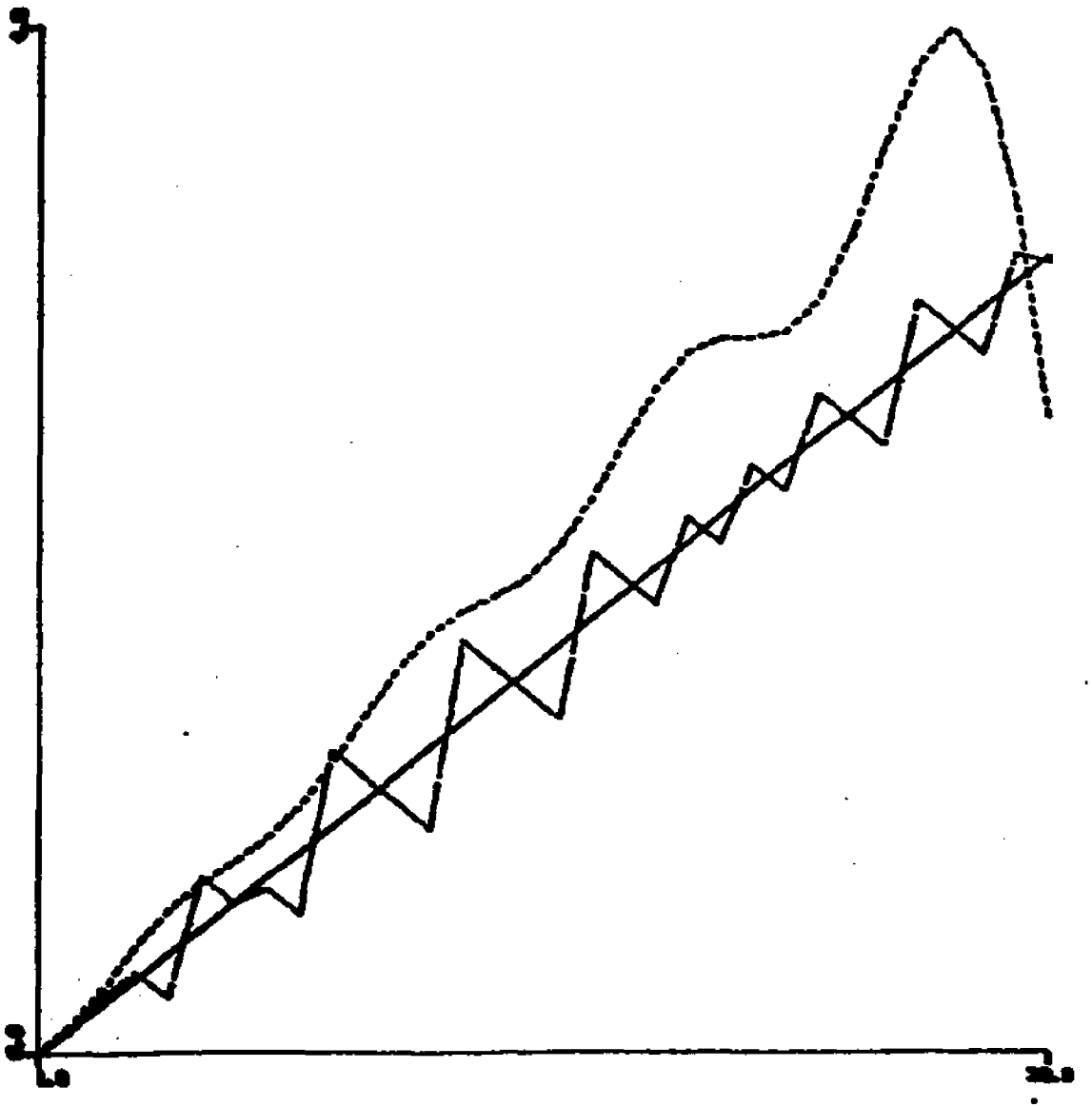

Fig. 3.6-18 Restoration of linear smooth curve with first order smoothness constraints.

Fraction of Rayleigh Distance between Samples	Condition Number		Pseudo-Rank	
	Coherent	Incoherent	Coherent	Incoherent
$\frac{1}{10}$	10^{18}	3×10^{17}	5	4
$\frac{1}{8}$	2×10^{17}	3.5×10^{16}	7	5
$\frac{3}{16}$	10^{17}	10^{16}	9	6
$\frac{1}{2}$	2×10^{16}	7×10^{15}	12	8

Fig. 3.6-19 Comparison of pseudo-rank and condition numbers between coherent and noncoherent restoration

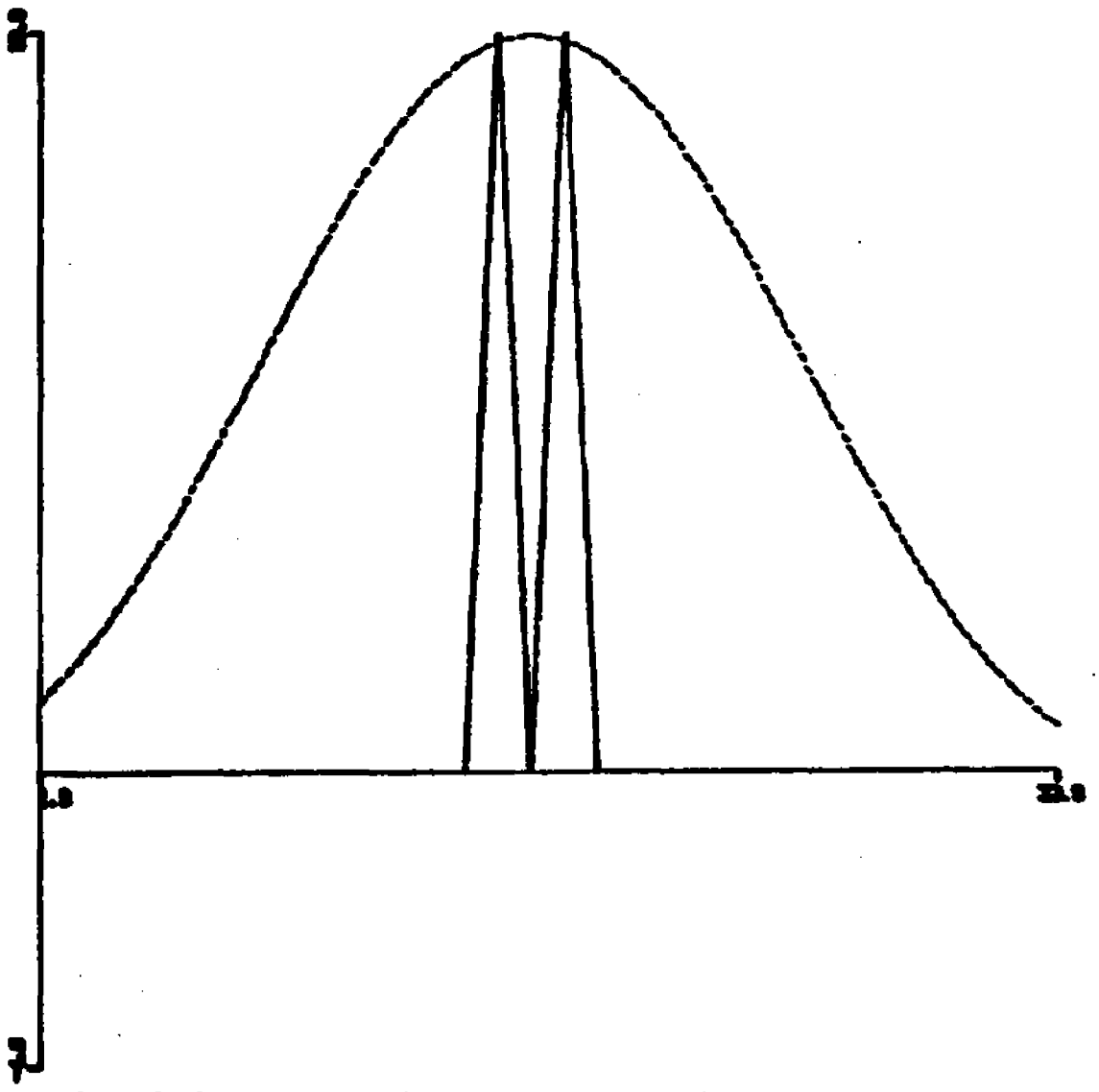

Fig. 3.6-20 Noncoherent restoration of two impulses separated by 1/10 the Rayleigh distance

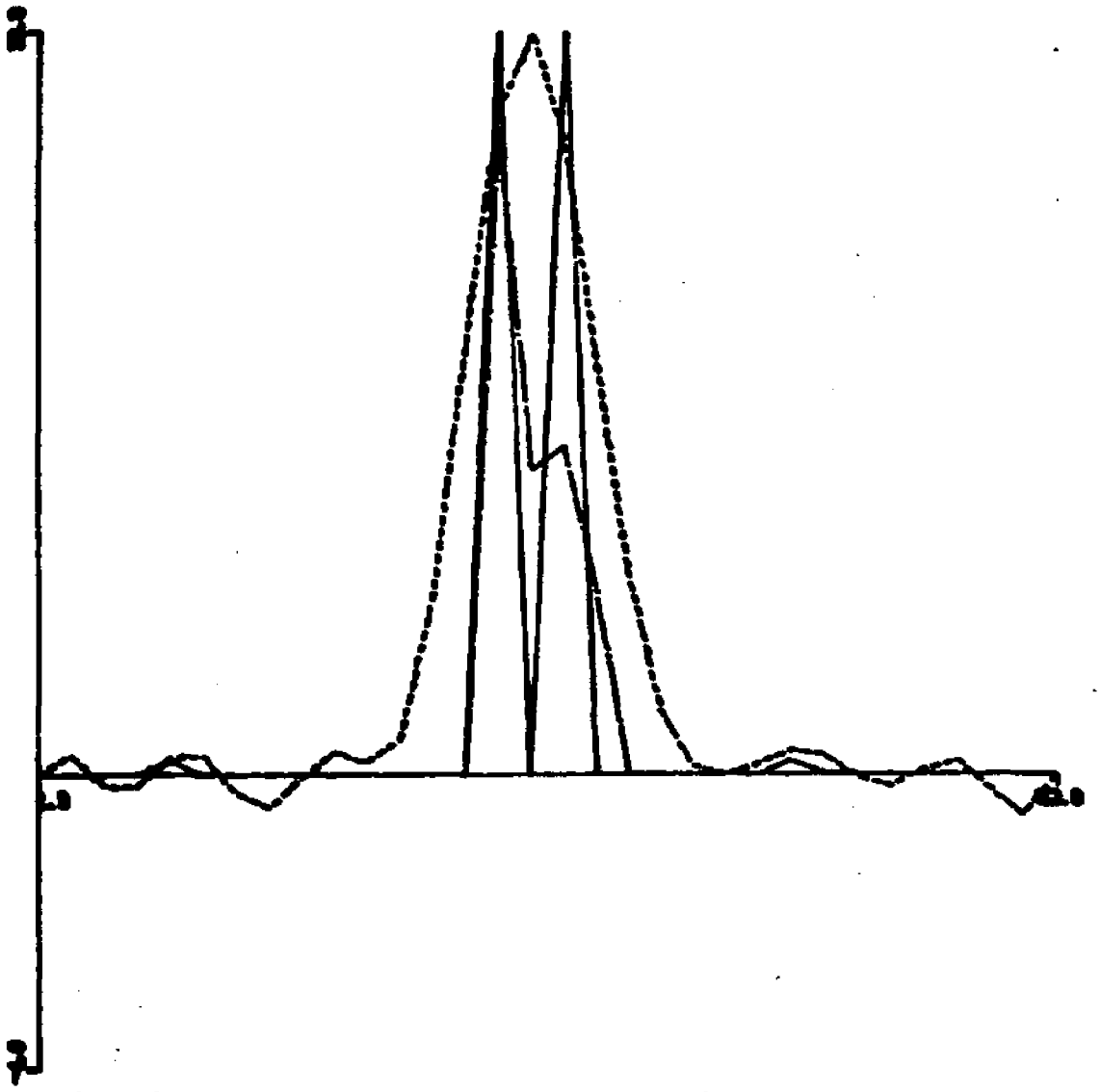

Fig. 3.6-21 Noncoherent restoration of two impulses separated by ½ the Rayleigh distance with SNR of 20 db

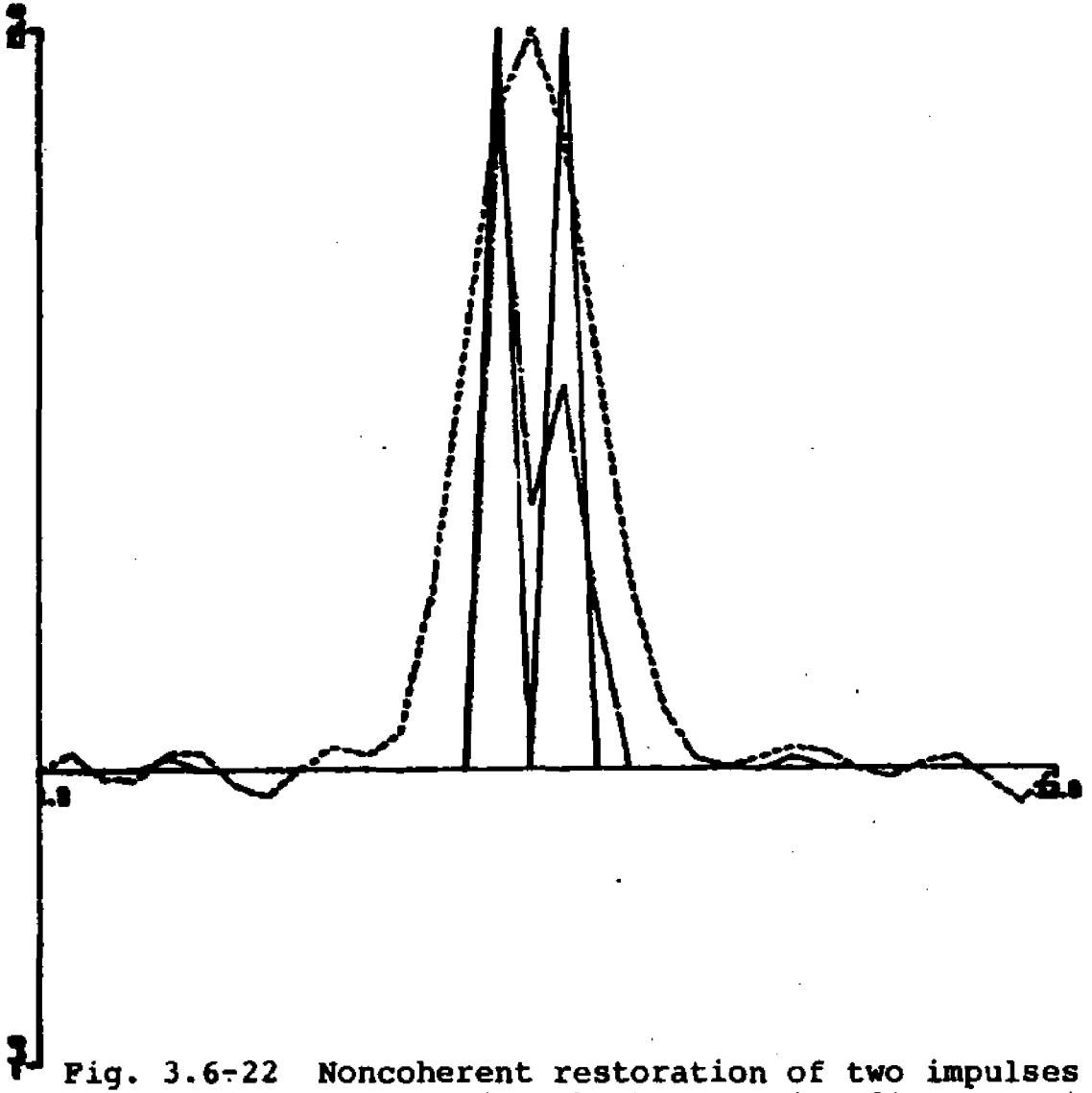

Fig. 3.6-22 Noncoherent restoration of two impulses separated by ½ the Rayleigh distance with SNR of 22 db

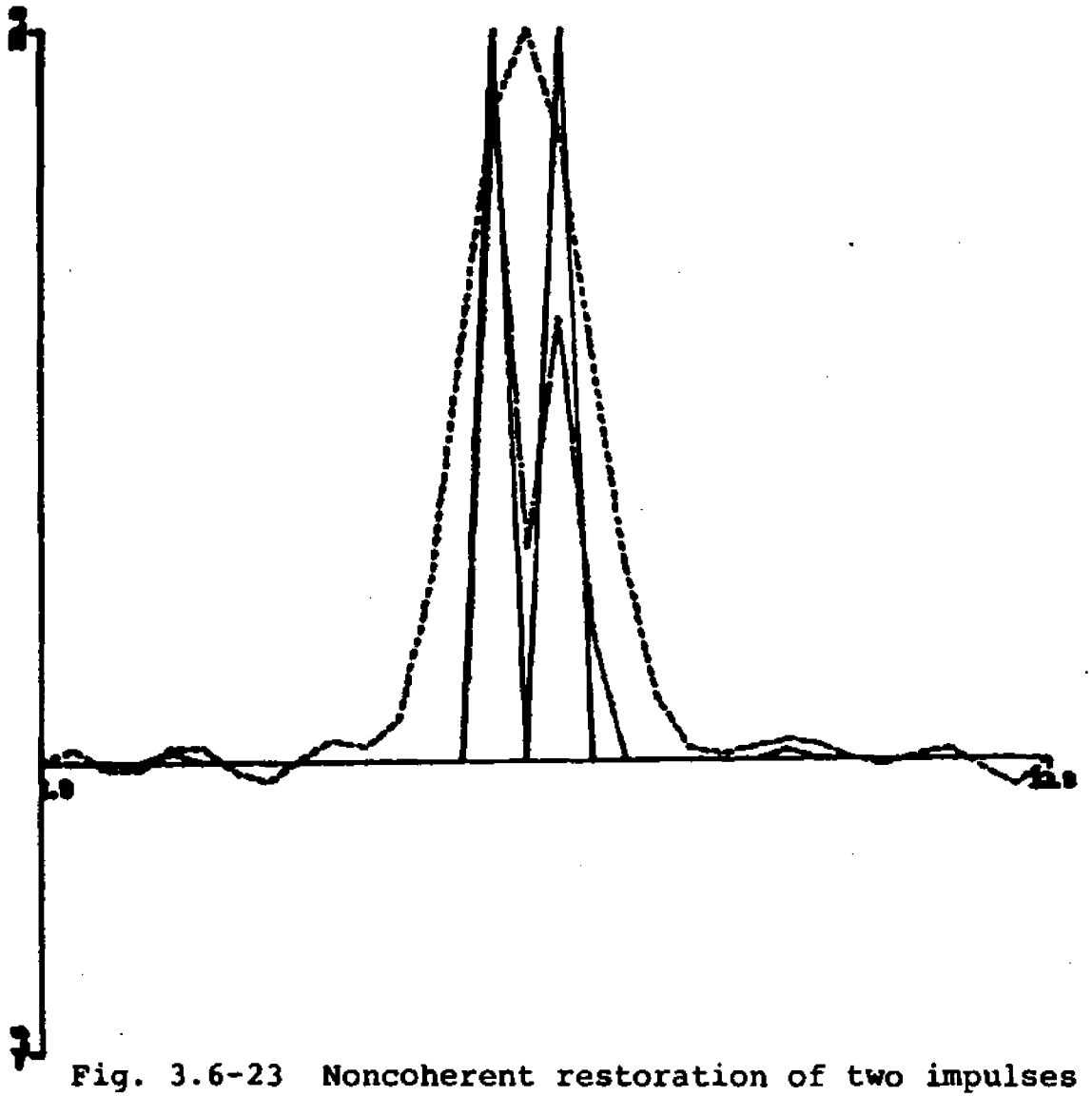

Fig. 3.6-23 Noncoherent restoration of two impulses separated by ½ the Rayleigh distance with SNR of 24 db

Chapter 4

SUPERRESOLVING SPECTRAL ESTIMATION FROM AN INCOMPLETE OBSERVATION

4.0 Background

The estimation of the Fourier spectrum or the extrapolation in the time domain of a bandlimited function from an incomplete observation is a problem of long standing interest [11,12]. The recent renewed interest is largely due to several new algorithms [9,10] which provide some degree of deconvolutions of the time truncation operator of the measured spectrum. Although this deconvolution process can be obtained exactly in theory [2], the conversion of the truncation process is highly unstable in the presence of noise.

In this thesis we present a new robust method of superresolving spectral estimation (SSE) which employs a priori knowledge of the Fourier spectrum of the signal in the form of linear inequalities. The advantage of imposing constraints on the problem have long been recognized [19]. For the formulation of the deconvolution problem, subject to these a priori constraints, there are many "solutions." In this paper we select the solution vector which minimizes the ℓ_1 norm of the difference between the Fourier spectrum of the

measured signal and the convolved estimate.

For a bandlimited signal, truncated in time, the frequency resolution limit is usually given as the uncertainty principle [1]

$$T\omega_R = 1 \qquad (4.0\text{-}1)$$

where T is the duration of the observed signal and ω_R is the resolvable units of frequency. If some signal processing algorithm can provide greater resolution than this limit, the process is called superresolving. This problem is the dual problem of inverse filtering an ideal low pass filter (ILPF), discussed in the previous chapter. That is, the roles of time and frequency have been interchanged. This problem is also complicated by the fact that the convolution operates in the frequency domain. Since the inversion must operate in the convolved domain, we are forced to deal with complex numbers.

The Discrete Fourier transform (DFT) will be used to approximate the Fourier transform. This is done to facilitate the evaluation of the Fourier transform through the use of the fast Fourier transform (FFT) algorithm. The DFT is an approximation of a Fourier transform of a signal f(t) of finite duration T

$$F(\omega) = \int_{-T/2}^{T/2} f(t)\ e^{-j\omega t}\ dt \qquad (4.0\text{-}2)$$

and the inverse relationship is given by

$$f(t) = \frac{1}{2\pi} \int_{-\infty}^{\infty} F(\omega)\ e^{+j\omega t}\ d\omega \qquad (4.0\text{-}3)$$

If f(t) is extrapolated outside the interval [-T/2, T/2] to be a periodic function, we have

$$f_p(t) = f(t) * \sum_{i=-\infty}^{\infty} \delta(t-iT) \qquad (4.0\text{-}4)$$

where * represents the convolution operator. We shall make use of the transform pair

$$\sum_{i=-\infty}^{\infty} \delta(t-i\ T) \leftrightarrow \frac{1}{T} \sum_{k=-\infty}^{\infty} \delta(\omega-k\ \frac{2\pi}{T}) \qquad (4.0\text{-}5)$$

where → indicates Fourier transform, ← indicates inverse Fourier transform, and ↔ indicates a Fourier transform pair. If we take the Fourier transform of both sides of (4.0-5) and using the convolution theorem, we obtain

$$F_p(\omega) = \left\{\frac{1}{T} \sum_{k-\infty}^{\infty} \delta(\omega-k\ \frac{2\pi}{T})\right\} \cdot F(\omega) \qquad (4.0\text{-}6)$$

This equation states that the transform of the constructed periodic sequence is a sampled version of the actual Fourier transform with the sample spacing $2\pi/T$. This spacing can be made arbitrarily small by increasing the effective period. The effective period may be increased by simply

zero padding. In the limit, as T goes to infinity, the spacing becomes infinitesimally small and the continuous Fourier transform is obtained.

If most of the signal energy is in the band of frequencies from $[-W_c, W_c]$ we can approximate the transform as zero outside this band. Since this assumption violates the uncertainty principle we introduce aliasing error into the approximation. This error can be minimized by choosing the bandwidth ($2W_c$) sufficiently large. We now construct this finite sequence of Fourier transform samples into a periodic sequence

$$F_p(K) = T \sum_{k=-\infty}^{\infty} \delta(\omega - kW_c) * F(\omega) \qquad (4.0\text{-}7)$$

The inverse Fourier transform of Eq. (4.2-6) gives the sampled time sequence

$$f(n) \triangleq f'_p(t) = \left\{ \sum_{n=-\infty}^{\infty} \delta\left(t - n\,\frac{2\pi}{W_c}\right) \right\} \cdot f_p(t) \qquad (4.0\text{-}8)$$

where f(n) is a sampled version of f(t) with sample spacing $2\pi/W_c$ and a period T. The distance between the time samples is $T_s = 2\pi/W_c$ and the distance between frequency samples is $\Delta\omega_s = 2\pi/T$. The number of points in either the time or frequency interval is

$$N = \frac{f_c}{f_R} = \frac{T}{T_s} \qquad (4.0\text{-}9)$$

Thus the same number of samples appears in both the time and the frequency sequence. This is a result of the assumption that we sample at exactly the Nyquist rate $1/T_s$ for the duration T. We can also sample at a finer spacing than T_s or sample longer than the duration T, i.e. zero padding. Either of these processes would increase the number N leading to a more computationally expensive processing. But this increase in computational complexity is offset by definite advantages in either case. Finer sampling in the time domain allows the DFT to span a larger frequency band. This is very useful for this application. Since the signal is known to be bandlimited to angular frequency W_c, any frequency component at a frequency higher than W_c can be eliminated since it can only be due to noise. Since the goal of the signal processing is to increase the resolution, the frequency scale must be more dense. This is done by zero padding the time sequence until the desired frequency resolution ω_R is achieved, i.e.

$$\omega_R = \frac{2}{T'} \qquad (4.0\text{-}10)$$

where T' is the effective signal duration. The effective signal duration T' is the actual signal duration T plus the additional duration due to the zero elements.

Thus there are two desirable methods of increasing the effectiveness of the DFT approximation; finer sampling and

zero padding. But the degree to which we can improve the frequency range and resolution is limited only by the practical limitation on the number N with which it is possible to process the signal.

The DFT of an N element siquence $\{f_n\}$ (which usually represents a sampled time signal) is

$$F_k = \sum_{n=0}^{N-1} f_n \, e^{-j\ 2\omega kn/N} \quad k=0,1,\ldots,N-1 \qquad (4.0\text{-}11)$$

and the corresponding inverse DNT relationship is

$$fn = \frac{1}{N} \sum_{k=0}^{N-1} F_k \, e^{j\ 2\omega kn/N} \quad n=0,1,\ldots,N-1 \qquad (4.0\text{-}12)$$

To simplify the notation, let

$$W_N = e^{-j\ 2\pi/N} \qquad (4.0\text{-}13)$$

so (4.0-11) becomes

$$F_k = \sum_{n=0}^{N-1} W_N^{nk} \, f_n \quad k=0,1,\ldots,N-1 \qquad (4.0\text{-}14)$$

Each F_k can be viewed as a linear combination of the sample set $\{f_n\}$ with $\{W_N^{nk}\}$. We can write Eq. (4.0-14) in matrix form

$$F = \underline{W} f \qquad (4.0\text{-}15)$$

where F and f are the vectors corresponding to $\{F_m\}$ and

$\{f_n\}$ respectively, and the DFT matrix is given as

$$\underline{W} = \begin{bmatrix} 1 & 1 & 1 & 1 & . & . & 1 \\ 1 & w^0 & w^1 & w^2 & . & . & w^N \\ 1 & w^2 & w^4 & w^6 & . & . & . \\ 1 & w^3 & w^6 & . & . & . & . \\ . & . & & & & & \\ 1 & 1 & . & . & . & . & w^{7N} \end{bmatrix} \qquad (4.0\text{-}16)$$

The complex elements of the matrix $\underline{W}$ possess a great deal of redundancy. This can be seen by examining the cyclic nature of the elements $W_N^{nk} = W_N^L$ in Fig. 4.0-11 for the case N=8. Note that since L=nk is always an integer, and W^L is a root of unity of modulo N, then the same N complex values repeat in the matrix W. The first row or zeroth row can be obtained by starting at the zeroth element and rotating elements to obtain the next element. The second row is obtained by spacing one element in Fig. 4.0-1 between adjacent row elements. For the third row the element spacing is two and so on.

This high degree of symmetry allows one to significantly decrease the computational complexity when N is a highly composite number. The most frequently used radix of N is 2, i.e. $N=2^j$, where j is an integer. This allows a reduction in the number of complex multiplication which must be performed. As it is known, the FFT reduces the N^2 multiplications required to evaluate Eq. (4.2-14) to N&nN.

Circulant matrices of the form

$$\underline{C} = \begin{bmatrix} c_0 & c_1 \cdots & c_{N-1} \\ c_{N-1} & c_0 \cdots & c_{N-2} \\ \vdots & & \\ c_1 & c_2 \cdots & c_0 \end{bmatrix} \qquad (4.0\text{-}17)$$

occur in a variety of investigations. This type of matrix when used to premultiply a vector x will yield the cyclic convolution of the vector $c^T = [c_0, c_1, \ldots, c_N]$ with the vector x i.e.

$$Y = c \textcircled{N} x \qquad (4.0\text{-}18)$$

where $\textcircled{N}$ indicates cyclic as opposed to linear convolutions. The eigenvectors of a circular matrix are the DFT orthonormal vector set. That is, if a SVD of $\underline{C}$ is performed, i.e.

$$\underline{C} = \underline{U}\underline{\Lambda}^{\frac{1}{2}}\underline{V}^T \qquad (4.0\text{-}19)$$

then it can be shown that $\underline{U}$ and $\underline{V}^T$ are the DFT and inverse DFT matrix and $\underline{\Lambda}^{\frac{1}{2}}$ is a diagonal matrix with elements that are the DFT of the vector c. This can be seen by examining the characteristic roots and vectors of the matrix $\underline{C}$.

Let r_1 be a complex root of the scalar equation

$$r^N = 1 \qquad (4.0\text{-}20$$

and set

$$y_1 = c_0 + c_1 r_1 + \ldots + c_{N-1} r_1^{N-1} \qquad (4.0\text{-}21$$

Then we see that y_1 satisfies the following system of equations

$$\begin{aligned} y_1 &= c_o + c_1 r_1 + \ldots + {}_{N-1}\, r_1^{N-1} \\ r_1 y_1 &= c_{N-1} + {}_o r_1 + \ldots + c_{N-2}\, r_1^{N-2} \\ &\vdots \\ r_1^{N-1} y_1 &= c_1 + c_2 r_1 + \ldots + c_o r_1^{N-1} \end{aligned} \tag{4.0-22}$$

It follows that y_1 is a characteristic root of $\underline{C}$ with associated characteristic vector

$$x' = \begin{bmatrix} 1 \\ r_1 \\ \vdots \\ r_1^{N-1} \end{bmatrix} \tag{4.0-23}$$

Since the equation $r^N = 1$ has N distinct roots, we see that we obtain N distinct characteristic vectors. Consequently, we have the complete set of characteristic roots and vectors. Thus any circulant matrix can be diagonalized by the DFT and inverse DFT matrices, where the diagonal elements are the DFT of the c vector. The sequence resulting from a cyclic convolution of two sequences has an associated DFT sequence which is the product of the DFTs of the two sequences

$$\text{IDFT}\{f_1(n) \circledN f_2(n)\} = \text{DFT}\{f_1(n)\} \cdot \text{DFT}\{f_2(n)\} \tag{4.0-24}$$

where $\cdot$ represents element by element multiplication.

The converse of this statement is also true, i.e.

$$\text{DFT}\{f_1(n) \cdot f_2(n)\} = \frac{1}{N} \text{DFT}\{f_1(n)\} \textcircled{N} \text{DFT}\{f_2(n)\} \tag{4.0-25}$$

The last relationship will be used in our analysis to model the time truncation operator.

4.1 Formulation

It will be helpful in the following discussion to define what is meant by negative time and frequency samples. The first N/2 + 1 elements of the sequence $\{F_K\}$ or $\{f_n\}$ correspond to the positive frequency or time samples in a forward order and the remaining N/2-1 elements correspond to the negative frequency or the time samples in a backward order. This is consistent with the idea of extending the sequences in a periodic manner. The time truncation operation is characterized by multiplication of the time sequence by the rectangular sequence $\{R_n\}$ as shown in Fig. 4.1-1. The DFT of this rectangular sequence is a real sequence, since $\{R_n\}$ is even, similar to a sampled sinc function. Let

$$h = \text{DFT}\{R_n\} = \{h_N\} \tag{4.1-1}$$

In order to examine the relationship of the DFT of the truncated and the exact sequence, we shall use the convolution theorem for DFT's. The linear discrete convolution of two sequences can be characterized by a Toeplitz matrix (comprised of shifted versions of a sequence) which multiplies

the other vector. For the DFT the analog of linear convolution is cyclic convolution which is characterized by a circulant matrix. For the time truncation operator the frequency cyclic convolution matrix is

$$\underline{H} = \begin{bmatrix} h_0 & h_1 & \cdots & h_N \\ h_N & h_1 & \cdots & h_{N-1} \\ \vdots & & & \\ h_1 & h_2 & \cdots & h_0 \end{bmatrix} \qquad (4.1\text{-}2)$$

If we let

$$G = \underline{H}F + n \qquad (4.1\text{-}3)$$

where G and F are the DFT of the measured and the input sequence, and n is the complex error (noise) vector. Since G, F and n are complex, Eq. (4.1-3) represents 2N equations. But all the time sequences are real and, therefore, the DFT sequences have symmetry which introduce redundancy into Eq. (4.1-3). The elimination of this redundancy reduces the 2N to N equations. In order to generate these N equations we must examine some properties of the DFT.

In analogy to the properties of the Fourier transform, the DFT of a real sequence possess an even real and an odd imaginary part. We plan to use the computationally efficient FFT radix 2 algorithm with $N = 2^j$. Thus the sequence consists of an even number of points. However, a discrete even function must contain an odd number of points.

Therefore, even symmetry will be redefined in the following way. There is one element for the DC or zeroth component, (N/2-1) negative elements, (N/2-1) positive frequency elements and one remaining element, the center element. This center frequency component is always real. This can be seen by noticing that the $N/2^{th}$ row of the DFT matrix is a sequence of alternating 1's and -1's. Thus the center frequency and DC frequency components are always real. The remaining N-2 elements consist of complex conjugate pairs, between the first and last elements and the second and the second for the last elements and so on. Thus this Hermittian relationship obtained by reordering yields an even symmetry.

There are N/2+1 distinct real and N/2-1 imaginary elements. We form the concatenated sequence of the distinct elements. Let the real and imaginary parts of the i^{th} element be denoted by a subscript R and I, respectively, then

$$\tilde{G} = \begin{bmatrix} G_{RO} \\ G_{R1} \\ \vdots \\ G_{R_{N/2+1}} \\ G_{I_{N/2-1}} \\ \vdots \\ G_{I1} \end{bmatrix} \quad \tilde{F} = \begin{bmatrix} F_{RO} \\ F_{R1} \\ \vdots \\ F_{RN/2+1} \\ F_{IN/2-1} \\ \vdots \\ F_{I1} \end{bmatrix} \quad \tilde{N} = \begin{bmatrix} N_{RO} \\ N_{R1} \\ \vdots \\ N_{RN/2+1} \\ N_{IN/2-1} \\ \vdots \\ N_{I1} \end{bmatrix} \qquad (4.1\text{-}4)$$

The relation (4.1-3) can now be written in reduced form

$$\tilde{G} = \underline{\tilde{H}}\tilde{F} + \tilde{n} \qquad (4.1\text{-}5)$$

where

$$\underline{H} = \left[\begin{array}{c|c} A & B \\ \hline e\ C\ f & D \end{array}\right] \qquad (4.1\text{-}6)$$

with e and f as unused column vectors.

Here $\underline{A}$ is a $(N/2 + 1)\times(N/2 + 1)$, $\underline{B}$ is a $(N/2 + 1)(N/2 - 1)$, $\underline{C}$ is a $(N/2 -1)\times(N/2-1)$ and $\underline{D}$ is a $(N/2 - 1)\times(N/2 - 1)$ submatrix of $\underline{H}$. If we let ϕ and $\underline{\phi}$ denote the null vector and matric respectively. Define

$$\underline{\tilde{B}} = \left[\begin{array}{c|c|c} & & \\ \phi & \underline{B} & \phi \\ & & \end{array}\right] \qquad (4.1\text{-}7)$$

$$\underline{\tilde{D}} = \left[\begin{array}{c|c|c} & & \\ \phi & \phi & \underline{D} \\ & & \end{array}\right] \qquad (4.1\text{-}8)$$

$$\underline{\tilde{C}} = \left[\begin{array}{c|c|c} & & \\ \phi & \phi & \underline{C} \\ & & \end{array}\right] \qquad (4.1\text{-}9)$$

then

$$\underline{\tilde{H}} = \left[\begin{array}{c|c} \underline{A} + \underline{\hat{B}} & \underline{\phi} \\ \hline \underline{\phi} & \underline{\tilde{D}} - \underline{C} \end{array}\right] \tag{4.1-10}$$

For example, for the case N = 4 we have four complex equations:

$$\begin{bmatrix} G_0 \\ G_1 \\ G_2 \\ G_3 \end{bmatrix} = \begin{bmatrix} h_0 & h_1 & h_2 & h_3 \\ h_3 & h_0 & h_1 & h_2 \\ h_2 & h_3 & h_0 & h_1 \\ h_1 & h_2 & h_3 & h_0 \end{bmatrix} \begin{bmatrix} F_0 \\ F_1 \\ F_2 \\ F_3 \end{bmatrix} + \begin{bmatrix} \eta_0 \\ \eta_1 \\ \eta_2 \\ \eta_3 \end{bmatrix} \tag{4.1-11}$$

We can rewrite (4.1-11) as two sets of four real equations, one set for the real part of (4.1-11)

$$\begin{bmatrix} G_{R0} \\ G_{R1} \\ G_{R2} \\ G_{R3} \end{bmatrix} = \begin{bmatrix} h_0 & h_1 & h_2 & h_3 \\ h_3 & h_0 & h_1 & h_2 \\ h_2 & h_3 & h_0 & h_1 \\ h_1 & h_2 & h_3 & h_0 \end{bmatrix} \begin{bmatrix} F_{R0} \\ F_{R1} \\ F_{R2} \\ F_{R3} \end{bmatrix} + \begin{bmatrix} \eta_{R0} \\ \eta_{R1} \\ \eta_{R2} \\ \eta_{R3} \end{bmatrix} \tag{4.1-12}$$

and one set for the imaginary part of (4.1-11), i.e.

$$\begin{bmatrix} G_{I0} \\ G_{I1} \\ G_{I2} \\ G_{I3} \end{bmatrix} = \begin{bmatrix} h_0 & h_1 & h_2 & h_3 \\ h_3 & h_0 & h_1 & h_2 \\ h_2 & h_3 & h_0 & h_1 \\ h_1 & h_2 & h_3 & h_0 \end{bmatrix} \begin{bmatrix} F_{I0} \\ F_{I1} \\ F_{I2} \\ F_{I3} \end{bmatrix} + \begin{bmatrix} \eta_{I0} \\ \eta_{I1} \\ \eta_{I2} \\ \eta_{I3} \end{bmatrix} \tag{4.1-13}$$

But the real part of the transform sequences are even and the imaginary part of the transform sequences are odd since they are the DFT of a real signal

$$F_{R1} = F_{R3} \tag{4.1-14}$$

Using (4.1-14) in (4.1-13) to eliminate F_{R3}, we obtain from (4.1-11)

$$\begin{bmatrix} G_{R0} \\ G_{R1} \\ G_{R2} \\ G_{R1} \end{bmatrix} = \begin{bmatrix} h_0 & h_1+h_3 & h_2 \\ h_3 & h_0+h_2 & h_1 \\ h_2 & h_3+h_1 & h_0 \\ h_1 & h_2+h_0 & h_3 \end{bmatrix} \begin{bmatrix} F_{R0} \\ F_{R1} \\ F_{R2} \end{bmatrix} + \begin{bmatrix} \eta_{R0} \\ \eta_{R1} \\ \eta_{R2} \\ \eta_{R1} \end{bmatrix} \tag{4.1-15}$$

where we have taken advantage of the even symmetry, i.e. $G_{R1} = G_{R3}$ and $\eta_{R1} = \eta_{R3}$. Since there are only three independent variables, the fourth equation is redundant and we can write

$$\begin{bmatrix} G_{R0} \\ G_{R1} \\ G_{R2} \end{bmatrix} = \begin{bmatrix} h_0 & h_1+h_3 & h_2 \\ h_3 & h_0+h_2 & h_1 \\ h_2 & h_3+h_1 & h_0 \end{bmatrix} \begin{bmatrix} F_{R0} \\ F_{R1} \\ F_{R2} \end{bmatrix} + \begin{bmatrix} \eta_{R0} \\ \eta_{R1} \\ \eta_{R2} \end{bmatrix} \tag{4.1-16}$$

for the solution (F_{R0}, F_{R1}, F_{R2}) to (4.1-15), the fourth real element F_{R3}, obtained by using its equivalence to F_{R1}. We shall also take advantage of the odd symmetry in the equations resulting from the imaginary part of Eq.

(4.1-10), i.e.

$$F_{I3} = -F_{I1} \tag{4.1-17}$$

we can then rewrite (4.1-13)

$$\begin{bmatrix} G_{I0} \\ G_{I1} \\ G_{I2} \\ -G_{I1} \end{bmatrix} = \begin{bmatrix} h_0 & h_1 & h_2 & h_3 \\ h_3 & h_0 & h_1 & h_2 \\ h_2 & h_3 & h_0 & h_1 \\ h_1 & h_2 & h_3 & h_0 \end{bmatrix} \begin{bmatrix} F_{I0} \\ F_{I1} \\ F_{I2} \\ -F_{I1} \end{bmatrix} + \begin{bmatrix} \eta_{I0} \\ \eta_{I1} \\ \eta_{I2} \\ -\eta_{I1} \end{bmatrix} \tag{4.1-18}$$

where we have used the fact that

$$G_{I3} = -G_{I1} \text{ and } \eta_{I3} = -\eta_{I1}$$

We also know that since the solution F must be the DFT of a real sequence, then by even symmetry

$$F_{I0} = F_{I2} = 0 \tag{4.1-19}$$

So there are only two unknown variables F_{I1} and F_{I3}. From (4.1-14) we see that there is only one unknown needed, either F_{I1} or F_{I3}. Thus we take

$$G_{I1} = [h_3 \; h_0 \; h_1 \; h_2] \begin{bmatrix} 0 \\ F_{I1} \\ 0 \\ -F_{I1} \end{bmatrix} \tag{4.1-20}$$

Thus,

$$G_{I1} = [h_0 - h_2] \; F_{I1} \tag{4.1-21}$$

(4.1-16) and (4.1-21) now comprise the four equations for the four unknowns that we seek. This is the basis of the tilted equations (4.1-5).

In this case we obtain

$$\tilde{G} = \begin{bmatrix} G_{R0} \\ G_{R1} \\ G_{R2} \\ G_{R3} \end{bmatrix} \quad \hat{F} = \begin{bmatrix} F_{R0} \\ F_{R1} \\ F_{R2} \\ F_{R3} \end{bmatrix} \quad \tilde{N} = \begin{bmatrix} N_{R0} \\ N_{R1} \\ N_{R2} \\ N_{R3} \end{bmatrix} \tag{4.1-22}$$

$$\underline{A} = \begin{bmatrix} h_0 & h_1 & h_2 \\ h_3 & h_2 & h_1 \\ h_2 & h_3 & h_0 \end{bmatrix} \quad \underline{C} = [0 \; 0 \; h_2] \tag{4.1.23}$$

$$\underline{\tilde{B}} = \begin{bmatrix} 0 & h_3 & 0 \\ 0 & h_2 & 0 \\ 0 & h_1 & 0 \end{bmatrix} \quad \underline{\tilde{D}} = [0 \; 0 \; h_0] \tag{4.1-24}$$

then

$$\underline{\tilde{H}} = \begin{bmatrix} h_0 & h_1+h_3 & h_2 & 0 \\ h_3 & h_0+h_2 & h_1 & 0 \\ h_2 & h_1+h_3 & h_0 & 0 \\ 0 & 0 & 0 & h_0-h_2 \end{bmatrix} \tag{4.1-25}$$

Thus the first three rows correspond to the equations (4.1-16) and the last row is (4.1-21).

The matrix $\underline{H}$ can be decomposed by SVD, i.e.

$$\underline{H} = \underline{U}\ \underline{\Lambda}^{\frac{1}{2}}\ \underline{V}^{T} \qquad (4.1\text{-}26)$$

where $\underline{U}$ and $\underline{V}$ are the orthogonal inverse DFT and DFT matrices, respectively, and the diagonal matrix $\underline{\Lambda}^{\frac{1}{2}}$ consists of the DFT of the cyclic vector h. The diagonal of Λ matrix is the time truncation sequence which contains zeros and ones. Thus, the $\underline{H}$ matrix is rank-deficient. The matrix $\tilde{H}$ is obtained by converting the matrix $\underline{H}$ into a real matrix and eliminating the redundancies. Thus, it is not surprising that $\hat{\underline{H}}$ is also rank deficient.

The formulation of the spectral estimation problem is very similar to that of the previous chapter. Again we shall use linear programming methods to solve for the exact spectrum. The minimal ℓ_1 norm of the difference between the spectrum of the measured image and the spectrum of the estimate is used since it was found superior to the ℓ_2 and ℓ_∞ norms. The formulation is given in terms of real and imaginary spectral components. Although in a magnitudinal and phase representation the magnitude is always positive and the phase bounded by $\pm\pi$, this representation leads to non-linear equations. The real and imaginary parts have negative and positive bounds. This requires more dummy (slack) variables to be introduced into the formulation so that we must define the new vectors F^{-} and F^{+}, where

$$F = F^{+} - F^{-} \tag{4.1-27}$$

as done previously for the noise.

We can impose bounds on the amplitude of the spectrum and bounds on the difference between adjacent elements. We can append these constraints to (4.1-5)

$$\tilde{G} = \underline{\tilde{H}}\,\tilde{F} + \tilde{N} \tag{4.1-28}$$

subject to

$$\begin{aligned} -B_{1L} &\leq F \leq B_{1h} \\ -B_{2L} &< F_i - F_{i+1} \leq B_{2h} \end{aligned} \tag{4.1-29}$$

where B_{1L}, B_{2h}, B_{1L} and B_{2h} are the upper and lower bound vectors.

The SVD prefiltering can be performed before this procedure to help reduce the effects of noise. Another noise eliminating filtering process can be accomplished in the DFT domain. If the signal is oversampled the maximal frequency in the DFT is greater than the bandwidth of the signal. Thus the high frequency components represent only noise which can then be eliminated. This smoothing of the measured signal was found to be an effective way of reducing the noise effects.

4.2 Computer Simulations and Results

In many applications the duration of the sample signal

may not correspond to $N = 2^i$ points. This can occur, for example, if the actual duration of the signal is not conformal or if the signal could only be sampled for a certain window due to speed limitations. If the remaining points ourside the sampled interval of the signal is simply filled with zeros, i.e. zero padding, the DFT yields the desired spectrum convolved with a discrete sampling function. The resolvable frequency difference is therefore smeared. Fig. 4.2-1 illustrates this lack of resolution. Here the exact spectrum is shown by the solid line as two impulses. The DFT, which is the chain-dot line, does not resolve the two impulses. This figure corresponds to sampling 23 points of cos $W_N t$ and performing a 32 point DFT on the zero padded sequence. Here no noise is added. The DFT approaches the true spectrum as the length of the sampled sequence increases. The DFT begins to resolve the two impulses when the sequence is sampled for 25 of the 32 samples as shown in Fig. 4.2-2.

The method described in Chapter 3 can be used to deconvolve the time truncation effect of the spectrum in the frequency domain. Fig. 4.2-3 illustrates a perfect restoration (dotted line) obscured by exact solution (solid line). The chain dot curve indicates the DFT of the Sequence. This figure corresponds to sampling less than one quarter of the time domain sequence. Fig. 4.2-4 shows the time domain extrapolation where the dotted line indicates the measured

segment of the signal. The reconstruction (chain-dot) again is obscured by the exact signal (solid line). The deconvolution is again robust. Fig. 4.2-5 illustrates the restoration of cos $W_N t$ from 15 samples from a 32 point DFT with white Gaussian noise added. The measured SNR is 27 db while the restored spectrum had a decrease in the SNR to 17 db. Thus a factor of two increase in resolution was obtained in the presence of significant noise. Fig. 4.2-6 illustrates the time domain extrapolation corresponding to the case depicted in the previous figure.

Higher frequency signals are less difficult to resolve since the separation between frequency domain impulses is greater. Thus a cos $5W_N t$ signal is exactly restored in Fig. 4.2-7 from 7 samples and a 32 point DFT. Fig. 4.2-8 illustrates the corresponding extrapolation in the time-domain. Fig. 4.2-9 indicates acceptable restoration, for the same case as that of Fig. 4.2-7, but with white gaussian noise added such that the SNR is 20 db. The restored image (dotted line) has SNR of 6 db. Note that this gives an increase by a factor of four in resolution. Fig. 4.2-10 illustrates the same case as (4.2-9) with the signal plotted in the time domain. Fig. 4.2-11 illustrates that even better noise immunity can be acquired for higher signal frequencies.

Fig. 4.2-12 indicates that more sample points are necessary

to resolve
the sum of cosines of the fundamental and fifth harmonics than are needed for either frequencies appearing alone (7 points). The restoration is seen to be almost perfect. The fundamental components have some artifacts on the upper edges. Fig. 4.2-13 illustrates the effects of noise here. Here we have 15 points of cos $5W_N t$ + cos $W_N t$ waveform with an SNR of 24 db, extrapolated in the time domain. Other spectral estimation methods are sensitive to phase shifts of the input sinusoid [8]. Figs. 4.2-14 to 4.2-17 illustrate this method is insensitive to phase. Here we document the perfect restorations for sin $W_N t$ and $\cos(W_N t+\pi/4)$, respectively, in the frequency and time domains.

Figs. 4.2-18 to 4.2-21 indicate the effects of noise. These figures show an 11 sample points of the waveform sin $W_N t$ + cos $W_N t$ with noise and restored. These figures correspond to the cases of SNR of the measured image equal to 20 db, 22 db, 24 db, and 27 db respectively. The restored images possess a SNR of 2.6 db, 2.7 db, 3.3 db, and 4.0 db, respectively. These results are not as immune to noise as could be obtained if we were to relax the desired frequency resolution, i.e. we have obtained an increase of over a factor of two.

4.3 Summary and Conclusion

A new method of spectrum estimation is presented. The method provides superresolving restorations of the frequency spectrum. That is, spectrums of incomplete signals were obtained with frequency resolution greater than that dictated by the uncertainty principle. The method is highly robust to noise. There are two areas where noise components can be eliminated. First noise components are eliminated in the SVD domain of the constructed degradation operator, and the second method is to eliminate high frequency components in the estimated spectrum.

The reconstruction of the Fourier spectrum and phase was obtained from signals truncated to 1/8 of their actual durations without noise. The method is very robust to measurement error providing restorations from 1/2 their actual durations with SNR of 20 db.

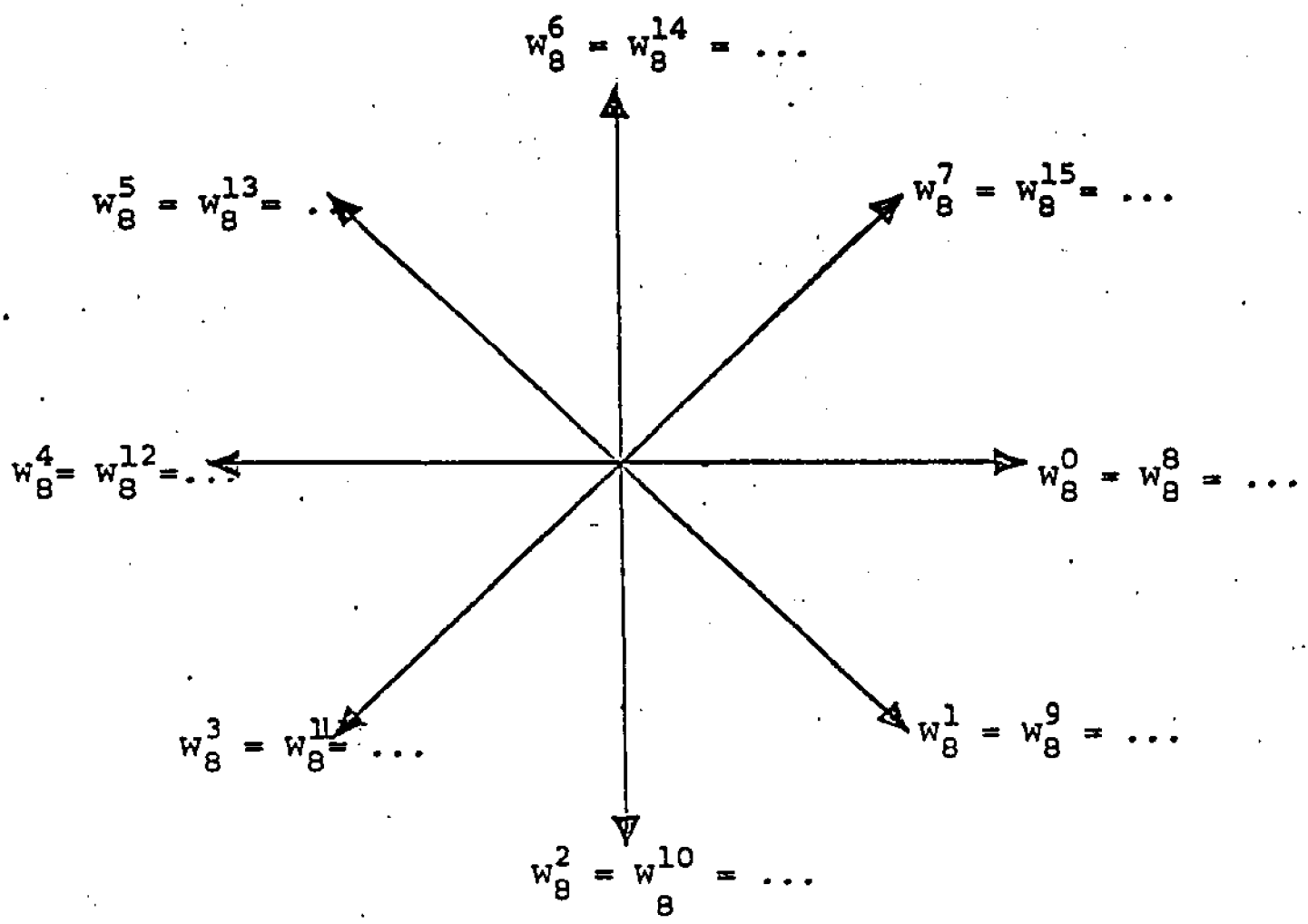

Fig. 4.0-1 Illustration of the equivalence of different powers of W_N with N=8

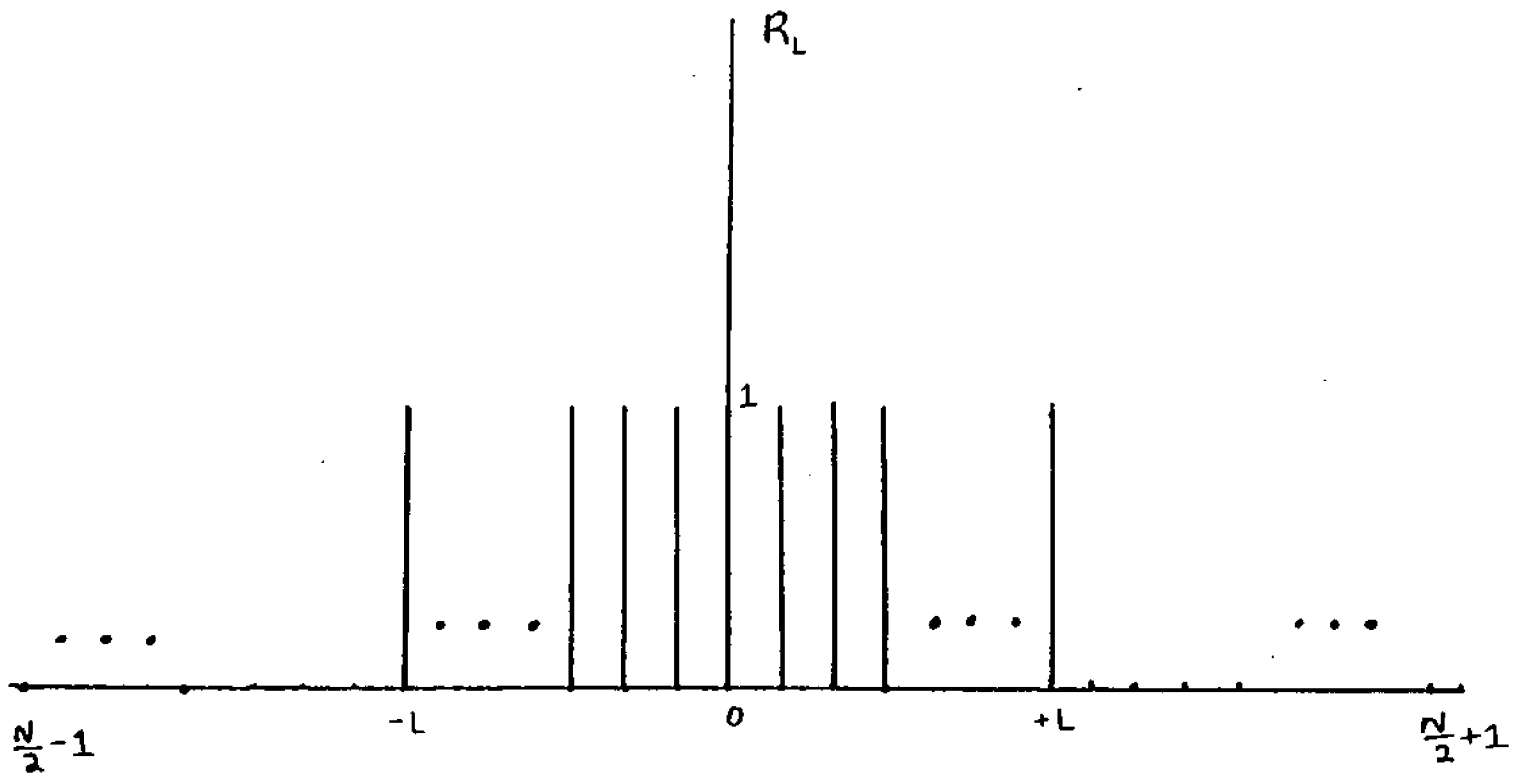

Fig. 4.1-1 The Discrete Time Operator

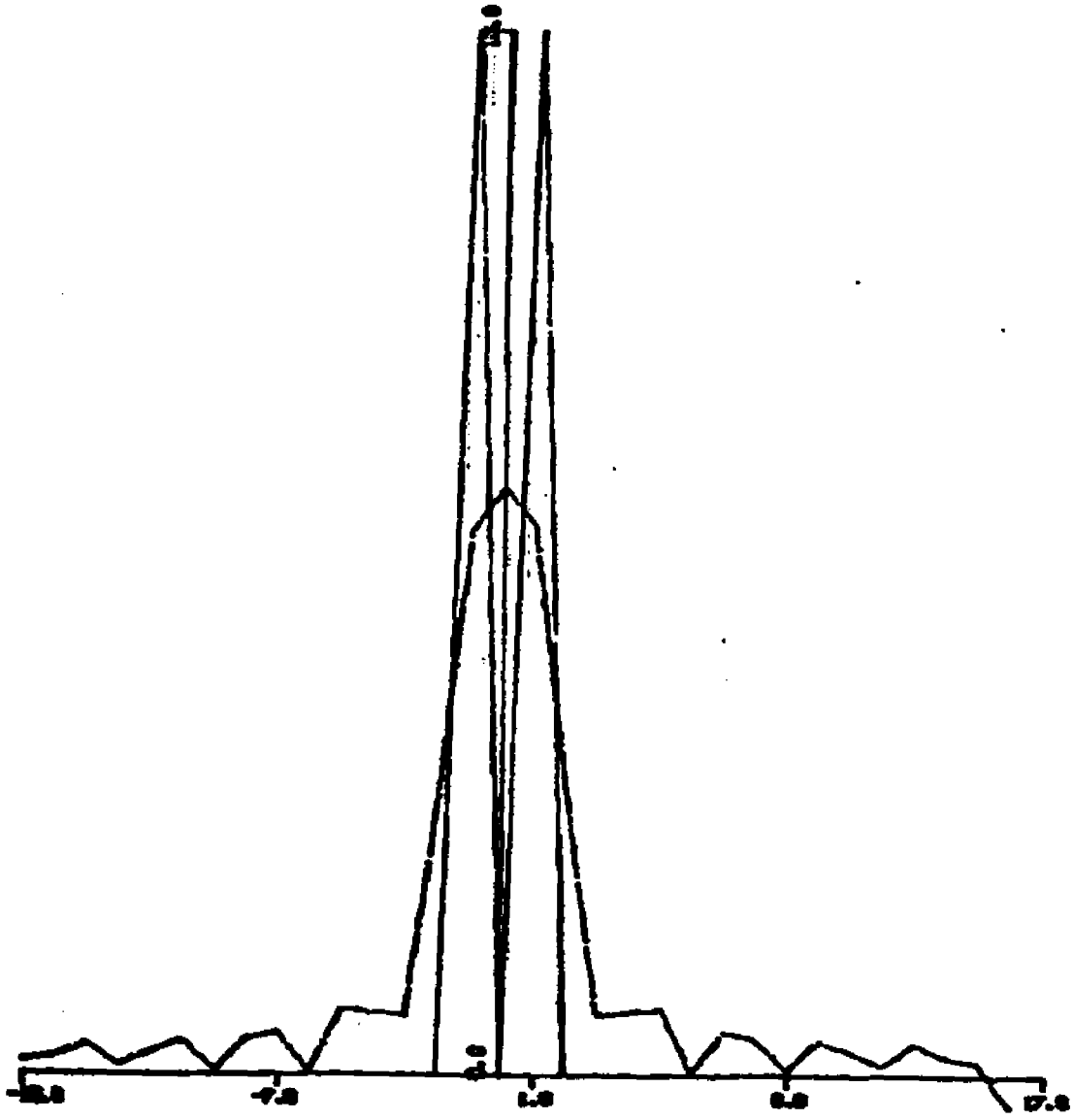

Fig. 4.2-1 The 32 point FFT of 23 points of cos $W_N t$

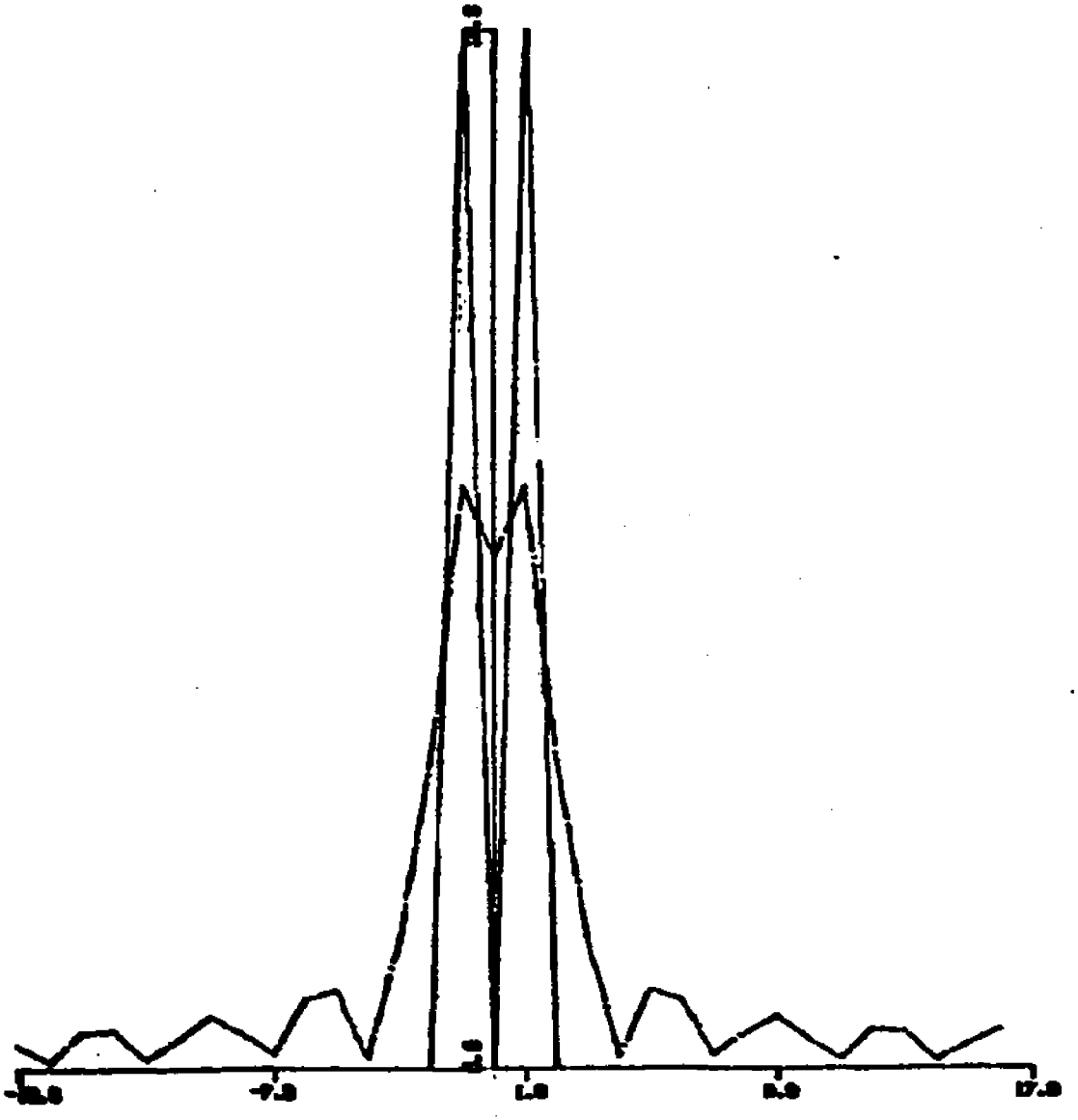

Fig. 4.2-2 The 32 point FFT of 25 points of cos $W_N t$

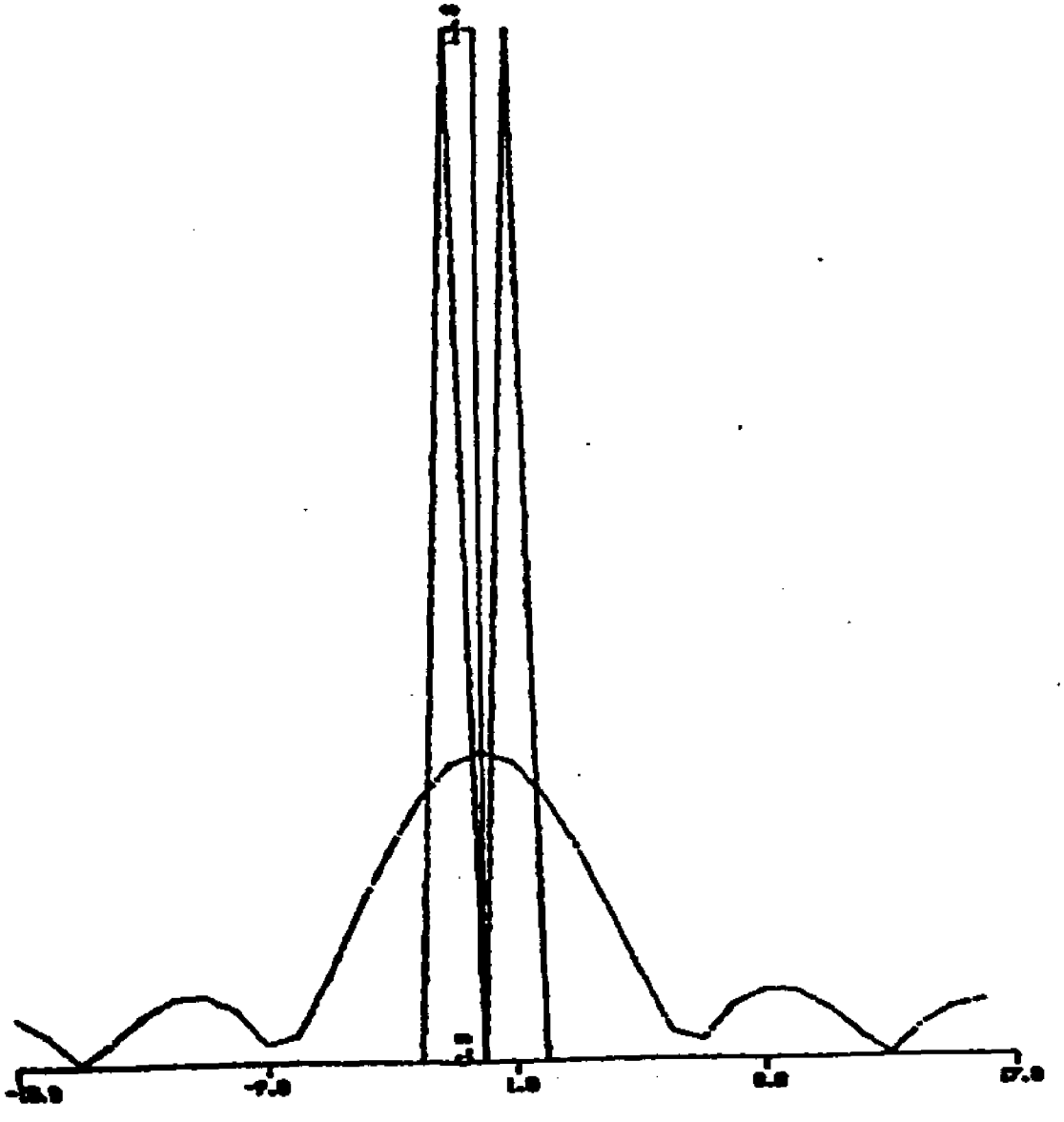

Fig. 4.2-3 Restoration of cos $W_N t$ from 7 points (frequency domain)

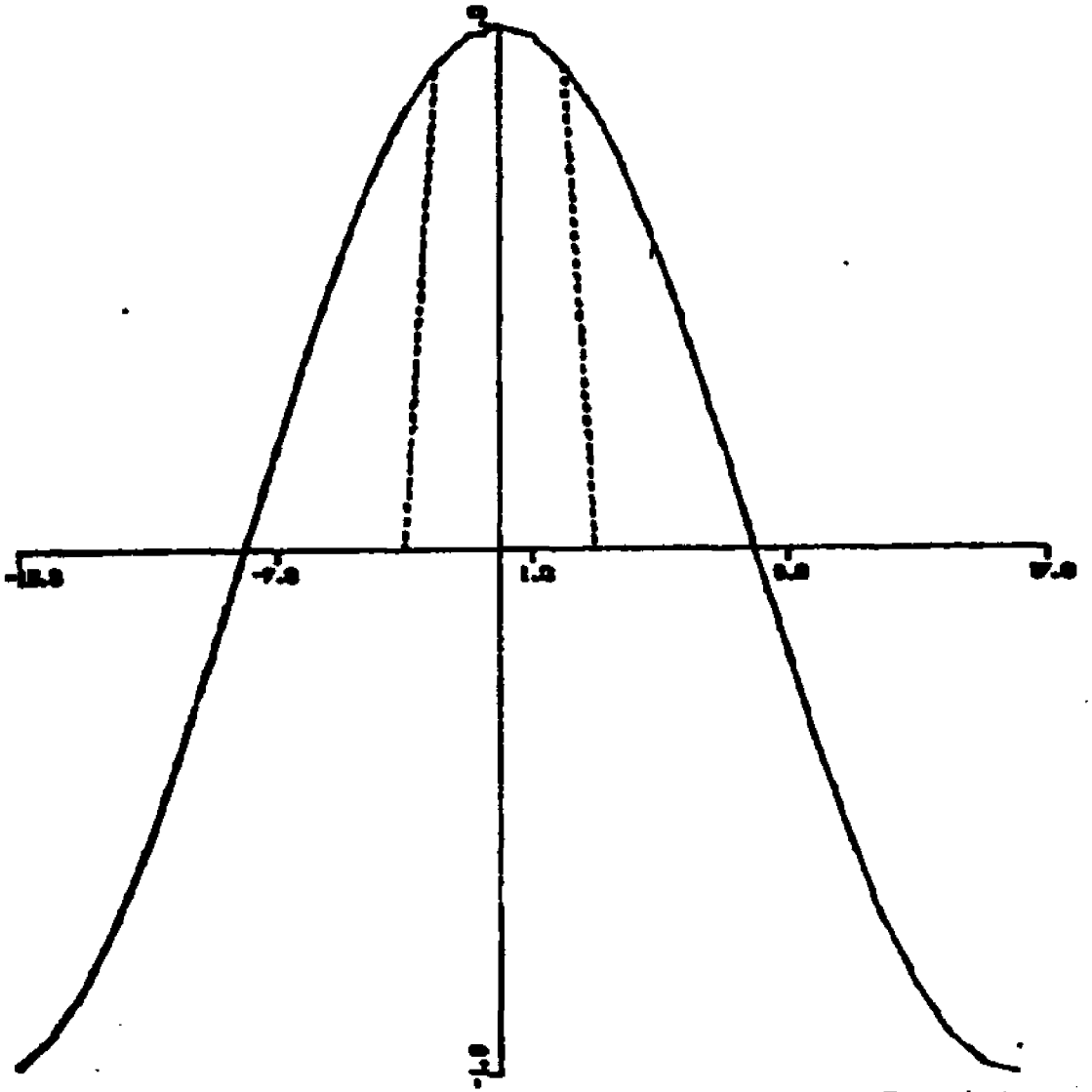

Fig. 4.2-4 Extrapolation of cos $W_N t$ from 7 points (time domain)

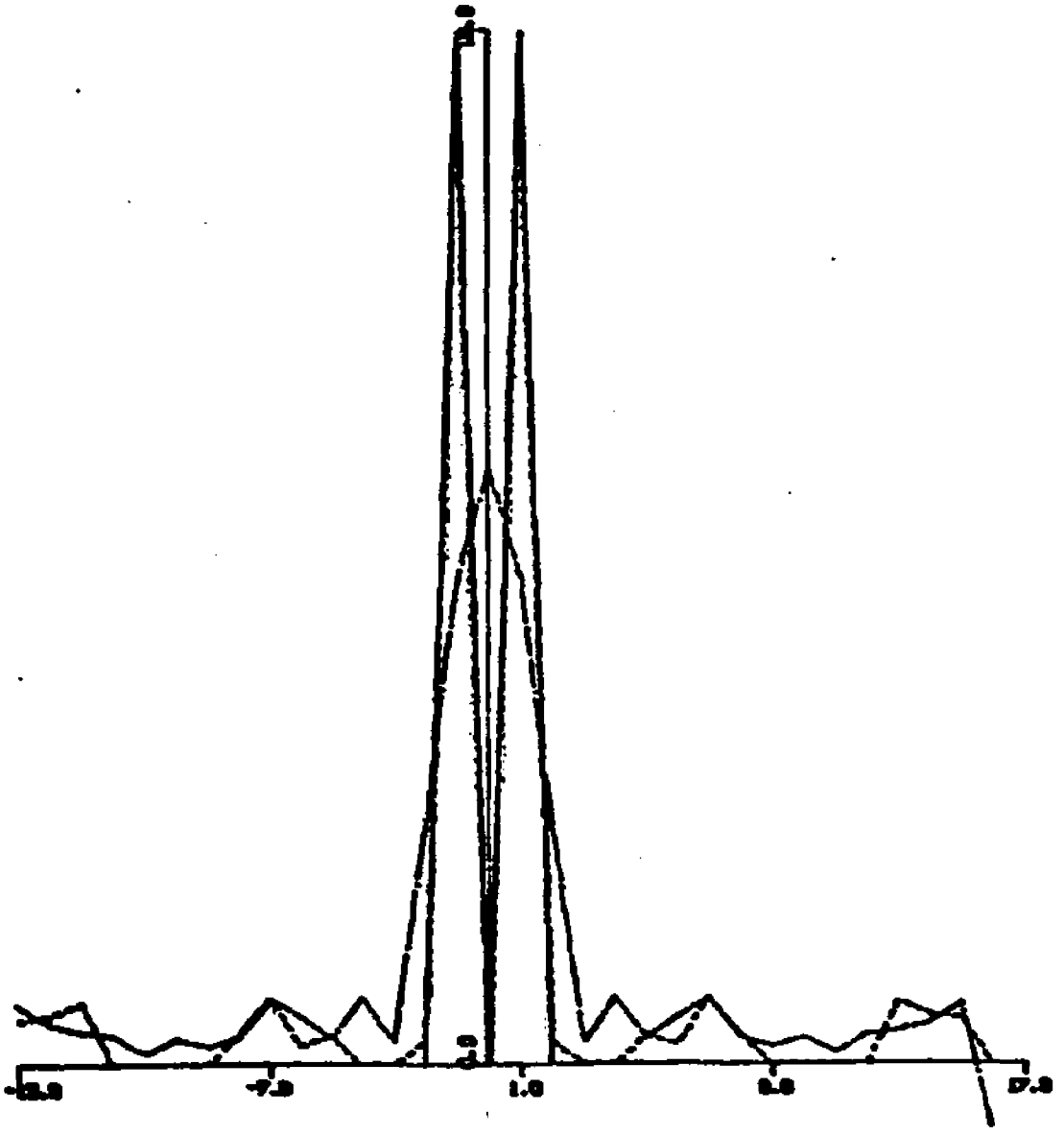

Fig. 4.2-5 Restoration of cos $W_N t$ from 15 points with noise SNR = 27 db (frequency domain)

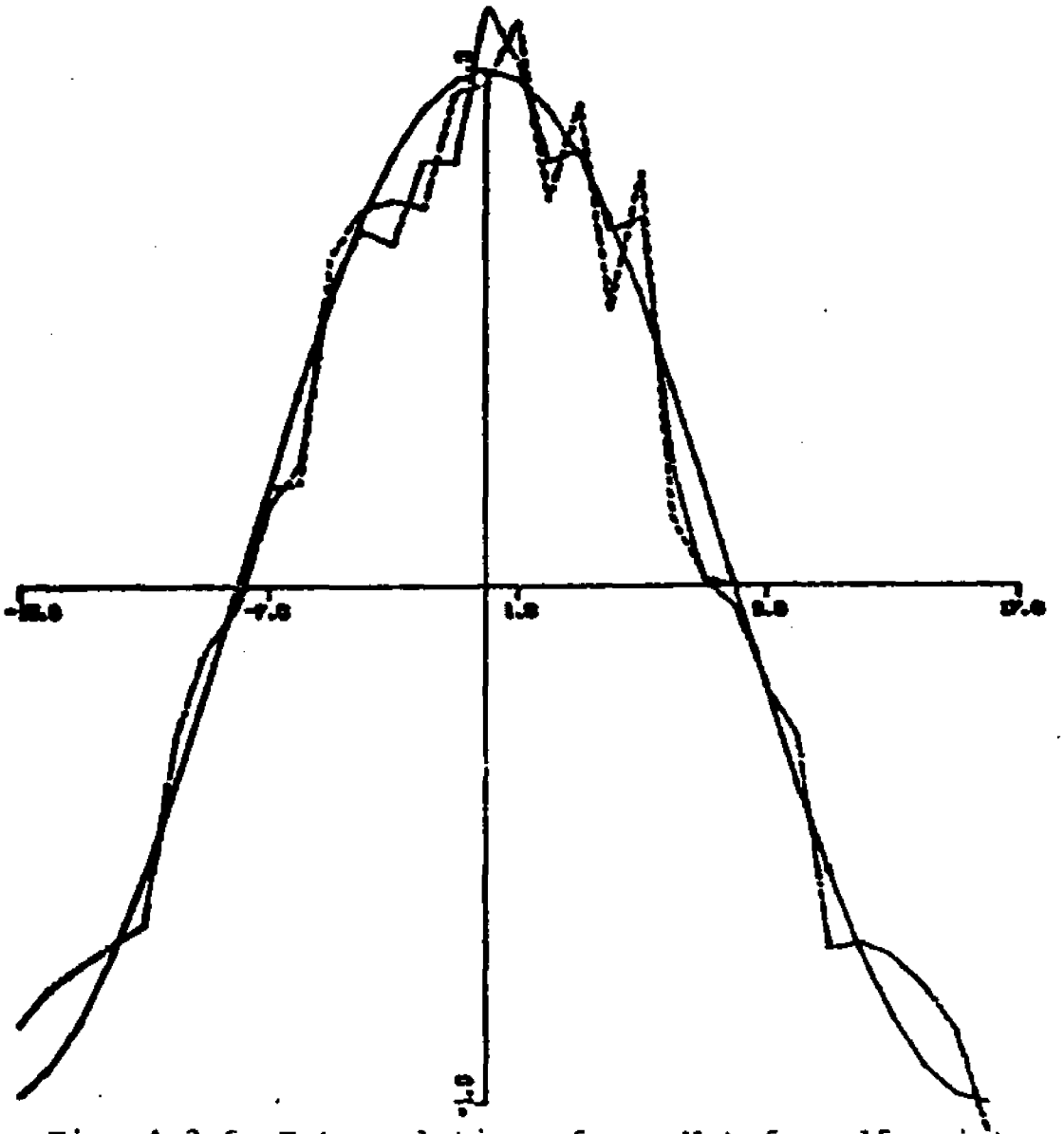

Fig. 4.2-6 Extrapolation of cos $W_N t$ from 15 points with noise SNR = 27 db (time domain)

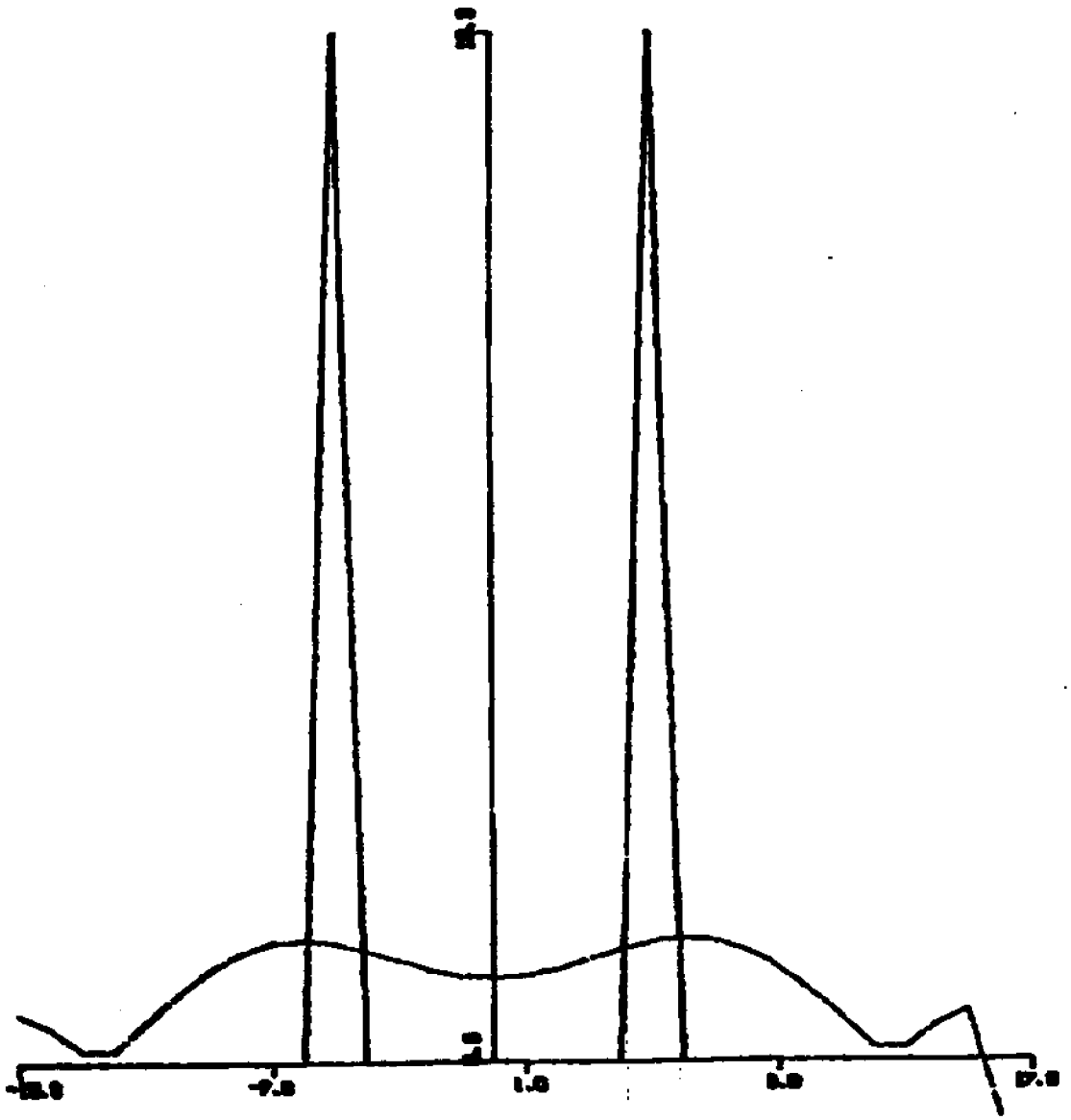

Fig. 4.2-7 Restoration of cos $5W_N t$ from 7 points (frequency domain)

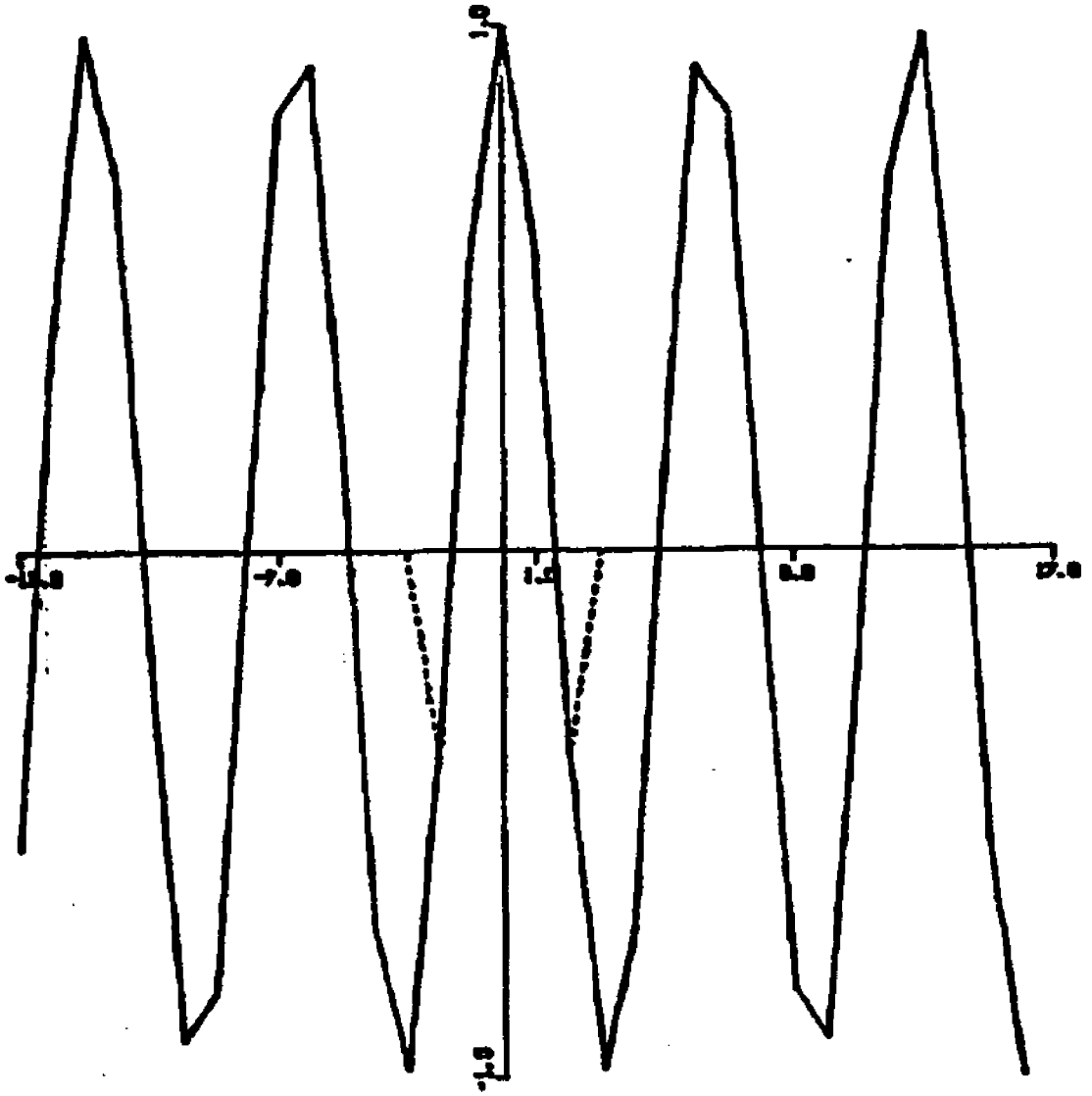

Fig. 4.2-8 Extrapolation of cos $5W_N t$ from 7 points (time domain)

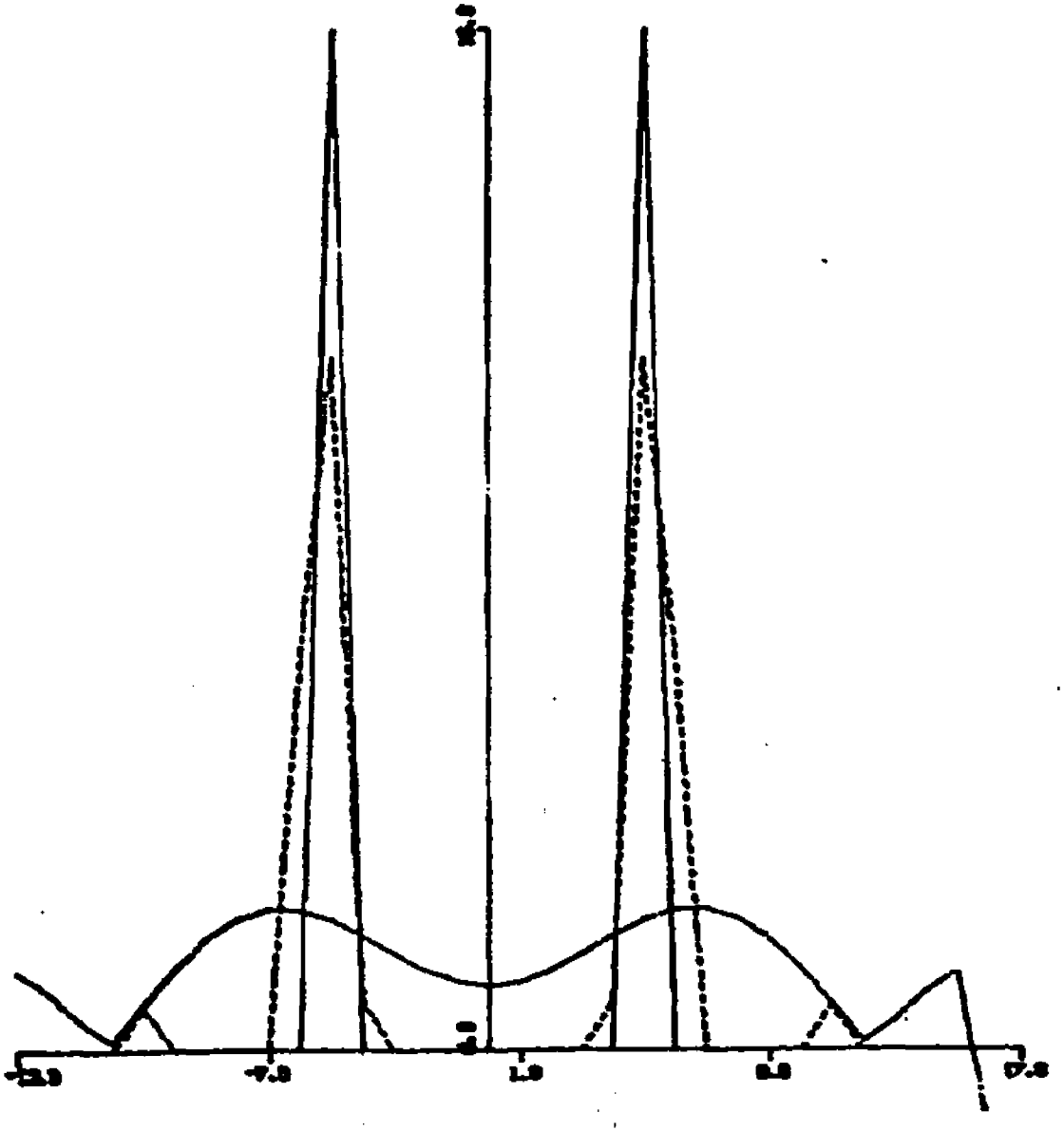

Fig. 4.2-9 Restoration of cos $5W_N t$ from 7 points with noise such that SNR = 20 db

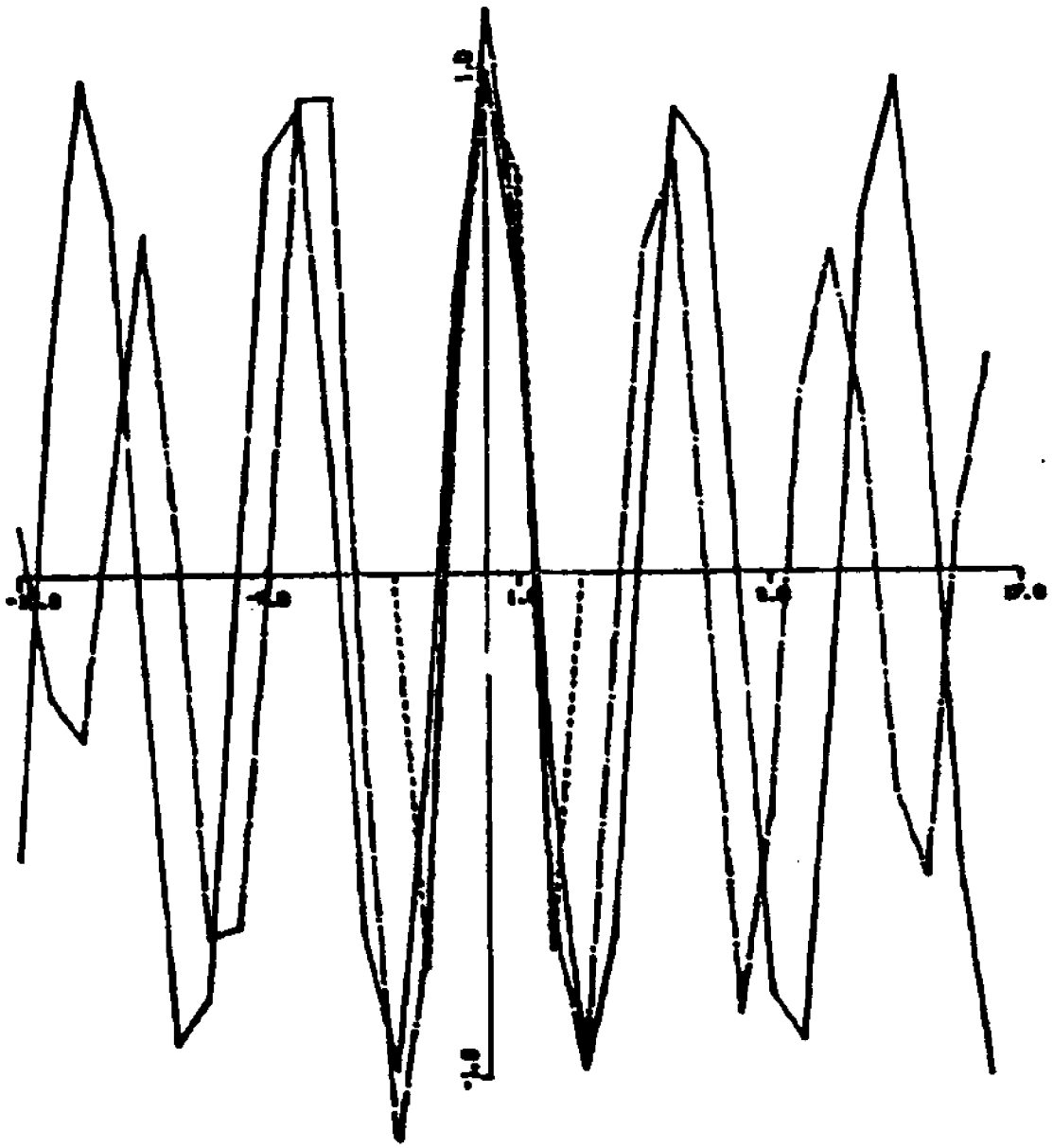

Fig. 4.2-10. Extrapolation of cos $s_N t$ from seven points from 7 points with SNR $\stackrel{\Delta}{=}$ 20dB (time domain)

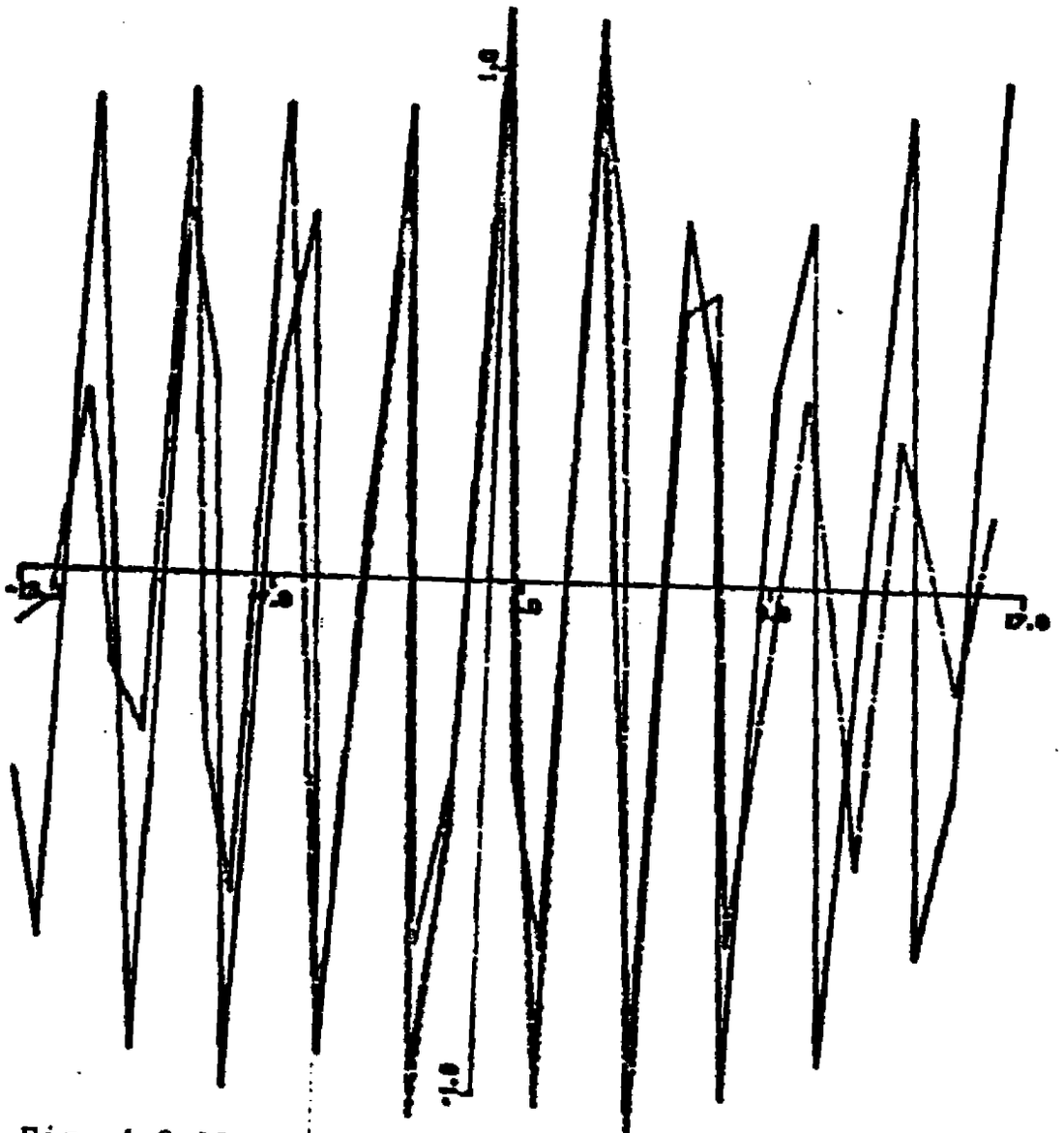

Fig. 4.2-11 Extrapolation of $\cos 10W_N t$ from 9 points with SNR = 19 db

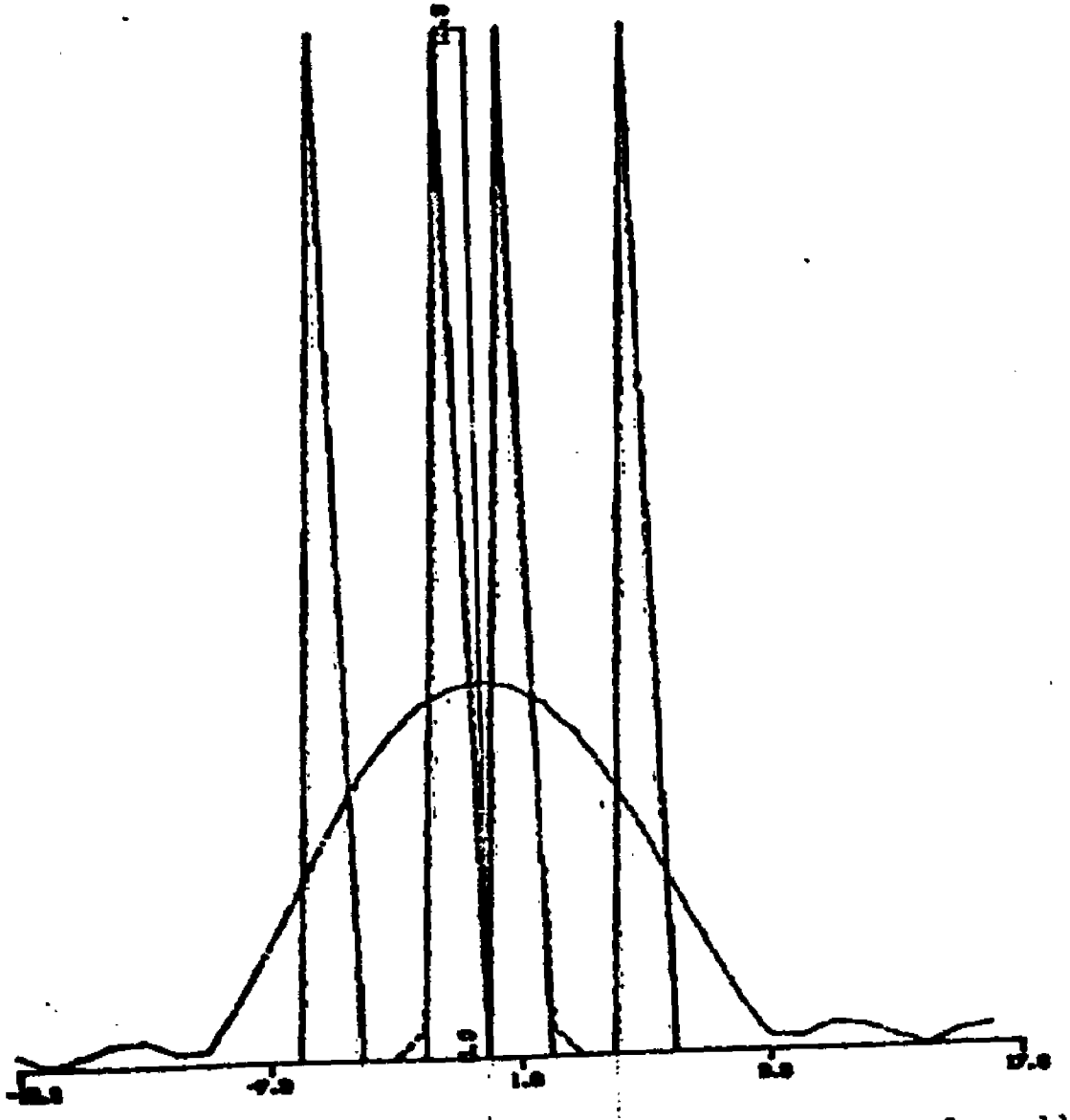

Fig. 4.2-12 Restoration of cos $W_N t$ + cos $5W_N t$ from 11 points

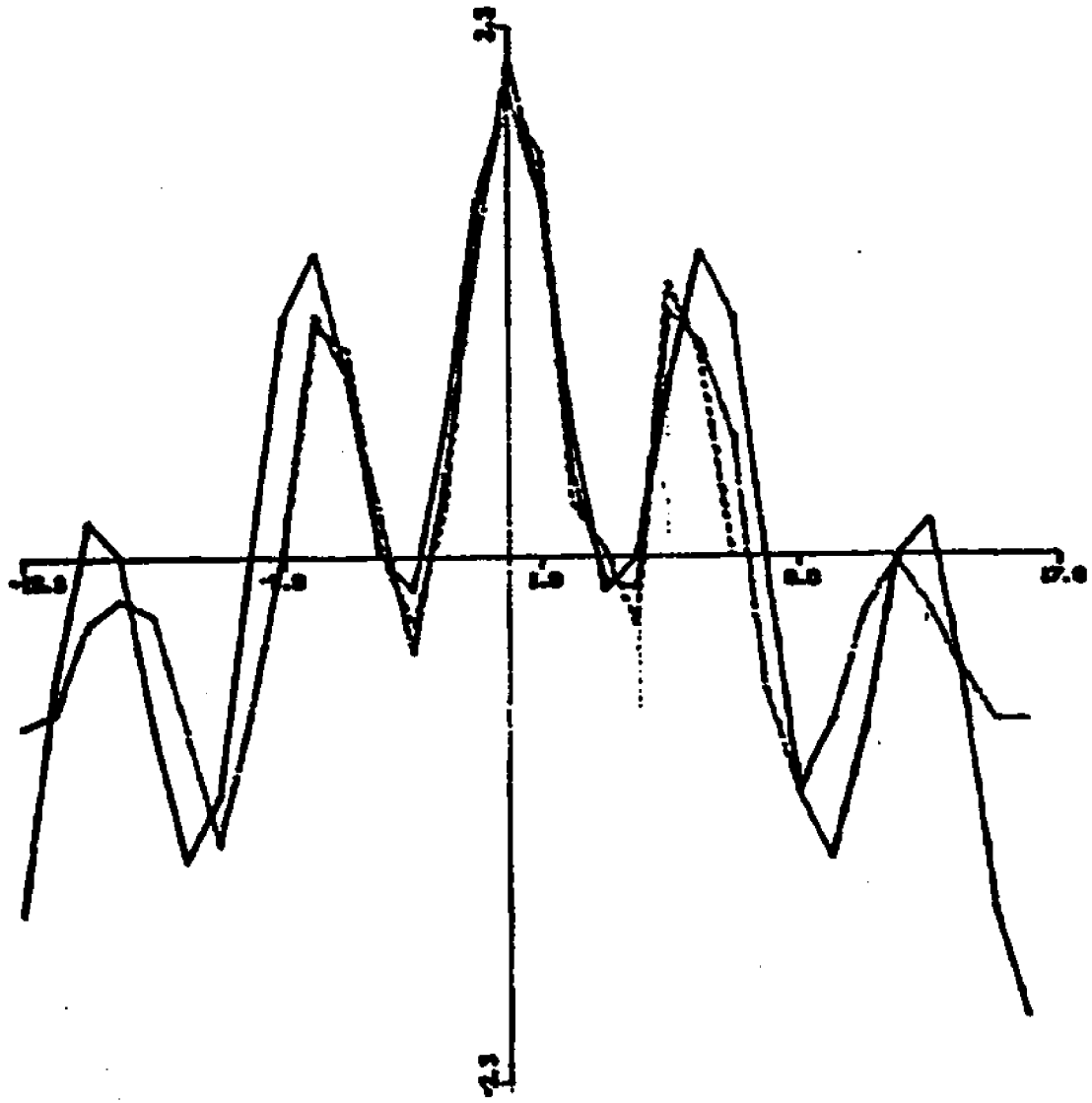

Fig. 4.2-13 Extrapolation of cos $W_N t$ + cos $5W_N t$ from 15 points with SNR = 24 db

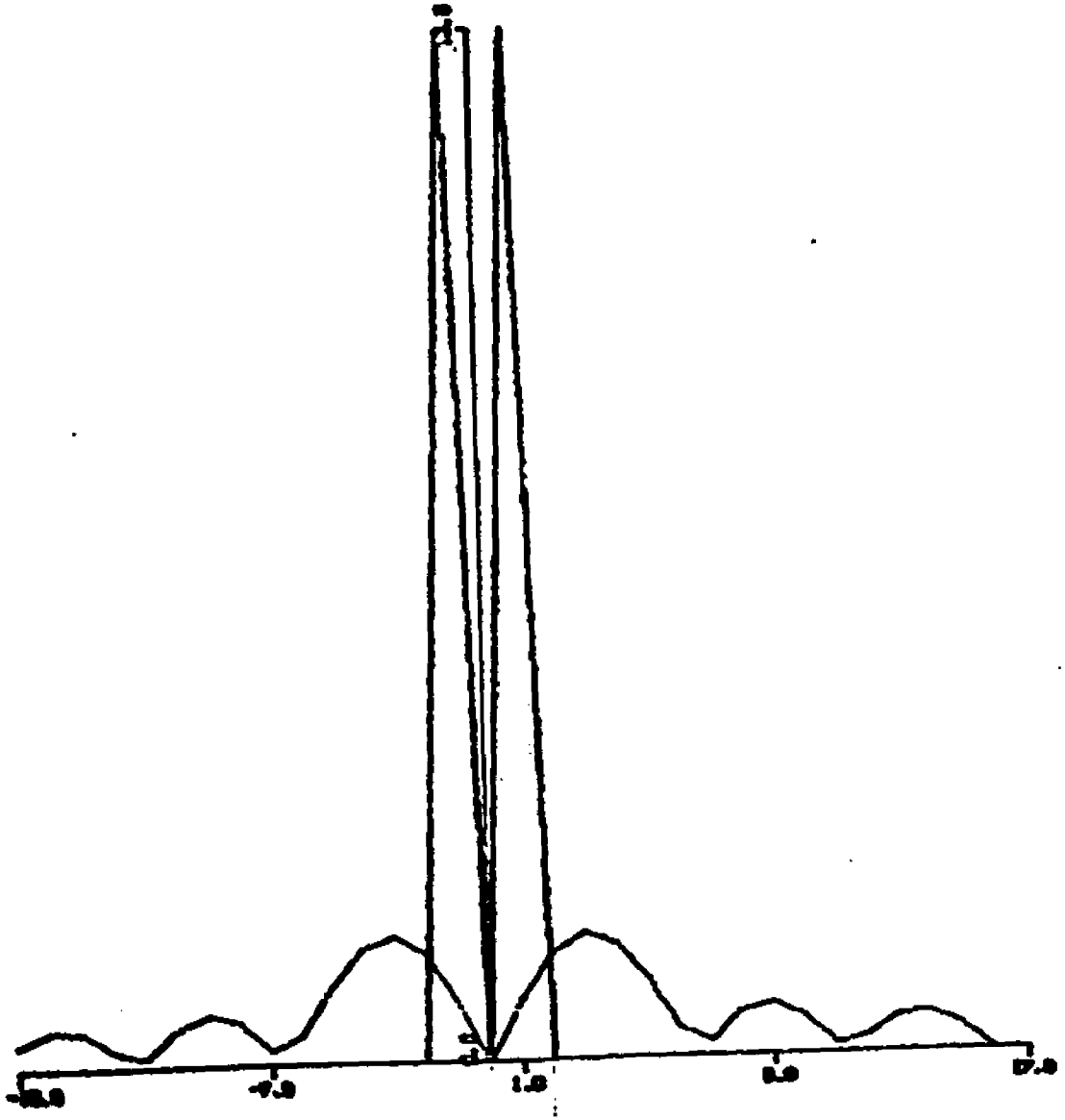

Fig. 4.2-14 Restoration of sin $W_N t$ from 7 points

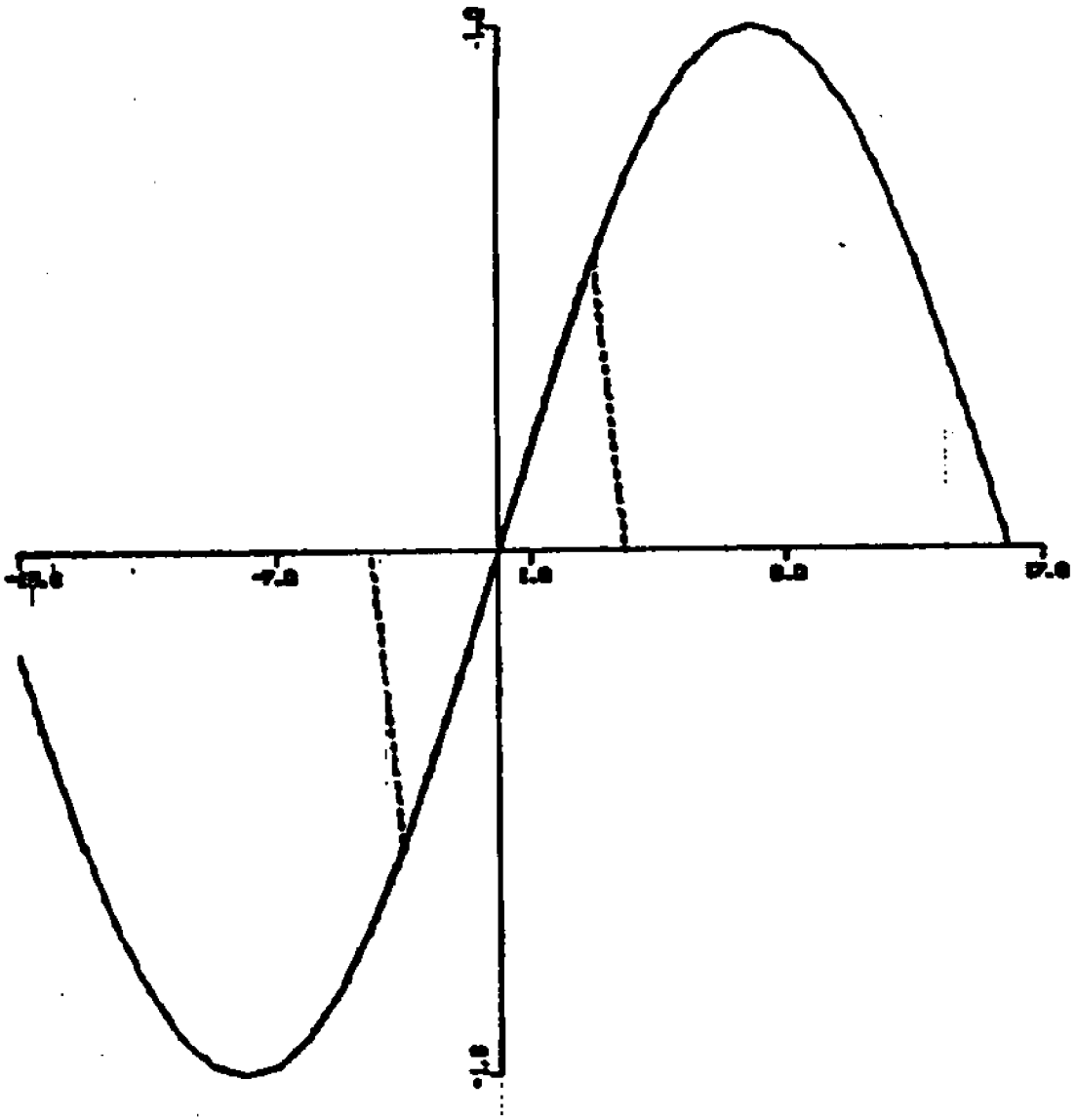

Fig. 4.2-15 Extrapolation of sin $W_N t$ from 7 points in the time domain

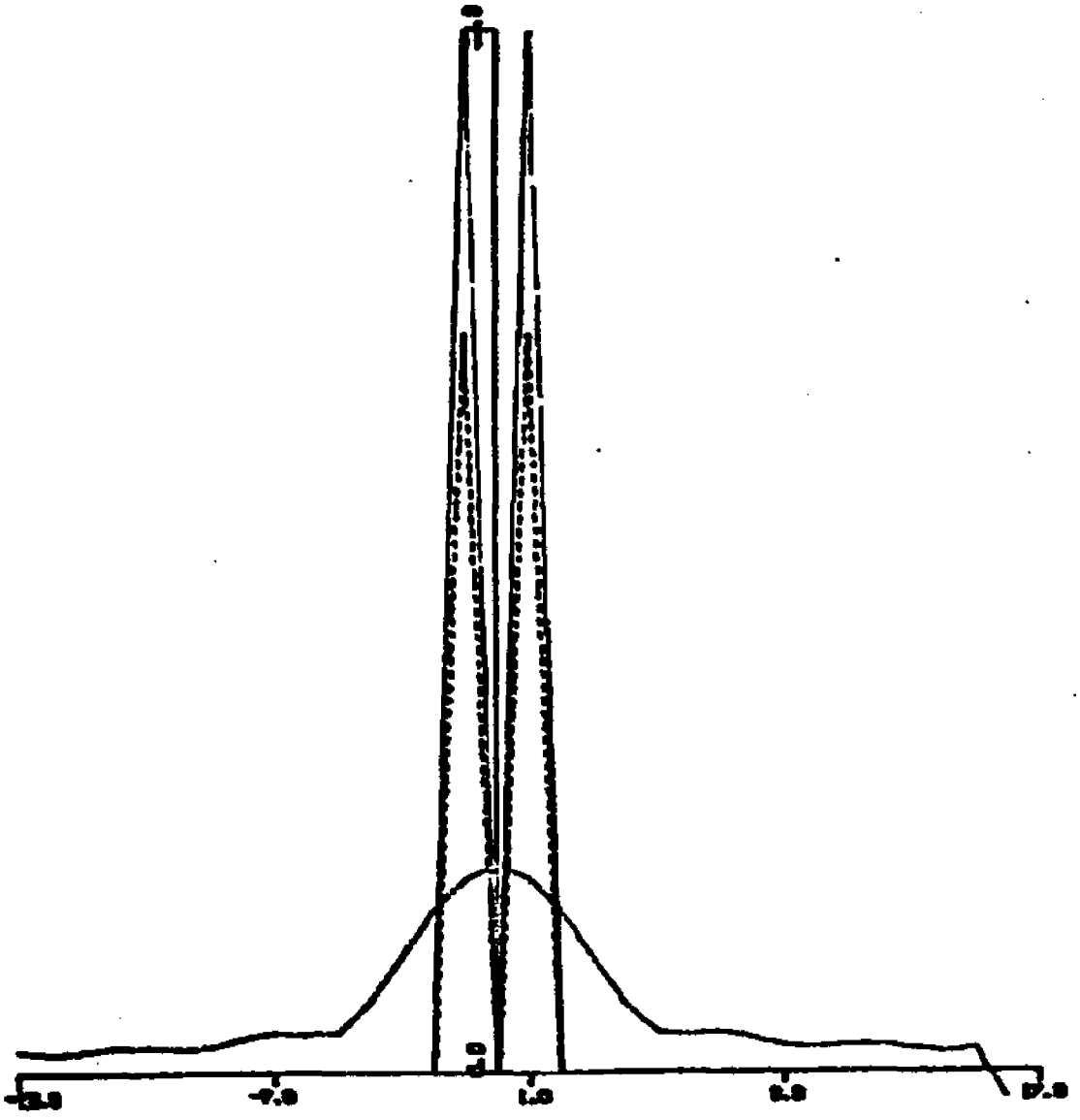

Fig. 4.2-16 Restoration of cos $W_N t$ + sin $W_N t$ from 7 points (frequency domain)

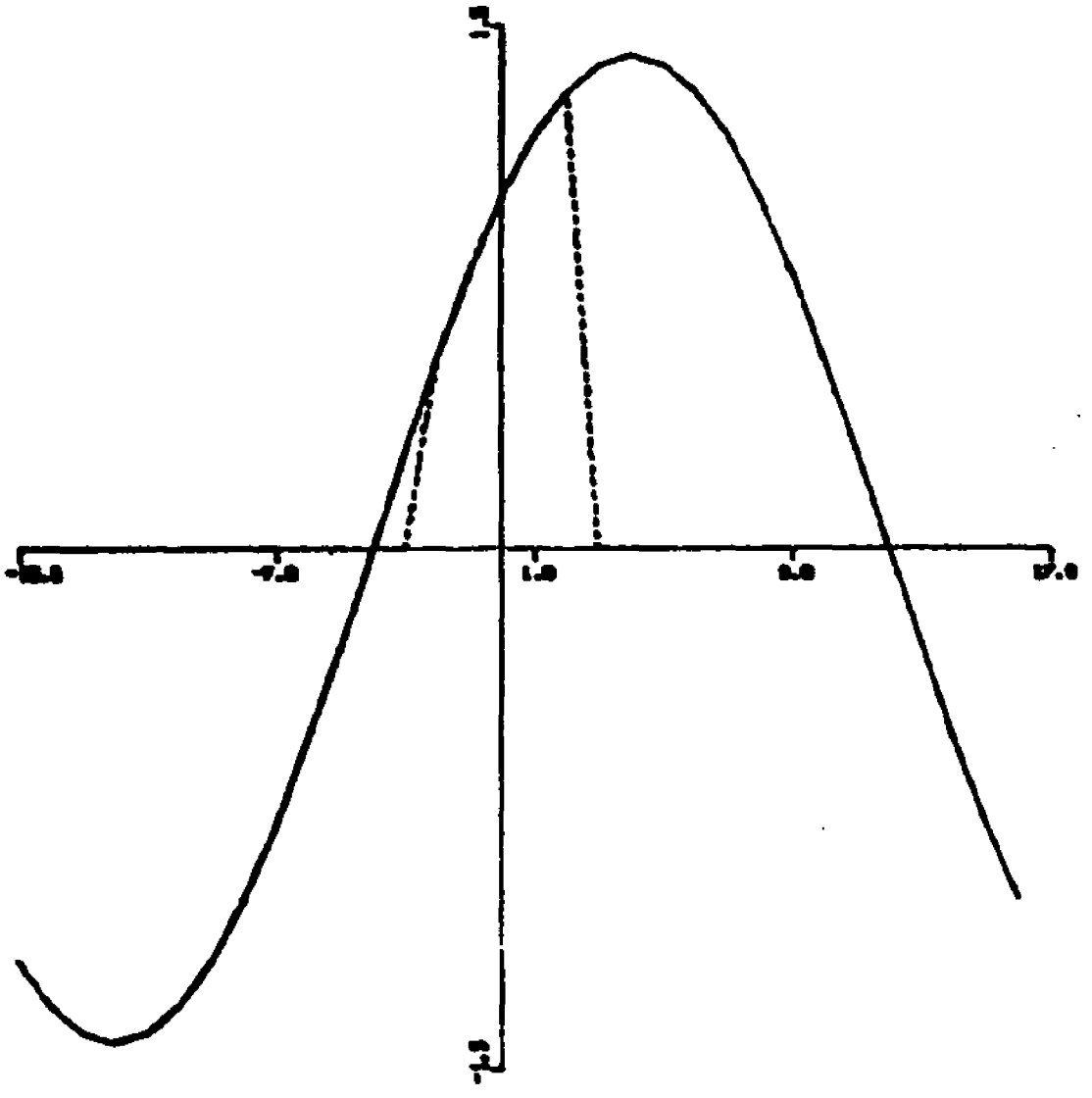

Fig. 4.2-17 Extrapolation of cos $\omega_N t$ and sin $\omega_N t$ from seven points (time domain)

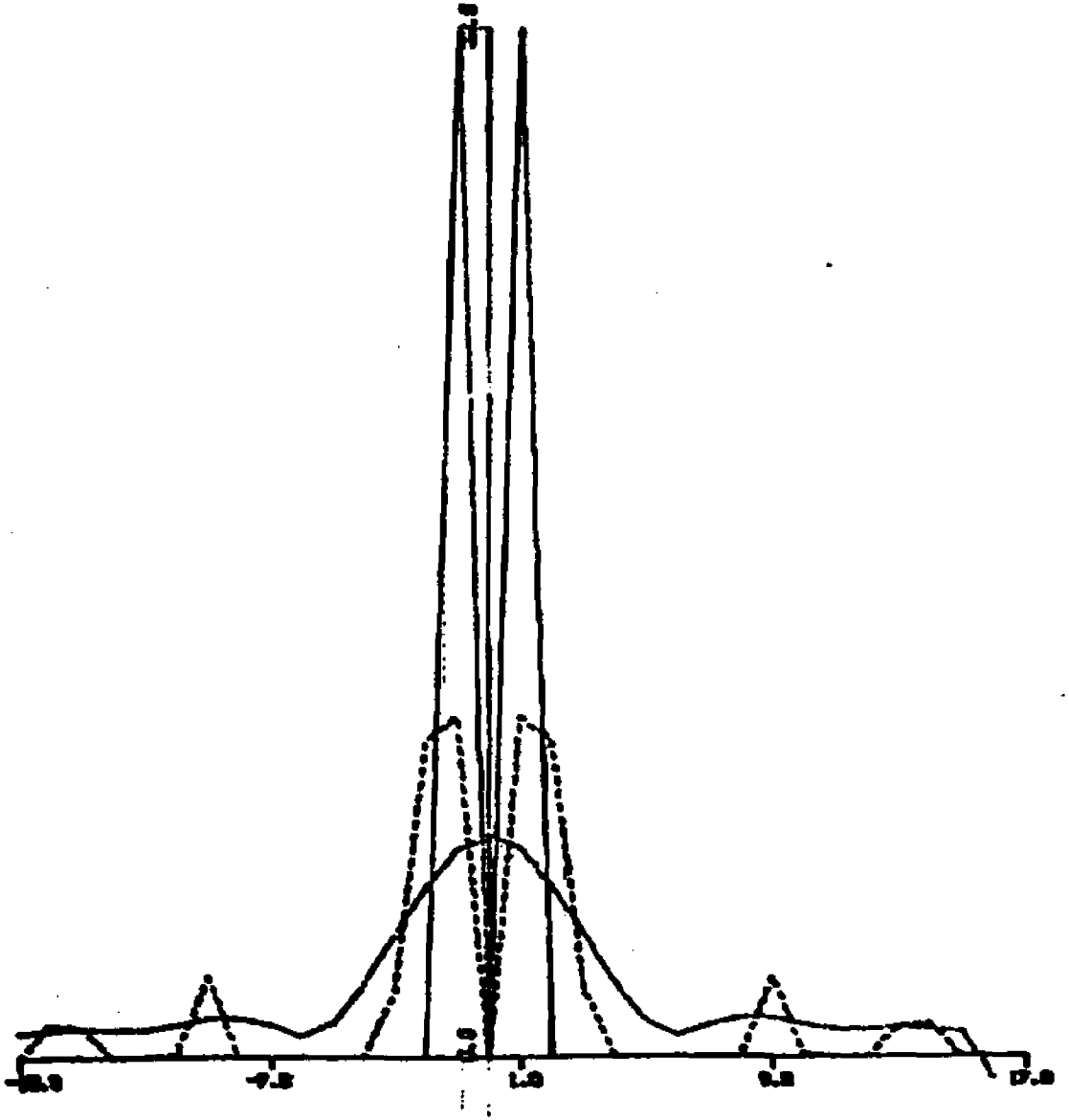

Fig. 4.2-18 Restoration of 11 points of cos $W_N t$ + sin $W_N t$ with an SNR = 20 db

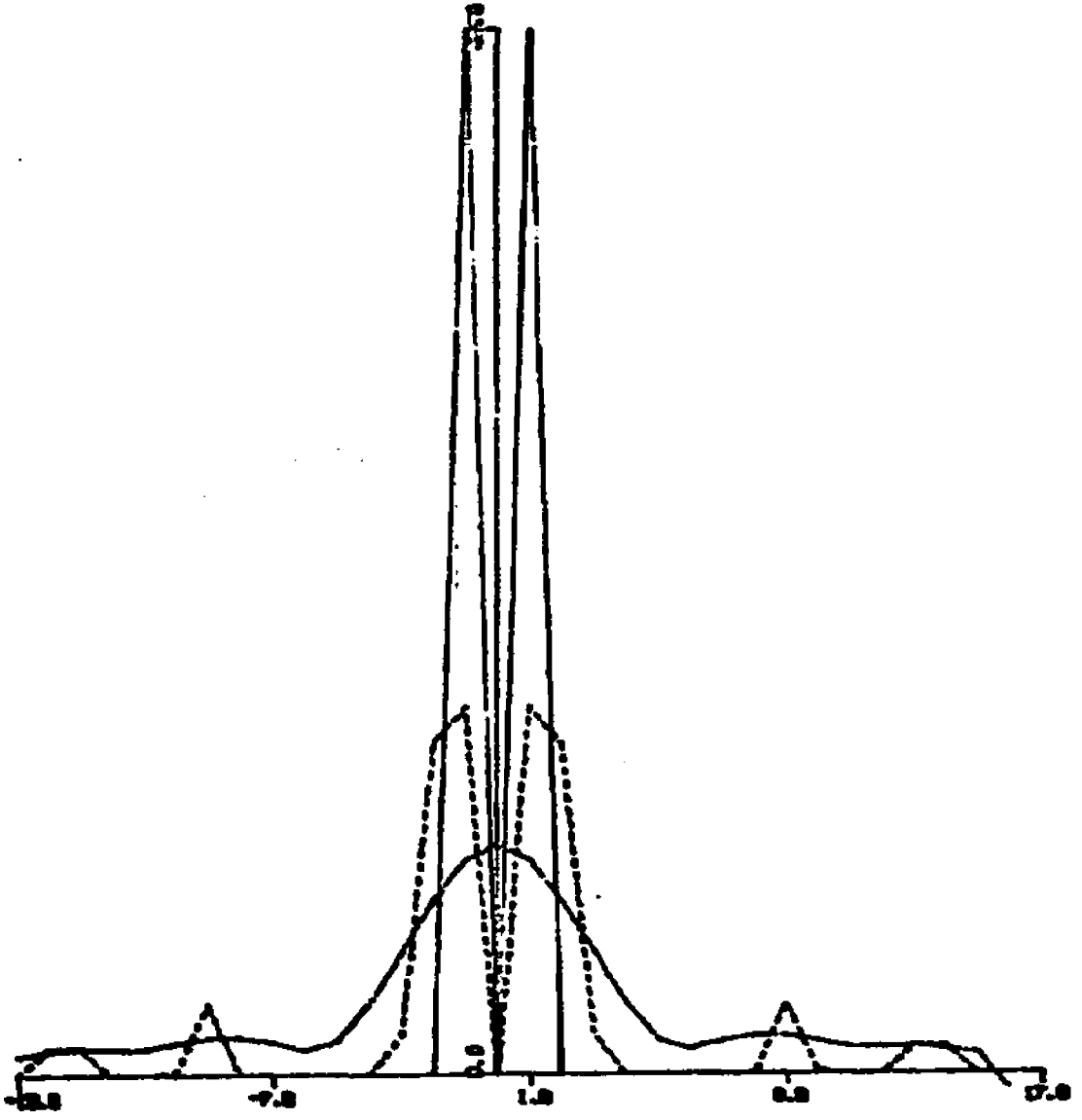

Fig. 4.2-19 Restoration of 11 points of cos $W_N t$ + sin $W_N t$ with an SNR = 22 db

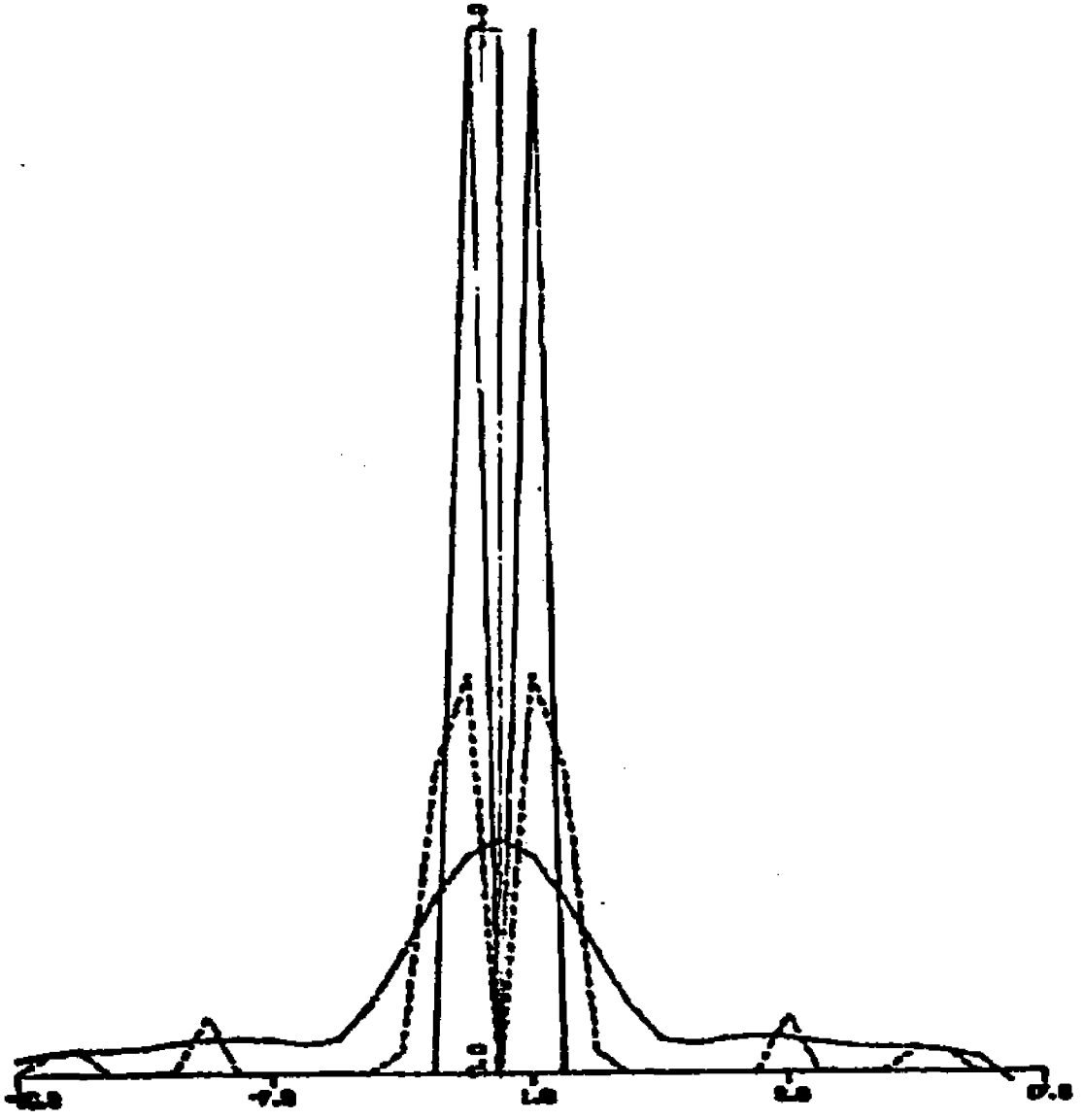

Fig. 4.2-20 Restoration of 11 points of cos $W_N t$ + sin $W_N t$ with an SNR = 24 db

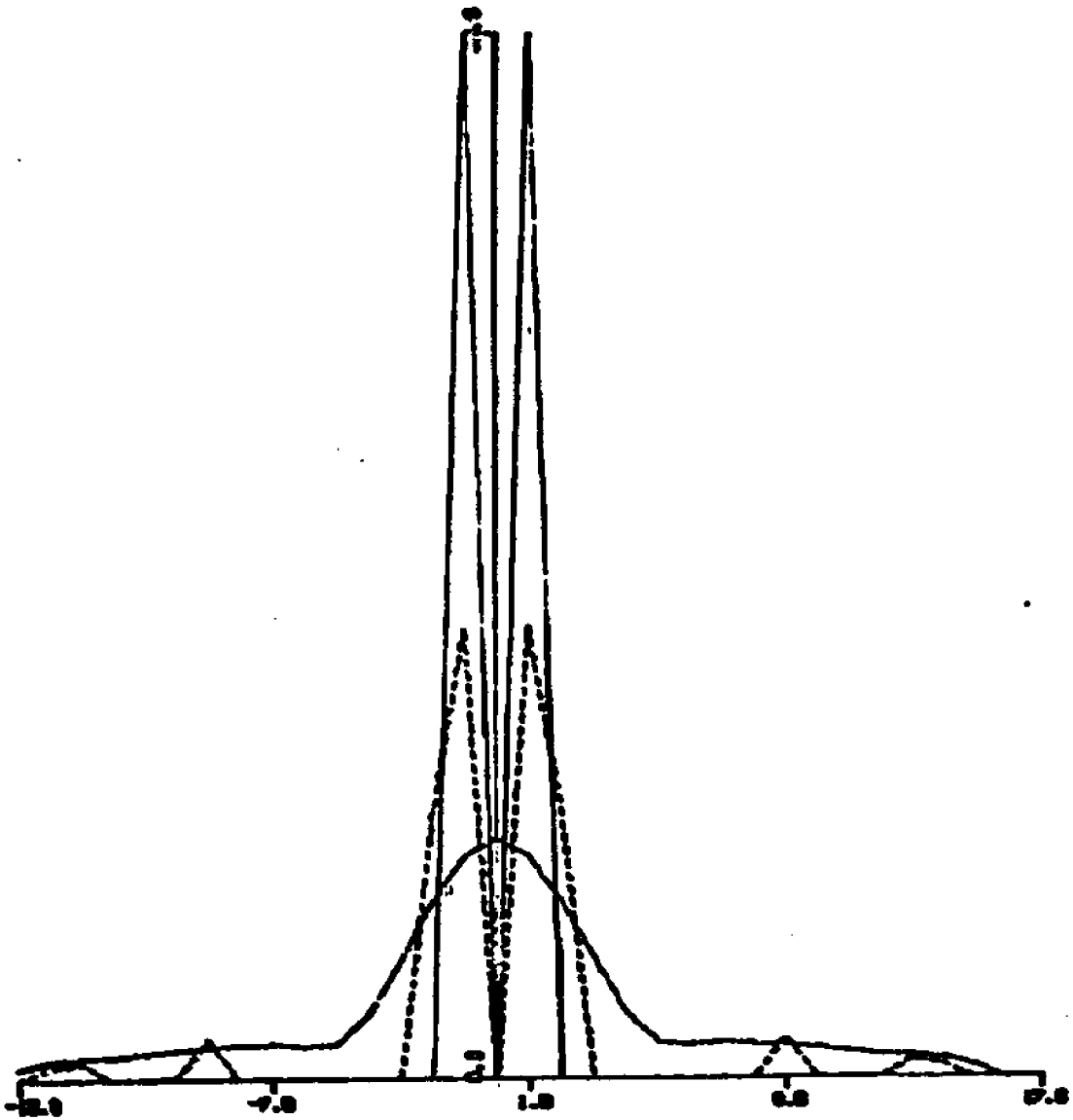

Fig. 4.2-21 Restoration of 11 points of cos $W_N t$ + sin $W_N t$ with an SNR = 27 db

Chapter 5

SUPERRESOLVING APODIZATION

5.0 Introduction

In many optical applications it is desired to shape the intensity profile at the focal plane [38]. This shaping is performed by placing a window function in front of the imaging system (Apodization). If the concentration of the energy distribution in the focal plane lies within a smaller area with the window function, then the Apodization is called superresolving [39]. The back and front focal planes of an imaging system are linked by a two dimensional transform relationship. Thus the uncertainty principle applies. Here the uncertainty statement is a relationship between the size of the input aperture and the spot size in the focal plane. Thus a smaller spot size in the focal plane corresponds to a larger effective numerical aperture. This can be seen by the scaling principle of the Fourier transform, i.e.

$$f(at) = \frac{1}{a}F(\omega/a) \qquad (5.0\text{-}1)$$

This is one reason for apodizing the entrance pupil of an imaging system. Another reason for apodizing for a smaller spot-size is for hole burning applications. For example, the recent development of video disks which employ holes

made by a laser could have increased storage density if each hole could be reduced in size and made more uniform. This application is the prime motivation of the research developed in this chapter.

5.1 Coherent Source Focusing System

For a coherent spherical lens system the two dimension front and back focal plane Fourier relationship can be reduced in the case of a rotationally symmetric input

$$g(r) = \int_0^1 f(u) J_0(ur)\ u\,du \qquad (5.1\text{-}1)$$

where g(r) and f(u) are the radially symmetric backfront focal plane amplitude distributions and J_0 is the Bessel function of the first kind and zeroth order. Eq. (5.1-1 is a Hankel Transform relationship between f and g. The Apodization problem for minimum uniform spot size can now be posed.

Given an amplitude distribution g(r) with minimal distance between the first zero crossings and minimal sidelobes find a transmission density profile which will yield the closest possible positive amplitude distribution to the desired g(r). The transmission profile can only take on values between zero and unity. n^+ and n^- represent the absolute value of the residual error between the Hankel Transform of the estimate and the desired g(r) focal plane amplitude distribution.

This problem can be formulated as a linear programming problem, i.e.

$$\text{Minimize:} \quad n_1^+ + n_1^- + n_2^+ + n_2^- + \ldots n_N^+ + n_N^- \tag{5.1-2}$$

$$\text{Subject to:} \quad g = Hf + \eta^+ \eta + \eta^- \tag{5.1-3}$$

$$f \leq I_1 \tag{5.1-4}$$

$$f \geq 0 \tag{5.1-5}$$

where g, f and n^+ and n^- are obtained from Eq. (5.1-1) in the same manner as in Chapter 3. $\underline{H}$ is the matrix representation of the integral operator in Eq. (5.1-1) obtained by a quadrature rule, and I_1 is column vector defined as

$$I_1 = \begin{bmatrix} 1 \\ 1 \\ \vdots \\ 1 \end{bmatrix} \tag{5.1-6}$$

The restrictions of Eq. (5.1-5) and (5.1-6) can be relaxed if phase-sensitive or holographic materials are used, allowing complex amplitude distributions. In this formulation it is assumed that the transparency is illuminated with a constant plane wave. Although in practice other, i.e. Gaussian distributions are also used.

5.2 Incoherent Source Focusing System

The basic numerical Apodization approach can be applied to an incoherent-Source Focusing System. The imaging equation of Eq. (5.1-1) is now changed to

$$g'(r) = \int_0^1 f(u) J_0^2(ru)\, u\, du \tag{5.2-1}$$

where g'(r) and f'(u) are the intensities of the light distribution in the back and front focal planes, respectively.

The new kernel is the square of the zero order Bessel function. Note here the unknown represents light intensity whereas previously the unknown was a light amplitude. The new Apodization problem can be set up in the same fashion as the coherent case. The only change is in the degradation kernel and in the interpretation of the quantities under consideration.

5.3 Computer Simulation and Results

Fig. 5.3-1 illustrates the amplitude distribution for a spherical lens system with no Apodization. Fig. 5.3-2 shows the effect of Apodization. Note the central lobe has been compressed by ~25% and with very little side lobe gain. The transmission profile is illustrated on the same illustration by the chain dot curve. The scale for the transmission profile is 1/10 that of the amplitude distribution. Fig. 5.3-3 illustrates the incoherent case with no apodization. Note the lack of zero intensity due to lack of total destructive interference. Fig. 5.3-4 illustrates the optimal apodization intensity pattern. Again, a compression of about 25% is realized. The sidelobe level of the apodized pattern is not increased at all; this is very desirable for many applications.

We have found optimal design for Apodization Masks for both coherent and incoherent optical systems. The designs offer approximately 25% compression of the main lobe with very little gain in the sidelobe levels.

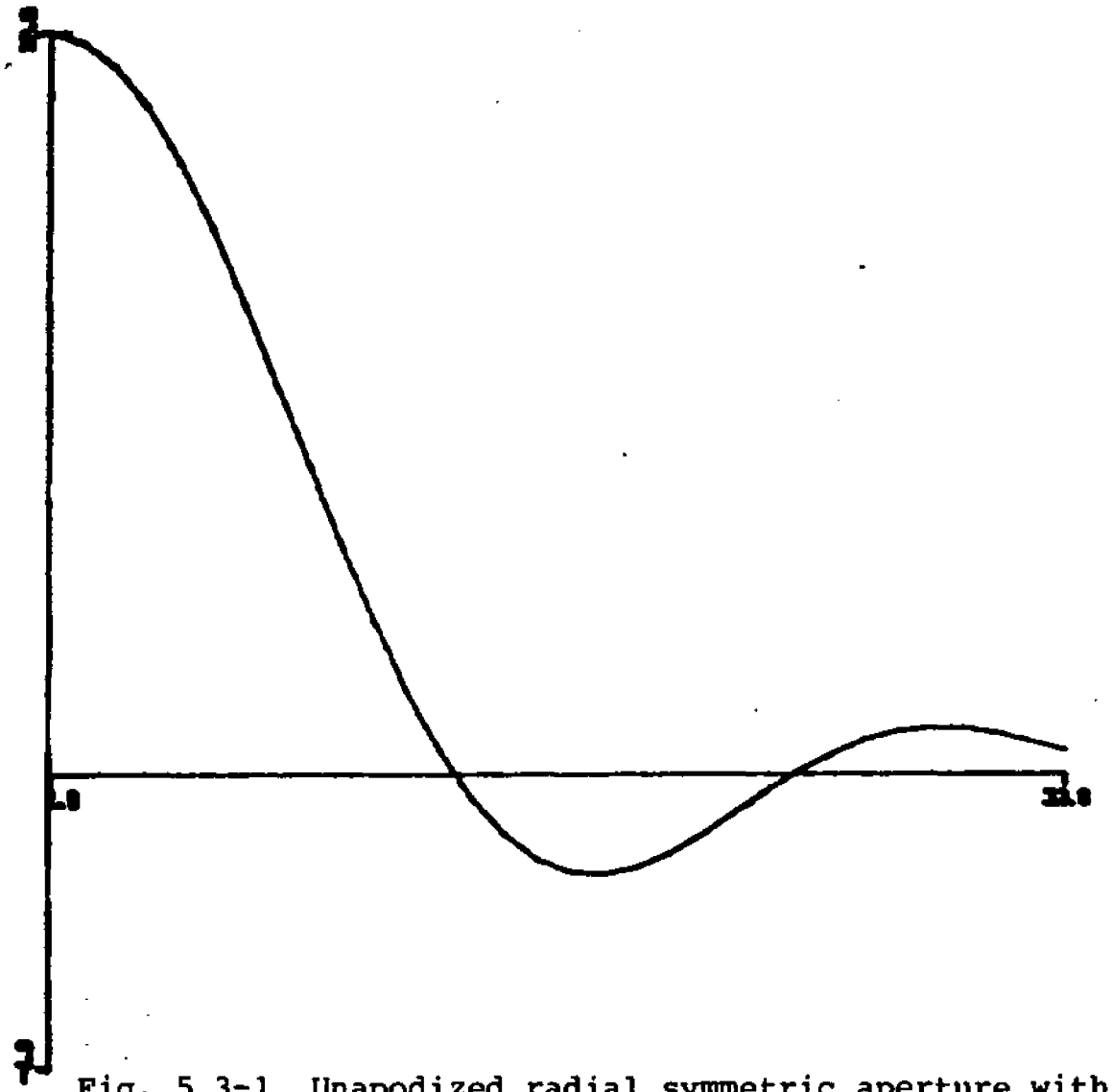

Fig. 5.3-1 Unapodized radial symmetric aperture with a coherent source

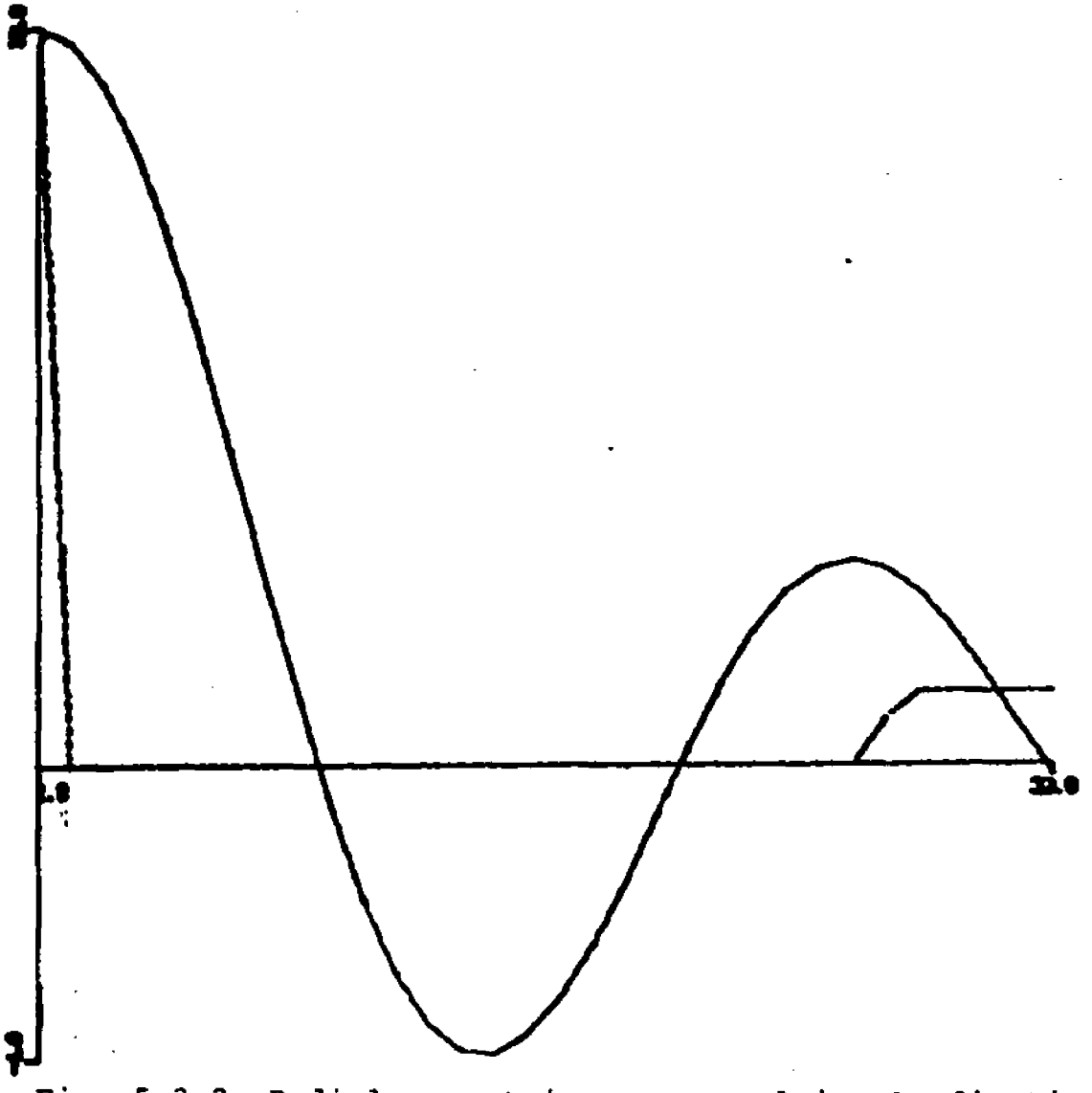

Fig. 5.3-2 Radial symmetric superresolving Apodization of a coherent source

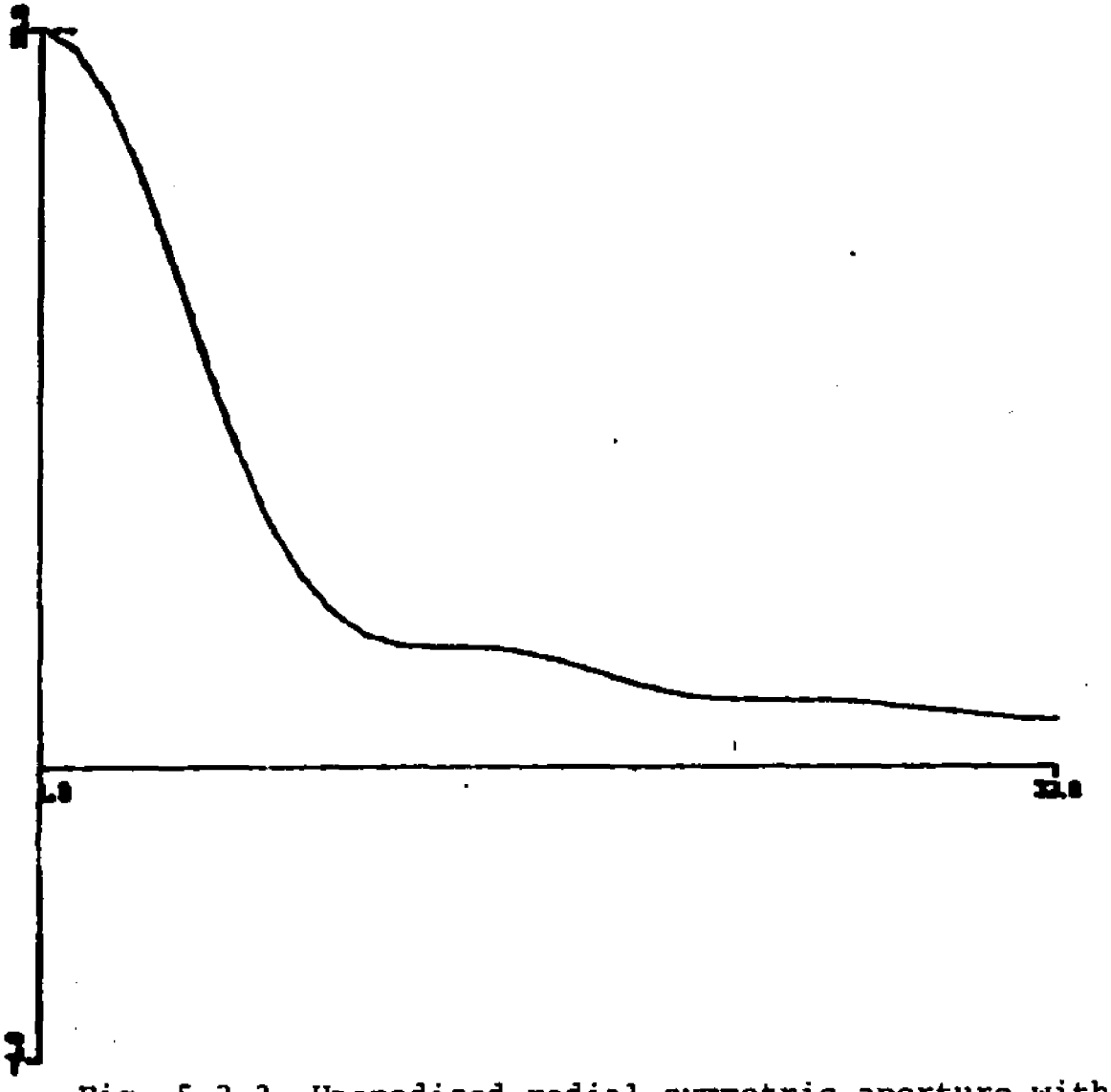

Fig. 5.3-3 Unapodized radial symmetric aperture with a noncoherent source

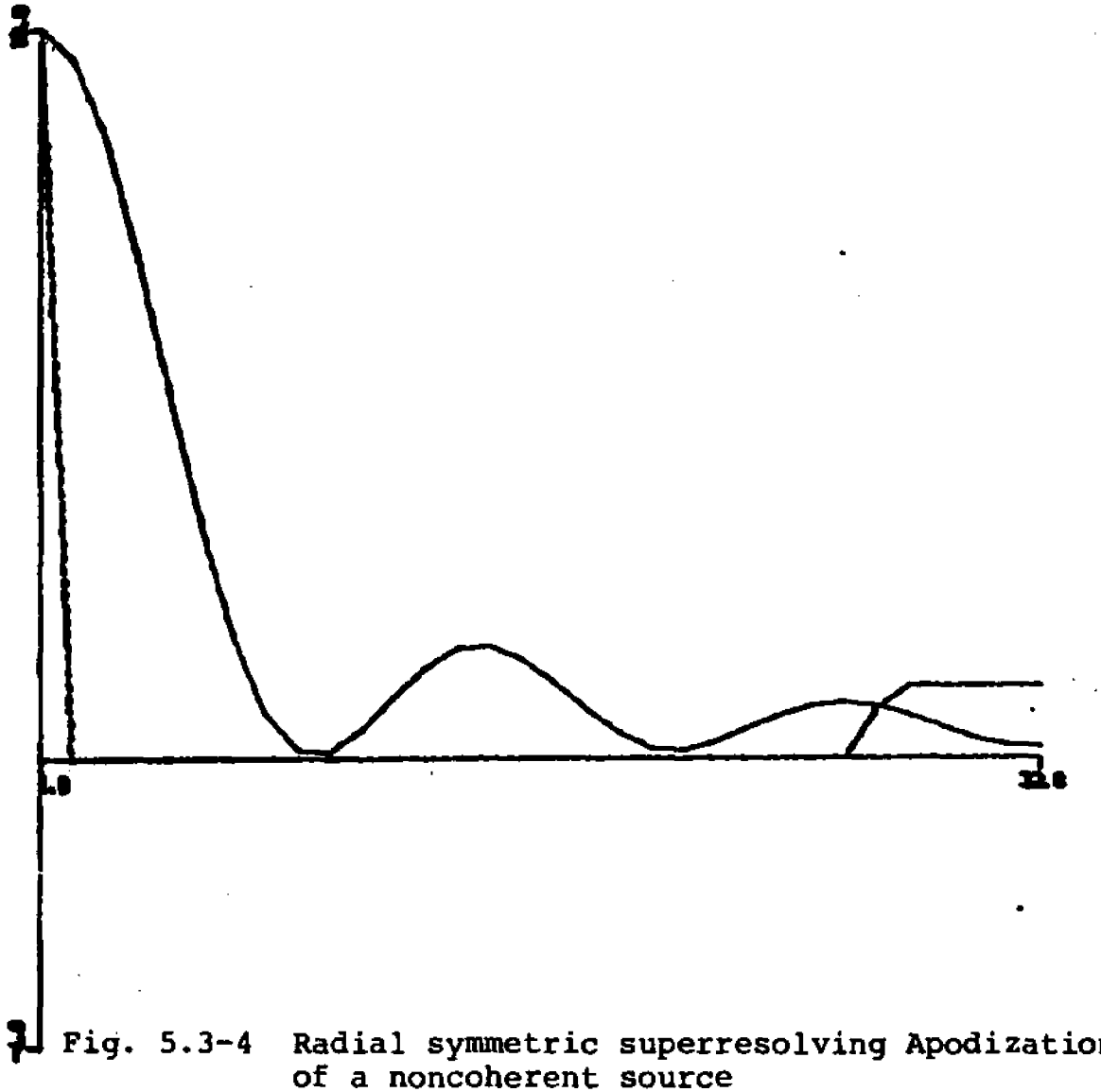

Fig. 5.3-4 Radial symmetric superresolving Apodization of a noncoherent source

Chapter 6

SUMMARY AND ALTERNATE APPLICATIONS

6.0 Summary

A new robust method of solving ill-conditioned problems is presented. The method employs a priori constraints on the estimate, i.e. that the estimate, the first and/or higher order differences are bounded. The ill-conditioned system is reduced by elimination of the effectively redundant equations. This provides a reduction in computational complexity and acts to stabilize the inversion problem.

Since the resulting reduced system of equations is underdetermined, there are many possible "solutions." We shall select that particular vector for the solution which yields the minimal norm of the residual error. Since this solution vector is of the same dimension as the effective rank, the method prefers restorations of inputs with sparse vector representations. The method is demonstrated in three applications: image processing, spectral estimation, and Apodization. Each application pertains to increasing the resolution of a measured signal. The resolution is increased beyond the limit imposed by the uncertainty principle of signal

processing (superresolving). The method is demonstrated to be very effective in all three applications via computer simulations. The first chapter of this thesis contains material of an introductory nature. In Chapter 2 the contemporary methods of increasing resolution or equivalently extrapolating the spectrum of a signal are given. In general, these methods are found to be computationally very expensive and highly sensitive to noise. In Chapter 3, a new method of increasing the resolution of an image is presented. The method reduces the computational effort necessary to restore images degraded by an ill-conditioned operator. The restorations of noncoherent and coherent diffraction limited images are treated in detail. In Chapter 4, exptrapolation in the time domain of a bandlimited signal is investigated. Alternately, the resolution of the frequency spectrum is increased. Thus, superresolving spectral estimation is demonstrated. Chapter 5 presents the design of a superresolving Apodization screen. This screen will permit a spot-size of smaller circumference than previously possible. This smaller spot-size finds immediate application in the recent development of laser video discs. The video information is in the form of holes in the video disc. This Apodization will allow smaller holes to be burnt into the disc; thus discs of higher density can be made. Future research is suggested in further

applications of the algorithm presented.

6.1 Alternate Applications

Further research efforts should address the wealth of further applications possible. The extension of this superresolving restoration method can be made to a wide variety of disciplines. The list of possible applications includes: Geophysics (signal restoration from seismographs), Neurophysics (EEG signals), Speech Communication, i.e. given a particular speech signal, it is fo interest to determine the general type of sound it is, voiced or fricated. In addition, one is interested in the identity of the sound which can be obtained from the spectrum. Such derived information can then be used in an automatic speech recognition system or a speech compression system. Further investigation should be pursued of the superresolving capabilities of this method for image enhancement of electron-microscope images, video images received from onboard space and aircraft and for image enhancement of medical diagnostic images, such as CAT-scans, B-scan, ultrasound images, conventional X-rays and Neutron Magnetic Resonance (NMR) images. The method presented could also be utilized to increase the resolution of existing sonar and radar systems.

REFERENCES

1. Papoulis, A. Signal Analysis. McGraw-Hill, 1977.

2. Slepian, D., and H.O. Polak. "Prolate Spheroidal Wave Functions, Fourier Analysis, and Uncertainty-I." Bell Syst. Tech. J. 40:43-63 (1961).

3. Slepian, D. "Prolate Spheroidal Wave Functions, Fourier Analysis and Uncertainty-V: The Discrete Case." Bell Syst. Tech. J. 57:1371-1430 (1978).

4. Gerhardt, L.A. "Topologically Optimum Adaptive Networks." ICC Conf. Washington, D.C. (1976).

5. Markel, J., and A. Gray. "Linear Prediction of Speech." Berlin, Springer Verlag (1976).

6. Akaike, H. "A New Look at the Statistical Model Identification." IEEE Trans. Autom. Control, Vol. AC-19:716-723 (1974).

7. Van den Bos, A. "Alternative Interpretation of Maximum Entropy Spectral Analysis." IEEE Trans. Inform. Theory, Vol. IT-17:493-494 (1971).

8. Griffiths, L.J., and R. Prieto-Dias. "Spectral Analysis of Natural Seismic Events Using Autoregressive Techniques." IEEE Trans. Geo Sci. Electron., Vol. GE-15:13-26 (Jan. 1977).

9. Papoulis, A. "A New Algorithm in Spectral Analysis and Band-Limited Extrapolation." IEEE Trans. Circuits Syst. Vol. CAS-22, No. 9, 735-742 (1975).

10. Gerchberg, R.W. "Super-resolution Through Error Energy Reduction." Optica Acta, 9, 21:709-720 (1974).

11. Cadzow, J.A. "Improved Spectral Estimation from Incomplete Sampled Data Observations." Proc. RADC Spectrum Estimation Workshop, pp. 109-123 (1978).

12. Sabri, M., and W. Steenaart. "An Approach to Band-Limited Signal Extrapolation: The Extrapolation Matrix." IEEE Trans. Circuits Sys., Vol. Cas-25:74-78 (1978).

13. Kadar, I., and L. Kurz. "A Robustized Vector Recursive Stabilizer Algorithm for Image Restoration." Information and Control 44, 3:320-338 (1980).

14. Backus, G., and F. Gilbert. Phil. Trans. Roy. Soc. (London). Vol. A266:123-ff (1970).

15. Schell, A.C. "Enhancing the Angular Resolution of Incoherent Sources." Radio Electron. Eng. 29:21-26 (1965).

16. Biraud, Y. "A New Approach for Increasing the Resolving Power by Data Processing." Astron. Astrophys. 1:124-127 (1969).

17. Van Cittert, P.H. "Resolution Enhancement of Spectra." Z. Physik, Vol. 69:298-301 (1931).

18. Jansson, P.A., R.H. Hunt, and E.K. Plyler. "Resolution Enhancement of Spectra." J. Opt. Soc. Am 60:596-599 (1970).

19. Frieden, B.R. "Image Enhancement and Restoration." In Picture Processing and Digital Filtering. T.S. Huang, Ed. Springer Verlag, New York (1975).

20. Twomey, S. "The Application of Numerical Filtering to the Solution of Integral Equations Encountered in Indirect Sensing Measurements." J. Franklin Inst., Vol. 279:95-109 (1965).

21. Burg, J.P. "Maximum Entropy Spectral Analysis." Presented at the 37th annual meeting of the Society of Exploration Geophysicists, Oklahoma City, OK (1967).

22. Phillips, D.L. "A Technique for the Numerical Solution of Certain Integral Equations of the First Kind." J. Ass. Comput. Mach. Vol. 9:84-96 (1962).

23. Helstrom, C.W. "Image Restoration by the Method of Least Squares." J. Opt. Soc. Am. 3, 57:297-303 (1967).

24. Andrews, H.C. and B.R. Hunt. Digital Image Restoration. Prentice-Hall, Englewood Cliffs, NJ (1977).

25. Tikhonov, A.N. "On the Solution of Incorrectly Posed Problems and the Method of Regularization." Soviet Math. 4:1035-1038 (1963).

26. Barrett, E.B., and R.N. Devich. "Linear Programming Compensation for Space-Variant Image Degradation." Proceedings SPIE/OSA Cong. on Image Processing. J.C.Urbach, Ed. Pacific Grove, CA, 74:152-158 (1976).

27. MacAdam, D.P. "Digital Image Restoration by Constrained Deconvolution." J.Opt. Soc. Am., 60, 12: 1617-1627 (1970).

28. Mascarenhas, N.D.H., and W.K. Pratt. "Digital Image Restoration Under a Regression Mode." IEEE Trans. Circuits and Systems, CAS-22, 3:252-266 (1975).

29. Frieden, B.R., and J.J. Burke. "Restoring With Maximum Entropy II; Superresolution of Photographs of Diffraction-Blurred Impulses." J. Opt. Soc. Am. 62:1202-1210 (1972).

30. Harris, J.L., Sr. "Image Evaluation and Restoration." J. Opt. Soc. Am. 56, 5:569-574 (1966)

31. Baker, C.T., L. Fox, U.F. Muyers, and K. Wright. "Numerical Solution of Fredholm Integral Equations of the First Kind. Comp. J. 7:141-152 (1964).

32. Hadley, G. Linear Programming. Addison-Wesley, Reading, MA (1962).

33. Beale, E.M.L. "On Quadratic Programming." Nav. Res. Log. Quart. g:227-243 (1959).

34. Wolfe, P. "The Simplex Method for Quadratic Programming." Econometrica, 27:382-398 (1959).

35. Kunzi, H.P., H.G. Tzschach and C.A. Zehnder. Numerical Methods of Mathematical Optimization. Academic Press, New York (1971).

36. Lawson, C.L. and R.J. Hanson. Solving Least Squares Problems. Prentice-Hall, Englewood-Cliffs, NJ (1974).

37. Andrews, H.C. and C.L. Patterson. "Singular Value Decompositions and Digital Image Processing." IEEE Trans. on Acous., SP, and Sig. Proc., Vol. ASSP-24, 1:26-53 (1976).

38. Jacquinot, P. and Mme. B. Roizen-Dossier. Apodization, "Progress in Optics." Ed. E. Wolf. Vol. III. John Wiley & Sons, Inc., New York (1964).

39. Toraldo di Francia, G. Suppl. Nuovo Cimento. Vol. 9: 426 (1952).